جامعة السودان للعلوم والتكنولوجيا

Sudan University of Science and Technology

College of Graduate Studies

Characterization of Normal Pineal Gland in Sudanese Population Using Magnetic Resonance Images

توصيف الغدة الصنوبرية السلمية لدى السودانيــن بإستخــدام التصوير بالرنيــن المغناطيسي

Thesis submitted for the Fulfillment the of PhD degree in Diagnostic Radiographic sciences

Prepared by :

Mazin Babikir Abdullah Hassib

Supervised:

Prof. Mohamed Elfadil Mohamed Garelnabi

Co-supervisor:

Dr. Asma Ibrahim Mohammad ElAmin

November - 2018

الآيـــة :

قال تعــــــالى :

بِسْمِ ٱللَّهِ ٱلرَّحْمَٰنِ ٱلرَّحِيمِ

ٱقْرَأْ بِٱسْمِ رَبِّكَ ٱلَّذِى خَلَقَ ﴿١﴾ خَلَقَ ٱلْإِنسَٰنَ مِنْ عَلَقٍ ﴿٢﴾ ٱقْرَأْ وَرَبُّكَ
ٱلْأَكْرَمُ ﴿٣﴾ ٱلَّذِى عَلَّمَ بِٱلْقَلَمِ ﴿٤﴾ عَلَّمَ ٱلْإِنسَٰنَ مَا لَمْ يَعْلَمْ ﴿٥﴾ كَلَّآ إِنَّ
ٱلْإِنسَٰنَ لَيَطْغَىٰٓ ﴿٦﴾ أَن رَّءَاهُ ٱسْتَغْنَىٰٓ ﴿٧﴾ إِنَّ إِلَىٰ رَبِّكَ ٱلرُّجْعَىٰٓ ﴿٨﴾ أَرَءَيْتَ
ٱلَّذِى يَنْهَىٰ ﴿٩﴾ عَبْدًا إِذَا صَلَّىٰٓ ﴿١٠﴾ أَرَءَيْتَ إِن كَانَ عَلَى ٱلْهُدَىٰٓ ﴿١١﴾ أَوْ أَمَرَ
بِٱلتَّقْوَىٰٓ ﴿١٢﴾ أَرَءَيْتَ إِن كَذَّبَ وَتَوَلَّىٰٓ ﴿١٣﴾ أَلَمْ يَعْلَم بِأَنَّ ٱللَّهَ يَرَىٰ ﴿١٤﴾ كَلَّا لَئِن
لَّمْ يَنتَهِ لَنَسْفَعًۢا بِٱلنَّاصِيَةِ ﴿١٥﴾ نَاصِيَةٍ كَٰذِبَةٍ خَاطِئَةٍ ﴿١٦﴾ فَلْيَدْعُ نَادِيَهُۥ
سَنَدْعُ ٱلزَّبَانِيَةَ ﴿١٧﴾ كَلَّا لَا تُطِعْهُ وَٱسْجُدْ وَٱقْتَرِب ۩ ﴿١٩﴾

۞صدق الله العظيم۞

﴿سورة إقراء﴾

Dedication:

I am honored to dedicate this work

To my loving family father, mother and brother.

In appreciation for their patience, understanding and never ending support . . .

ACKNOWLEDGMENT

Firstly my great thanks to Allah who led me until the end of this research; I thank my supervisors **Prof**. *Mohamed Elfadil Mohamed Garelnabi* **Dr.** *Asma Ibrahim* who helps advices and answers all my question .then I thank everyone who helps me, I also thank all my teachers in Sudan university of Science and Technology.

List of Tables

List of Figures

List of abbreviations

MRI: Magnetic resonance Images.

SWMR : Magnetic Susceptibility.

ROI: Region of Interest.

CAD: Computer-Aided Diagnosis

PX: Pixel.

FOS: First Order Statistic.

DSM: Disk Summation Method

DICOM: Digital Image communication in Medicine.

3D-FEE: Ultrafast Gradient Echo 3D.

IDL: Interactive Data Language

BMI: Body Mass Index.

Abstract

This study aim to estimation the volume of the pineal gland using disc summation method (DSM) and identification of shapes in normal Sudanese adult with classification to the region using MRI; defining the corpus, pineal gland, tectum, and third ventricle were carried out using Interactive Data Language (IDL) program as platform for the generated codes, 159 consecutive patients scanned for Brian MRI to pineal region using 1.5 Tesla, the sequence was3D-T1. Detailed Demographic Information of Population including; age, gender, weight, height, and BMI was recorded. DSM used to measure the normal pineal gland in normal individuals, and the shapes of pineal gland were evaluated in Axial & Sagittal images. On the other hand the features extraction was done by First Order Statistics. The results showed that the pineal gland volume showed inconclusive difference between gender 0.135±0.0063 0.137±0.0063 cm^3, for female and male respectively and using analysis of variance test for the age with body mass index BMI and the pineal gland volume were the *p*.value show that there is significant difference between the body mass index 0.000 and pineal gland volume 0.037 with age. The pineal gland volume can be estimated using the following linear equations: ***Pineal gland Volume = 0.0004 (Age/ys) + 0.1262***and***Pineal gland Volume = 0.0012 (BMI) + 0.1104.*** The distribution of shape of pineal gland showed three different shapes; pear, fusiform and cone shape. Where the pear shape found in 13.8%, of the cases, the fusiform shape 38.4% cases and the cone shape in47.8%. The result this study also showed that the mean ± S.D pineal gland volumes using Disk Summation Method were found to be 0.136 ± 0.007 cm^3.The classification showed that the pineal gland areas were classified well from the rest of the tissues although it has characteristics mostly similar to surrounding tissue. also the Gray Level variation and features give varies classification accuracy. Texture features are introduced using Gray Level variation, features and the FOS. FOS gives a classification score matrix generated by linear discriminate analysis with overall classification accuracy of 92.7%, where the classification accuracy of corpus 93.3%, pineal gland 97.9%, tectum 89.9%, while the third Ventricle showed classification accuracy of 88.5%. In conclusion these relationships are stored in a Texture Dictionary that can be later used to automatically annotate new MRI with the appropriate pineal gland.

المُستخلـص

عمد الباحث في هذه الدراسة على تقدير حجم الغدة الصنوبرية باستخدام طريقة تجميع الاقراص وتحديد أشكالها في البالغين السودانيين العاديين مع تصنيف منطقها في المخ باستخدام التصويربالرنين المغناطيسي الذي تم فيه تعريف الغشاء الرابط والغدة الصنوبرية والطبقة والبطين الثالث باستخدام برنامج لغة برمجة البيانات التفاعلية لذي اعتبر الاساس للحصول على خصائص الصورالتي تم تحليها. تم فحص 159 على التوالي وذلك باجراء صور الرنين المعناطيسي للراس لفحص الغدة الصنوبرية ومنطقتها باستخدام جهاز رنين مغناطيسي تبلغ شدة مجاله المغناطيسي 1.5 تسلا وكان البرتكول المستخدم لصورة في الزمن الاول ثلاثية الابعاد .لتقدير حجم الغدة تم استخدام طريقة قياس القرص ولمعرفة الشكل التشريحي للغدة كان عن طريق معايرة لصورة الرنين المحورية والجانبية للمريض . من ناحية اخرى تم استخدام الترتيب الاحصائي الاول لإستخراج خصائص الصورة و لتقسيم منطقة الغدة الصنوبرية لاربع اقسام.وضحت النتائج الاتي ، يوجد اختلاف ضئيل في حجم الغدة الصنوبرية بين الذكور والاناث حيث كان 0.135 ±0.0063 سم^{3}للإناث و 0.137 ±0.0063 سم^{3}للذكور . وبإستخدام التحليل الاحصائي للمتغيرات للعمر ومؤثر كلتة الجسم مع حجم الغدة كانت درجة المعنوية اقل من 0.00لموشر كتلة الجسم و 0.037 للعمر حيث يثبت وجود علاقة معهم و يمكن تقديرحجم الغدة الصنوبرية باستخدام المعادلات الخطية التالية : حجم الغدة الصنوبرية = 0.0004 × العمر + 0.13. ، حجم الغدة الصنوبرية = 0.0012 × موشر كلتة الجسم + 0.11 . أظهرتوزيع شكل الغدة الصنوبرية ثلاثة أنواع مختلفة من الاشكال ، الكمثرى والمغزلي والمخروطي حيث كان الشكل الكمثرى الموجود يمثل بنسبة 13.8٪ والمغزلي يمثل بنسبة 38.4٪ وشكل المخروطي يمثل 47.8٪.في هذه الدراسة ايضـا ،وجدأن متوسط حجم الغدة الصنوبرية باستخدام طريقة تجميع الأقراص هو 0.136 ± 0.007 سم^3. أظهرالتصنيف أنمناطق الغدة الصنوبرية صنف تبشكل جيد من بقية الأنسجة على الرغم من أن لها خصائص مشابهة في الغالب للأنسجة المحيطة بها. الترتيب الاحصائي الاول يعطي مصفوفة تصنيف للتحليل التمييز يالخطي بدقة تصنيف كلية 92.7٪ ،كانت دقة تصنيف الغشاء الرابط 93.3 ٪ ،الغدة الصنوبرية 97.9 ٪ ،الطبقة 89.9 ٪ والبطين الثالث دقة التصنيف 88.5 ٪.في الختام يتم تخزين هذه العلاقات في قاموس نسيجي مكن استخدامها لاحقً الإضافة تعليقات على التصويربالرنين المغناطيس يتلقائيًا مع للغدة الصنوبرية.

Contents

Chapter one:

Introduction:

1. 1 Introduction:

MRI is the modality of choice for evaluating the pineal region the gland appears as a small nodule of tissue with similar intensity to grey matter. It enhances vividly during contrast administration. The key to successful imaging of the region is the ability to clearly identify the relationship of any pathology to the surrounding structures and as such thin section high resolution imaging in all three planes (Buch S, et al 2016).

Magnetic Resonance Imaging (MRI) is a medical imaging technique. Radiologist used it for the visualization of the internal structure of the body. MRI provides rich information about human soft tissues anatomy. MRI helps for diagnosis of the brain abnormality. Images obtained by the MRI are used for analyzing and studying the behavior of the brain. Image intensity in MRI depends upon four parameters. One is proton density (PD) which is determined by the relative concentration of water molecules. Other three parameters are T1, T2, and T2* relaxation, which reflect different features of the local environment of individual protons. (Qurat-Ul-Ain et al-2014).

Recent advances in MRI imaging have led to the development of novel gradient echo (GRE) imaging techniques such as SWMR, which is based on magnetic susceptibility and sensitive to materials distorting the local Magnetic field. SWMR allows for a reliable differentiation of calcifications from tissue artifacts, hemorrhage and other causes of susceptibility differences by using T2. Diagnostic accuracy of SWMR for the evaluation of pineal gland calcification weighted magnitude and GRE filtered-phase information to generate a unique contrast (Haacke EM, et al 2009) (Nandigam RN, et al 2009).

Pineal gland is a very important neuroendocrine organ with many physiological functions such as regulating circadian rhythm. Radiologically, the pineal gland volume is clinically important because it is usually difficult to distinguish small pineal tumors.(Niyazi A, et al. 2012)

The Signs and symptoms related to pineal lesions are generally secondary to mass effect on adjacent structures. Compression of the tectal plate can result in obstruction of the sylvian aqueduct and obstructive hydrocephalus. Cerebellar, corticospinal or sensory disturbance can result from direct compression of the midbrain

(Klein P, Rubinstein LJ -1989). Infiltrative lesions of the pineal gland may interfere with normal pineal gland function and lead to precocious puberty, less commonly hypogonadism and diabetes insipidus.

Pineal parenchymal lesions account for less than 15 % of all pineal masses and less than 0.2 % of intracranial neoplasm's (Klein P, Rubinstein LJ -1989) (Surawicz TS et al 1999) These lesions commonly arise from pineocytes or their precursors and are classified by the World Health Organization (WHO) into the following entities: low-grade pineocytoma, pineal parenchymal tumour of intermediate differentiation (PPTID), papillary tumour of pineal region (PTPR) and highly malignant pineoblastoma (Louis DN et al 2007).

Stereological methods using the Cavalieri principle have been widely applied on magnetic resonance imaging (MRI) sections to estimate volume of brain and internal brain compartments. Researchers have employed these techniques to obtain volume estimations of various brain structures, including hippocampus, temporal lobe, Broca’s area, brain ventricles, cerebellum, and cerebral hemisphere .(S. Keller, et al-2002). (N. Aceret al-2010).

There are several packages that have been developed for volume estimation such as Analyze and Image J. This software has ROI function based on manual techniques. Manual techniques such as planimetry or tracing methods require the investigator to delineate a brain region based on reliable anatomical landmarks, whilst the software package provides information on volume. Tracing methods require the investigator to trace the brain region of interest (ROI) using a mouse-driven cursor throughout a defined number of MRI sections.

The cut surface areas, determined by pixel counting within the traced region, are summed and multiplied by the distance between the consecutive sections traced to estimate the total volume (S. S. Keller et al, 2009).

Classification of an MR Images is the technique for classifying the objects into corresponding classes. Ones the brain images acquired they are classified as normal and abnormal. For classification of the images different features of the image are extracted. These features are used for classifying the brain MR image as normal and abnormal. (Qurat-Ul-Ain et al-2014).

Computer-aided diagnosis (CAD) in medical images has been studied in many disciplines including the diagnosis of brainpathology. (S. Sahiner, H.et al -1998).Computer aided analysis and diagnosis of MRI brain images have become an important area of research in recent years.

(Namita Aggarwal, et al - 2012).

For proper analysis of these images, it is essential to extract a set of discriminative features which provide better classification of MRI images. In literature, various feature extraction methods have been proposed such as Independent Component Analysis (C.H.Mortiz et al , 2000) Fourier Transform (R. N. Bracewell, 1999) Wavelet Transform (S. Chaplot et al , 2006) and Texture based features (R. M. Haralick et al, 1973).

In literature (R. M. Haralick et al, 1973) (A. Materka et al , 1998). features based on First and Second Order Statistics that characterizes textures are also used for classification of images. Features based on statistics of texture gives far less number of relevant, non-redundant, interpretable and distinguishable features.

1.2 Research problem:

Knowledge of the characteristic of the normal pineal gland and its region is important for clinical assessments of abnormalities of it. And may it have variables dimensions, shape and texture features among different people so there is a normal range all along between different nations and individuals. Therefore several nations they got their own index which is attributed to their body characteristics which include the height, weight, and gender and sometimes body mass index. Also In this essence Sudanese index is crucial as well as normal textural identity of the variable structure of the pineal gland will inspire and promote the potential capacity of the diagnostic capabilities.

1.3Research Objectives:

1.3.1 General Objective:

The general objective of study is Characterization of Normal Pineal gland in Sudanese adult Using the Magnetic Resonance Images through Estimation the volume; evaluate the shape and textural analysis of it.

1.3.2 Specific Objectives:

The specific objectives are:

- To estimate the pineal gland volume for normal Sudanese adult.
- To generate the normal pineal gland volume index for Sudanese.
- To indentify the shapes of pineal gland.
- To correlate the pineal gland volume with Gender, Age, weight, High and body mass index.
- To find the shape distribution of pineal gland.
- To indentify the pineal region classes and classify coefficients in (FOS).
- To measure the accuracy of (FOS) to classification of pineal region.

Chapter Two:

Study Background:

2.1 Pineal Gland:

2.1.1 Pineal Gland Anatomy:

The human pineal gland also called the pineal body, epiphysis cerebri, epiphysis or the “third eye: is a small reddish-grey pine cone-like endocrine gland of a major regulatory importance located in between the superior colliculi. It is inferior to the splenium of the corpus callosum from which it is separated by the telachoroidea of the third ventricle and the contained cerebral veins .The pineal is about 8 mm long. Septa extend into the pineal gland from the surrounding pia mater. (Drake RL, et al, 2009).

Several surrounding structures are useful in grossly identifying the epiphysis cerebri.On a coronal section of the brain (vertically through the cerebellar hemispheres and pons), the following structural boundaries can be appreciated Superiorly, the splenium of the corpus callosum is observed ,Superolaterally, the choroid plexus of the third ventricle is seen bilaterally, Inferiorly, the superior and inferior colliculi are seen. In the sagittal section (along the longitudinal cerebral fissure).the quadrigeminal plate (in addition to the colliculi) is also readily observed inferiorly, the Habenular commissure and the thalamus are seen in anterosuperior relations to the gland. The great cerebral vein of Galen has a posterosuperior relation to the gland, and the posterior commissure, the cerebral peduncle and the cerebral aqueduct of Sylvius lies anteroinferiorly.(Drake RL, et al, 2009).

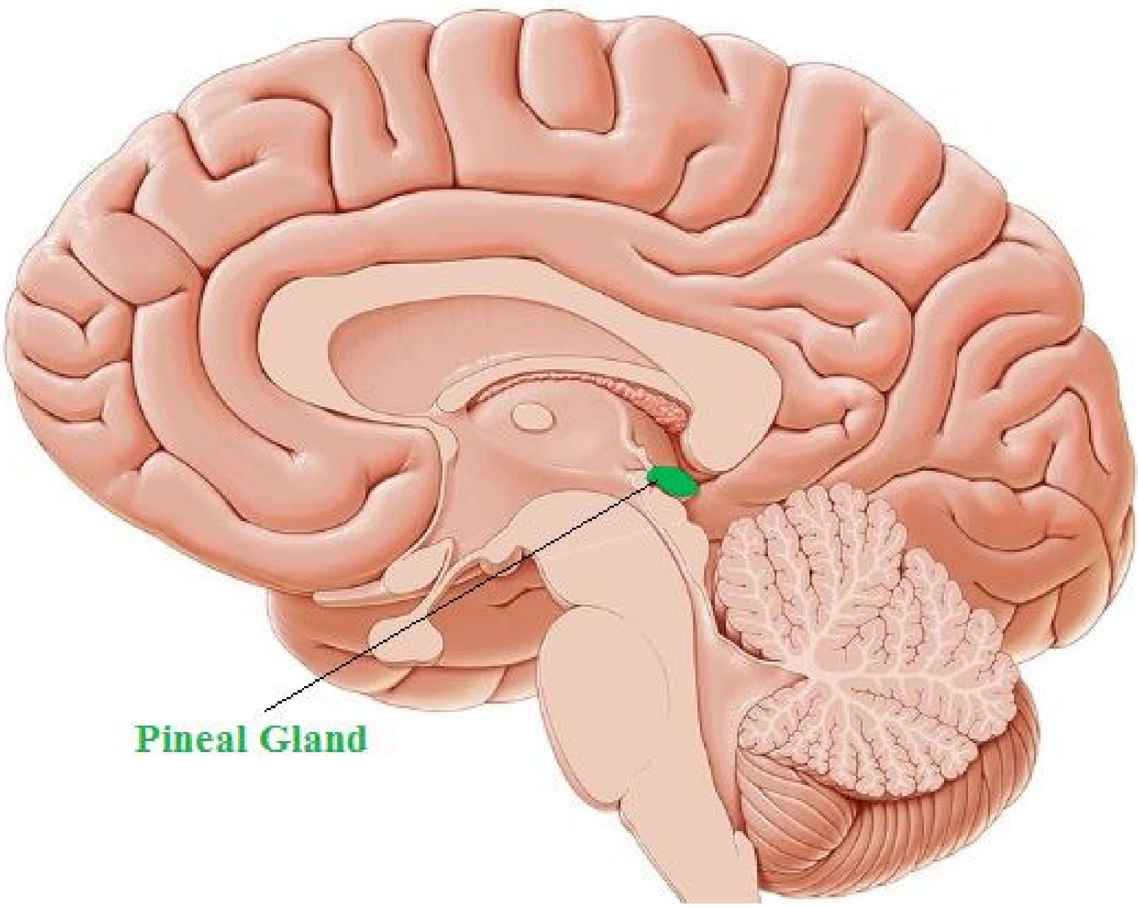

Fig (2-1):pineal Region anatomy sagittal (KEN HUB).

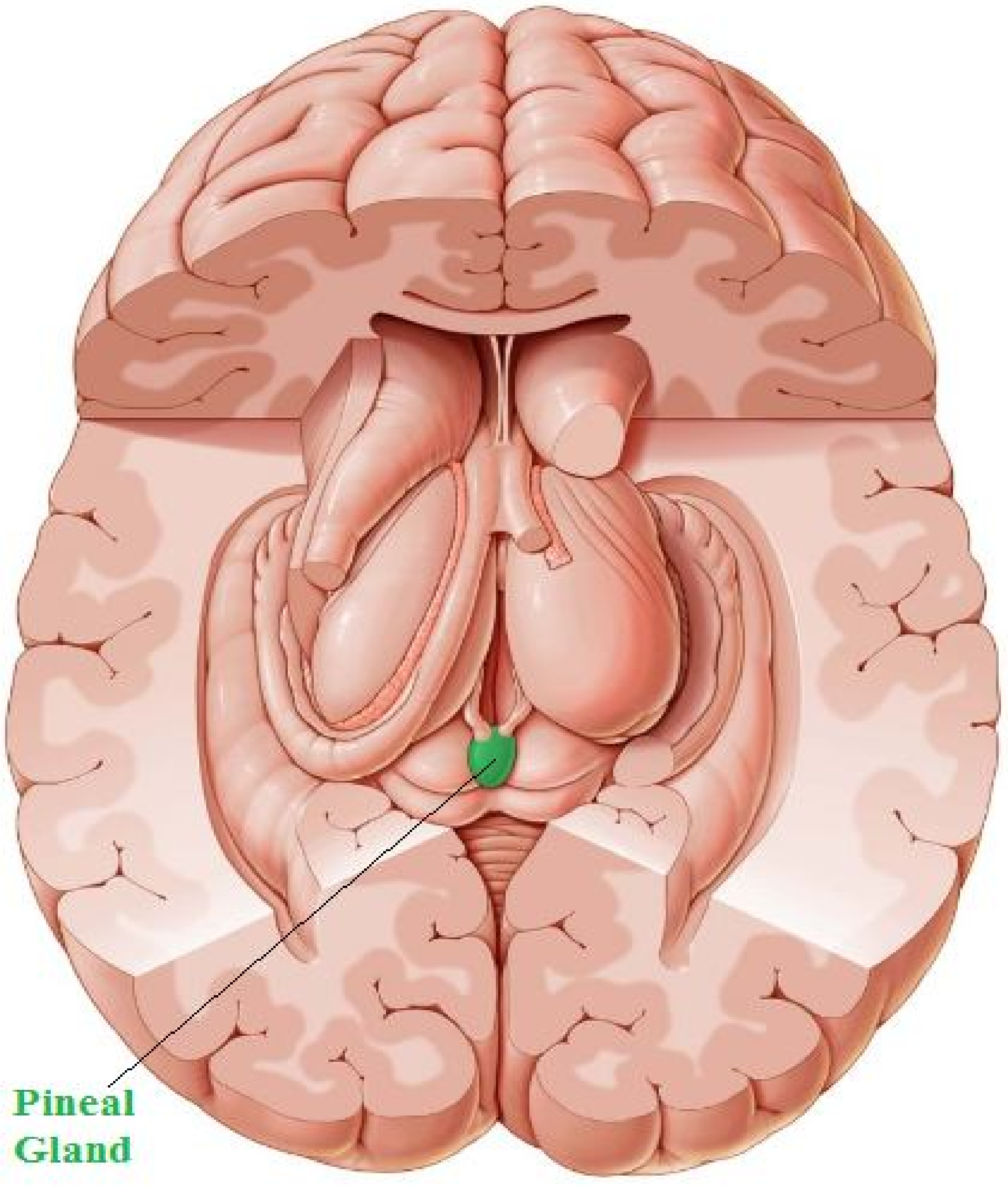

Fig (2-2):pineal Region anatomy section (KEN HUB).

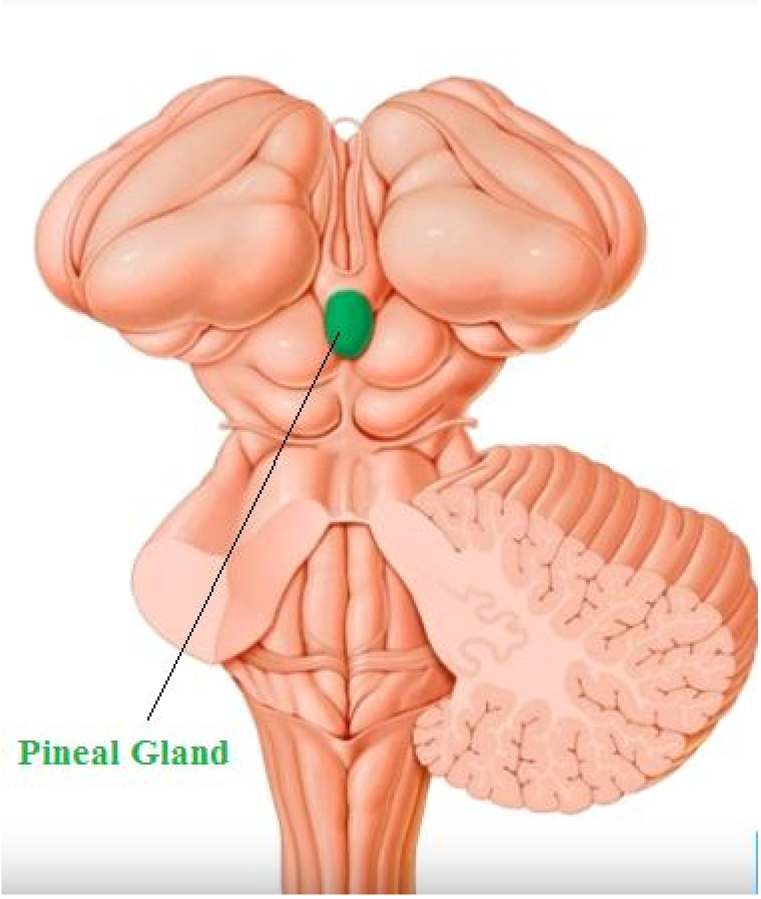

Fig (2-3):pineal Region anatomy section (KEN HUB).

The pineal gland receives its blood supply from fine branches of the posterior choroidal arteries and drains superiorly by multiple branches eventually into the great cerebral vein of Galen (Drake RL, et al, 2009).

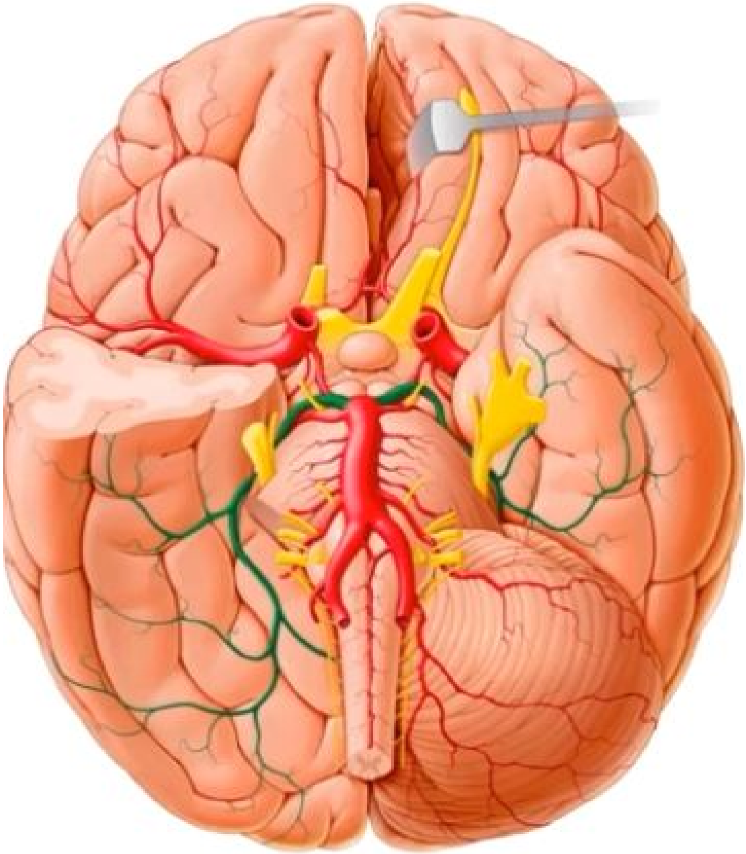

Fig (2-4):pineal Region anatomy blood supply Artery (KEN HUB).

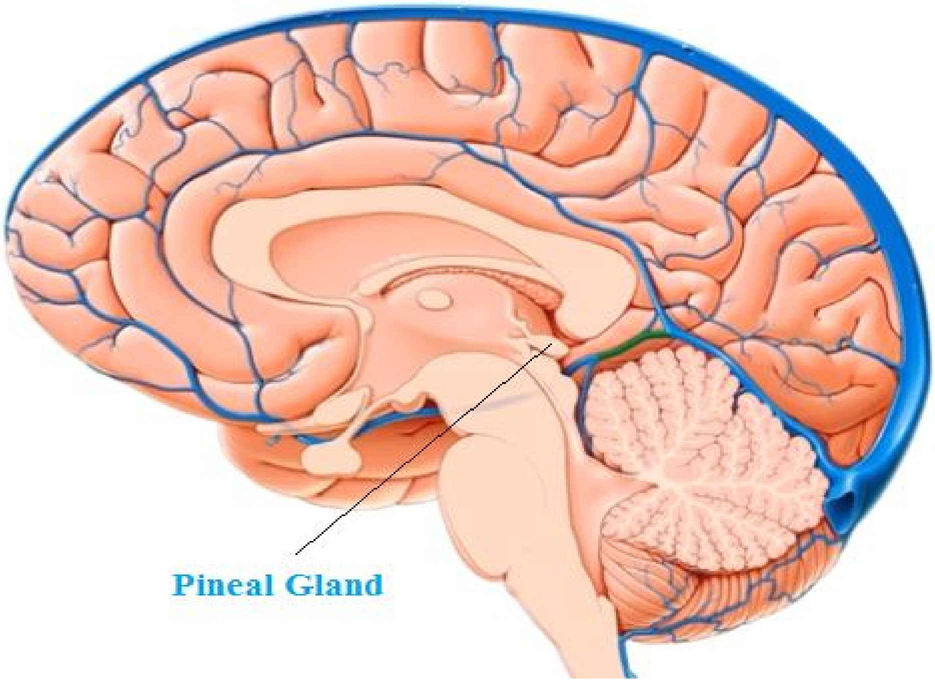

Fig (2-5):pineal Region anatomy blood supply Vein (KEN HUB).

Also it is attached by the stalk to the diencephalon and the stalk lines the pineal recess whose inferior lip links the pineal gland to the posterior commissure, and superior lip to the habenular commissure (H.M.Duvernoy et al, 2000). It has been stated that the pineal gland grows in size from birth until two years of age and then remains constant between 2 to 20 years of age(M. Sumida et al , 1996).

2.1.2 Pineal Gland Histology:

The pineal gland is encased by pia mater and lobulated by its connective tissue septae that projects into the gland. Within the epiphysis cerebri, there are pinealocytes and neuroglia cells.

Fig (2-6): pineal Gland Histology slide (KEN HUB).

The pinealocytes account for approximately 95% of the cellular content of the gland. They are irregularly shaped with peripheral processes, and lightly staining large round nuclei. Pinealocytes are primarily concerned with the photo-regulated production of melatonin. This hormone works with the body's circadian rhythm (which is controlled by the suprachiasmatic nucleus of the hypothalamus) to regulate the cycle of sleep and wakefulness. Additionally, some researchers believe that melatonin may alter sexual development in humans, contribute to thermoregulation, and cellularmetabolism.There are also the corpora arenacea (brain sand) bodies present within the gland. Calcification of these bodies is a common occurrence with increasing age. As a result, they appear as radiographic opacities on plain film radiography and can, therefore, be used as landmarks.(Edmund Tapp .2008).

2.1.3Pineal Gland Physiology:

The pineal gland contains cords and clusters of pinealocytes, where the melatonin and other pineal hormones are synthesized, associated with astrocyte-like neuroglia which is the main cellular component of the pineal stalk. The pineal body modifies the activity of the adenohypophysis, neurohypophysis, endocrine pancreas, parathyroids, suprarenal cortex, suprarenal medulla and gonads. Its effects are largely inhibitory. Pineal secretions may reach their target cells via the cerebrospinal fluid or the blood stream. (Macchi MM et al , 2004).

The pineal gland produces melatonin which affects the modulation of wake/sleep patterns circadian rhythms. And photoperiodic (seasonal) functions. It is also thought to have a reproductive function and has been associated with the onset of puberty(I. Nolte, A. et al, 2009).

The Pineal gland has several physiological or pathological conditions indeed alter the morphology of the pineal glands. For example, the pineal gland of obese individuals is usually significantly smaller than that in a lean subject (Grosshans.M ,et al .2016).

The pineal volume is also significantly reduced in patients with primary insomnia compared to healthy controls and further studies are needed to clarify whether low pineal volume is the basis or a consequence of a functional sleep disorder(Bumb, J.M, et al, 2014).These observations indicate that the phenotype of the pineal gland may be changeable by health status or by environmental factors, even in humans. The largest pineal gland was recorded in new born South Pole seals; it occupies one third of their entire brain

(Bryden, M. et al, 1986) (Cuello, A.C et al , 1969). The pineal size decreases as they grow. Even in the adult seal, however, the pineal gland is considerably large and its weight can reach up to approximately 4000 mg, 27 times larger than that of a human. This huge pineal gland is attributed to the harsh survival environments these animals experience (Tan, D.X, et al, 2005).

Also there are several diseases that can infect the pineal gland. Most of them are such as : Pineal Region Mass ,Cystic Non-Neoplastic Lesions, Pineal Cysts,Cavum Velum Interpositum ,Arachnoid Cyst, Pineal Parenchyma Tumours, Pineocytoma ,Pineal Parenchyma Tumor With Intermediate Differentiation ,Pineoblastoma and Papillary Tumor Of The Pineal Region (AFROZ.H , et al,2014).

2.2 Magnetic Resonance Imaging (MRI):

Magnetic resonance imaging (MRI) is a non-invasive medical imaging modality that has become more and more popular in recent years. MRI comes from the application of nuclear magnetic resonance (NMR). The extension of NMR to MRI was a great technical advance and greatly benefited radiologic imaging. The roots of MRI can be traced tothe initial discovery of the proton’s magnetic moment by Otto Stern in 1922 (W. Gerlach at el .1922)

Stern was awarded the Nobel Prize in1943 for discovering the proton's magnetic moment and for developing the molecular ray technology that makes possible

its observation. The famous Stern-Gerlach experiment verified the moment's existence by direct measurement and found its value to be twice that calculated from theory. Later, Isidor Rabi used the concept of magnetic resonance to probe the quantum spin states of the atomic nucleus. His work opened the door to many scientific developments, including nuclearmagnetic resonance (NMR).In 1946, scientists led by Felix Bloch from Stanford and Edward Purcell from Harvard independently observed the NMR signal (F. Bloch at el 1946)(E. M. Purcell , at el .1946) Using different methods, the two groups excited nuclear spins with radiofrequency (RF)electromagnetic fields. Knowing which frequencies are absorbed and re-emitted (i.e., the resonant frequencies) allowed them to detect the transition between nuclear magnetic energy levels. For their pioneering work in the field of NMR, BlochandPurcell shared the Nobel Prize in 1952.The idea of MRI was originally proposed by Lauterbur and Mansfield (P. Lauterbur, 1973)(P. Mansfield at el 1977), who were awarded the Nobel Prize forthis discovery in 2003.

In 1973, Lauterbur produced the first images using gradients to spatially encode the NMR signal (P. Lauterbur, 1973). He termed his method “zeugmatography” based on the Greek word “zeugmo,” meaning “that which joins.”Zeugmatography creates images using back projection in the same manner as computed tomography (CT) scans. In 1975,Richard Ernst showed that the nature of the MRI signal has the mathematical properties of a Fourier transformation, and heproposed using both frequency and phase encoding to generate data to produce superior images (R.R. Ernst at el 1975). One major reason for the better images is that the data may be sampled uniformly, using three orthogonal gradients. In the zeugmatography method, the sample must be subjected to gradients in several directions (accomplished with several different gradient vectors, or when practical, rotating the sample). Doing so oversamples the origin of frequency data, which results ininhomogeneous error distributions and coarser image quality. In 1977, Sir Peter Mansfield was able to dramatically shorten the lengthy zeugmatography process by implementing the Fourier method for image processing proposed by Richard Ernst. He is credited for using this concept to develop the fast imaging technique, echo planar imaging (P. Mansfield at el 1977). All of the above scientists received Nobel prizes for their work. Scientists from many fields continue to improve MRI. Parallel imaging techniques, radio frequency coil fabrication, pulse sequence design; functional, diffusion, perfusion, and angiographic imaging; and image-guided surgery are but a few of the areas of development underway in the field of MRI.

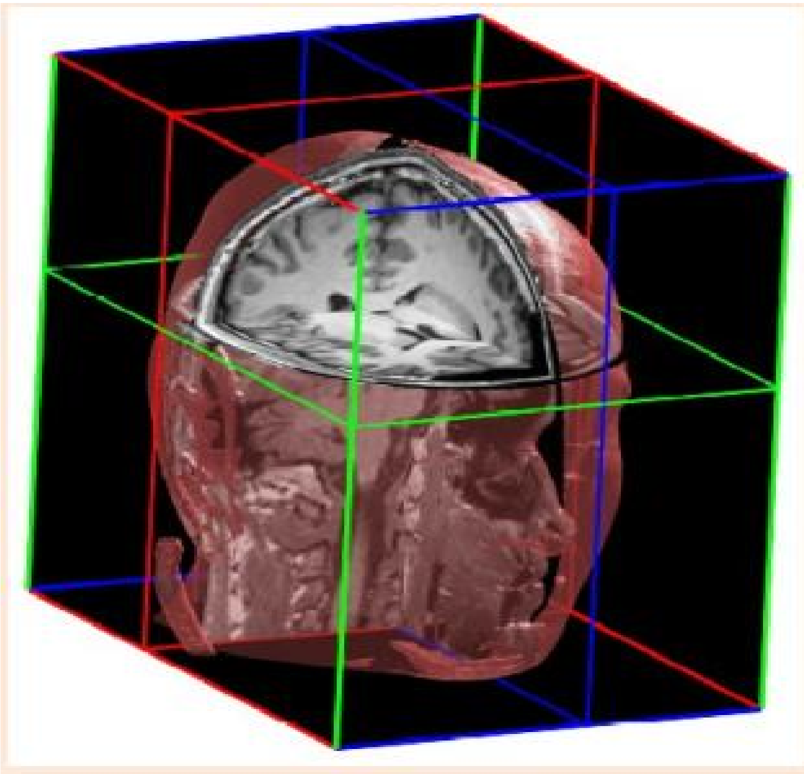

Fig (2-7):T1 -weighted MR image in sagittal (surrounded by the blue rectangle), coronal (red rectangle), and axial (green rectangle) views, combined with a semi-transparent view of the surface of the head. (Kathiravan S at el, 2013).

The basic principle of MRI is not very complicated. If a spatially varying magnetic field is introduced, the frequencies of the spins in the objects are also spatially varied. Different frequency components of the signal can be separated to give spatial information about the object. All modern MRIs still follow this basic idea, but they are quicker, more flexible and more powerful than their ancestors. Figure 1 illustrates the T1 -weighted MR image of the human head. MRI is one of the most important modalities in medical imaging. Hydrogen's (^1H), distributed throughout the human body in the form of water, fat and other chemical components, are the foundation for MRI signals. Each hydrogen can be visualized as spinning around an axis, yielding a tiny magnetic moment in the same direction as the angular momentum. Exerting external magnetic fields onto the spin generates the signals that are detected and measured by MR imaging devices and further transformed, via Fourier transforms, into the final image data that expose internal physical and chemical characteristics of the scanned object .Although the first MRI clinical scanners were not available until the early 1980s, MRI technology represented acumination of several physical discoveries spanning the twentieth century. An understanding of quantum mechanical spinin subatomic particles, the ability to manipulate a proton's spin with sophisticated apparatuses, experimental designs necessary to gain meaningful information from those manipulations, and development of mathematical frameworks to process the NMR signals, all contributes to the success of MRI. Figure 2 depicts an example of MR Brain Web data. The first row represents the HR T1 -weighted image (1×1mm2 in-plane resolution, 1 mm slice thickness) and the second row indicates the LR T2-weighted image (1×1mm2 in-plane resolution, 3 mm slice thickness)MRI is developing very fast. One report estimates that there were over 35 million MRI scans performed in 2001, and in2003, there were approximately 10,000 MRI units worldwide, with approximately 75 million MRI scans performed. The reare many advantages to MRI over other medical imaging modalities. It is very flexible and sensitive to a broad range of tissue properties. It is non-invasive and suitable for people of almost any age. Compared with other non-invasive procedures such as radiography and CT, it is a relatively safe operation because there is no radiation dose. (Kathiravan S at el, 2013).

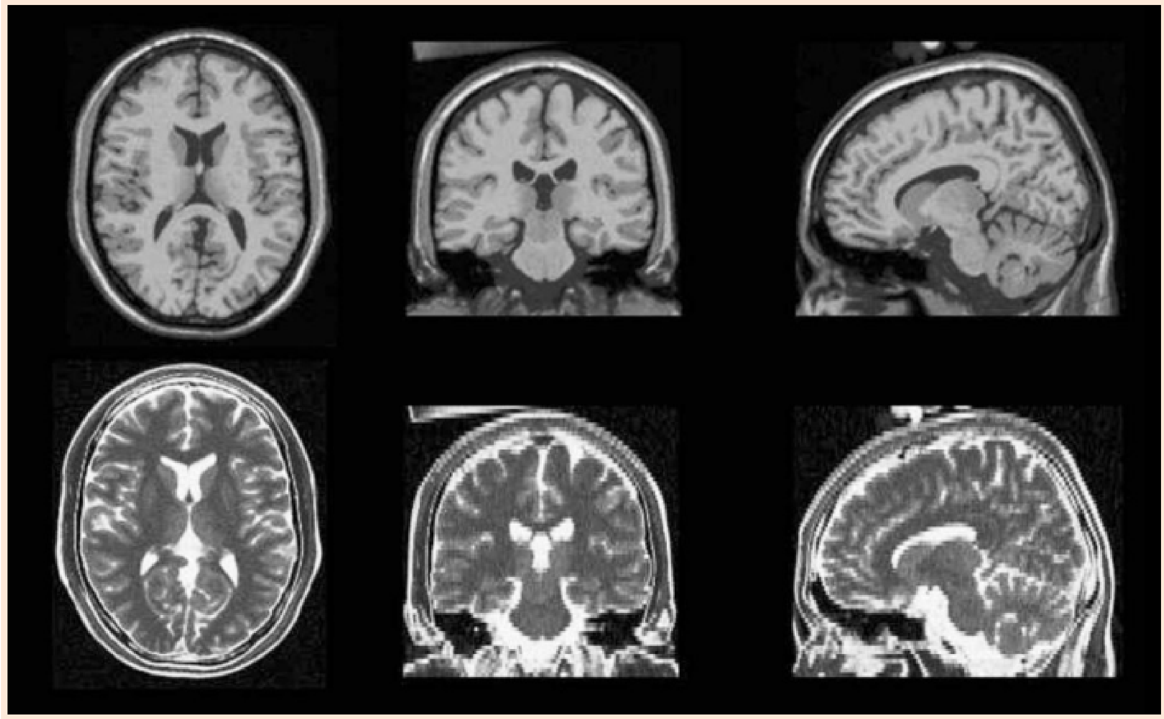

Fig (2-8): Example of MR BrainWeb data. First row: HR T1 -weighted image (1×1mm2 in-plane resolution, 1 mm slice thickness). Second row: LR T2-weighted image (1×1mm2 in-plane resolution, 3 mm slice thickness) (Kathiravan S at el, 2013).

2.2.1 Fast Magnetic Resonance Imaging:

One major disadvantage of magnetic resonance imaging is its comparatively slow scanning speed. This problem, together with normally expensive MR scanners, results in high expense for the patient who needs an MRI scan. Any improvement in MRI speed can greatly increase the quality of patient care. Fast-developing MR techniques bring more and more MR applications, such as interventional MRI, cardiac imaging, functional MRI, diffusion imaging, and so on. These new applications, on the other hand, spurred MR engineers and scientists to develop faster imaging methods .Improvements to MR hardware have provided the possibility of improving imaging speed in recent years. The main magnetic field has increased in strength from 0.2 Tesla (T) to 1.5 T and 3 T systems, which are becoming more and more popular. In some research facilities, 7 T and 9.4 T systems have been installed for human studies. The homogeneity of the main field was improved significantly, too. With the current shimming technique, the main field in homogeneity could be reduced to 1 part per million or even lower. The gradient system is another important sub-system that allows fast MR imaging. In a modern whole-body MRI system, the maximal gradient strength is about 10 to 50 mT/m and the maximum slew rate is about 10 to 200 T/m/s. These make some fast MR pulse sequences possible. The development of phased-array coils provides the necessary hardware conditions for parallel imaging techniques. Providing the advanced MR hardware, pulse sequence physicists developed many fast MRI sequences to greatly reduce the possible scanning time. Echo planar imaging (EPI) consists of a single RF excitation (or pair) of the imaging plane followed by the totality of gradient switching and sampling periods, yielding a complete encoding of the field of view(FOV). Rapid acquisition with relaxation enhancement and its variations rely on multiple RF spin echoes to sample k-space so that the total imaging time can be reduced. In the steady-state free precision technique, each type of gradient-echo sequence consists of a train of excitation pulses that are separated by a constant time interval, referred to as time of repetition (TR). Low tip angle allows short TR values, thus reducing the imaging time. More and more fast imaging sequences and protocols are being developed and applied to preclinical or clinical applications .Other methods could also be used to improve imaging speed. Selecting a good data acquisition mode and an appropriateK-space sampling scheme can sometimes greatly reduce scanning time. These efforts are sometimes combined with the development of new pulse sequences, but most of the time, they are independent techniques. The k-space trajectory is the path that was navigated in the Fourier domain. This path illustrates the acquisition strategy, influences the artifacts induced and requires the possible image reconstruction algorithms to be employed. The most popular k-space trajectory is a Cartesian raster in which a fast Fourier transform could be directly used for the reconstruction. One drawback of the

Cartesian acquisition is the relatively long scan time. Other popular trajectories include radial, spiral, and rosette. The coverage of k-space could be also different. In general, the sampling distance in k-space could be smaller than the inverse of the FOV; otherwise, aliasing artifacts will be observed based on the Nyquist theory .If multiple receiver coils and parallel imaging reconstruction techniques are used, the aliasing artifacts could be effectively reduced or removed, improving the actual scanning time; k-space could also be covered asymmetrically in the kx or ky directions, and special partial Fourier acquisition techniques could be applied for the reconstruction. The following illustrates one slice of a recorded MR image, in two-dimensional (2D) k-space and 2D image space. These two images arerelated through the Fourier transform.(Kathiravan S at el, 2013).

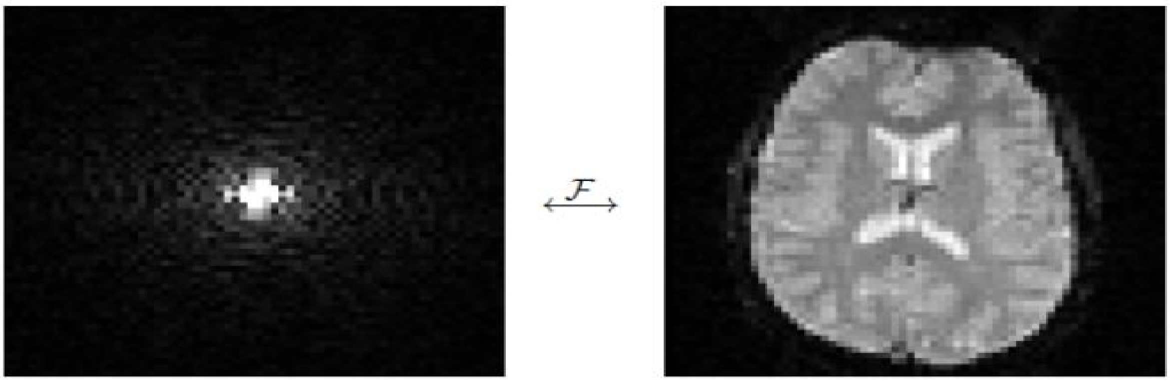

Fig (2-9): Two-dimensional (2D) k-space magnitude (left) and magnitude in 2D image space (right). (Kathiravan S at el, 2013).

Image quality is important in medical imaging because images are examined by physicians for diagnosis, therapy planning, application of therapy, and therapy assessment. Since the diagnostic task is often one of detecting a lesion, there is a long history in medical imaging of quantitatively measuring image quality as the ability to detect a target defect. Researchers use Experimental methods such as the receiver–operator characteristic(A. E. Burgess, 1995)and forced choice (P. Xue at el, 1998) and theoretical analyses using a variety of models of human detection (C. K. Abbey at el, 2000) (M. P. Eckstein at el , 2000)Most often, these were done in projection x-ray and nuclear medicine imaging, where ionizing radiation must be limited and quantum noise is often a factor. We are extending these methods to MRI.

Magnetic Resonance Imaging (MRI) is a medical imaging technique. Radiologist used it for the visualization of the internal structure of the body. MRI provides rich information about human soft tissues anatomy. MRI helps for diagnosis of the brain abnormality. Images obtained by the MRI are used for analyzing and studying the behavior of the brain. Image intensity in MRI depends upon four parameters. One is proton density (PD) which is determined by the relative concentration of water molecules. Other three parameters are T1, T2, and T2* relaxation, which reflect different features of the local environment of individual protons. (Qurat-Ul-Ain et al-2014).

MRI is the modality of choice for evaluating the pineal region the gland appears as a small nodule of tissue with similar intensity to grey matter. It enhances vividly during contrast administration. The key to successful imaging of the region is the ability to clearly identify the relationship of any pathology to the surrounding structures and as such thin section high resolution imaging in all three planes (Buch S, et al 2016).

The key to successful imaging of the region is the ability to clearly identify the relationship of any pathology to the surrounding structures and as such thin section high resolution imaging in all three planes is crucial. A typical protocol would include: Sagittal T1 and T2 (high resolution), Pre and post contrast T1 axial and coronal , FLAIR,DWI and SWI/gradient echo (to assess for presence of calcification). (J. Golan, et al , 2002).

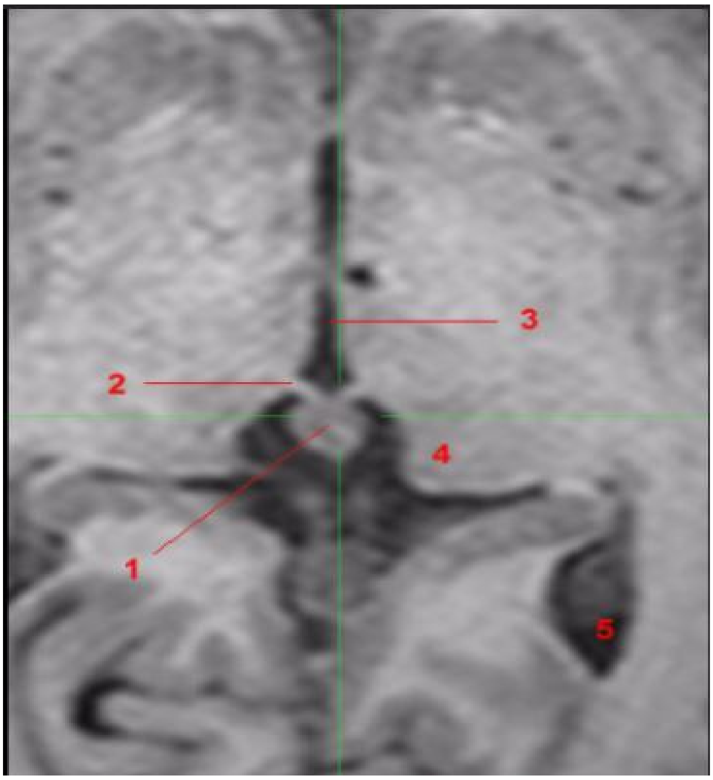

Fig (2-10): T1-weighted axial view.

Demonstrate (1, Pineal gland. 2, Habenula. 3, Third ventricle. 4, Pulvinar. 5, Lateral ventricle)(B. Sun, et al, 2009)

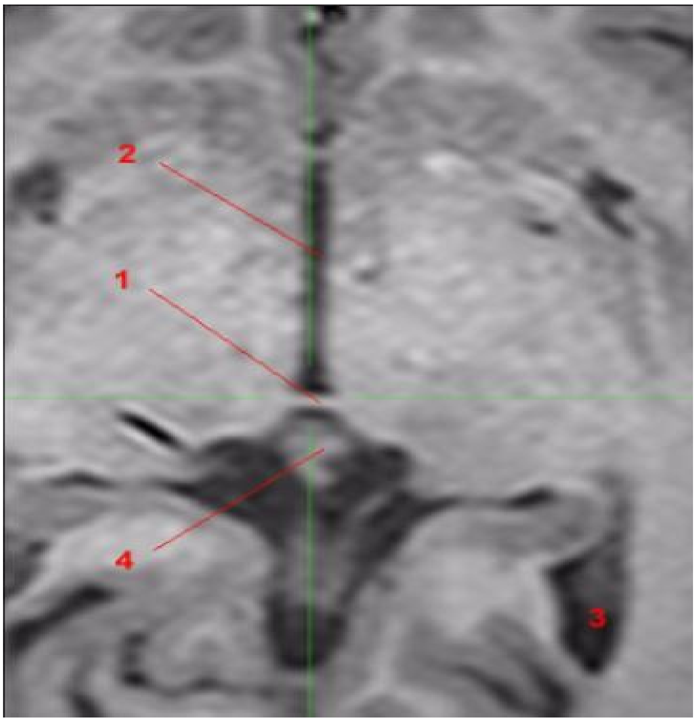

Fig (2-11): T1-weighted axial view.

Demonstrate (1, Posterior commissure. 2, Third ventricle. 3, Lateral ventricle. 4, Pineal gland)(B. Sun, et al, 2009)

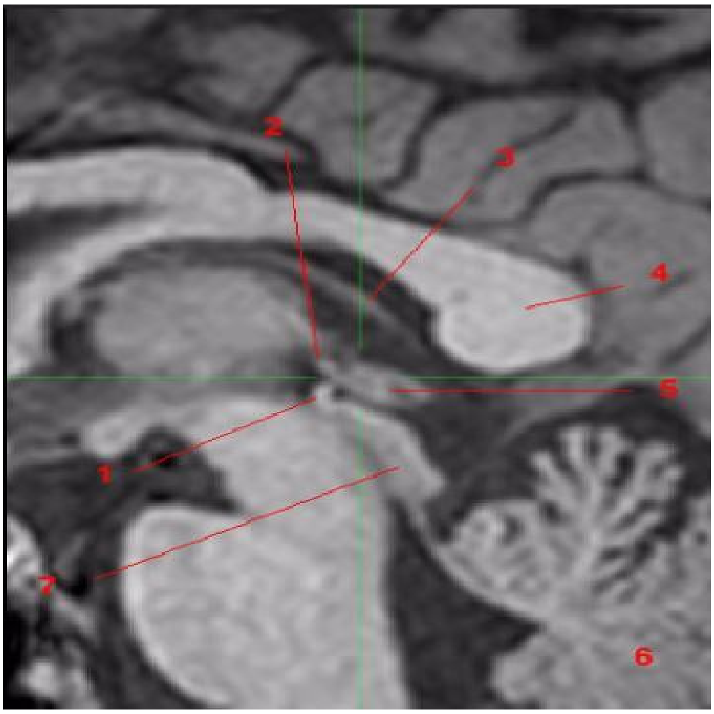

Fig (2-12): T1-weighted sagittal view.
Demonstrate (1, Posterior commissure. 2, Habenular commissure. 3, Internal cerebral vein. 4, Splenium, corpus callosum. 5, Pineal gland. 6,Cerebellum. 7, Tectum)(B. Sun, et al, 2009)

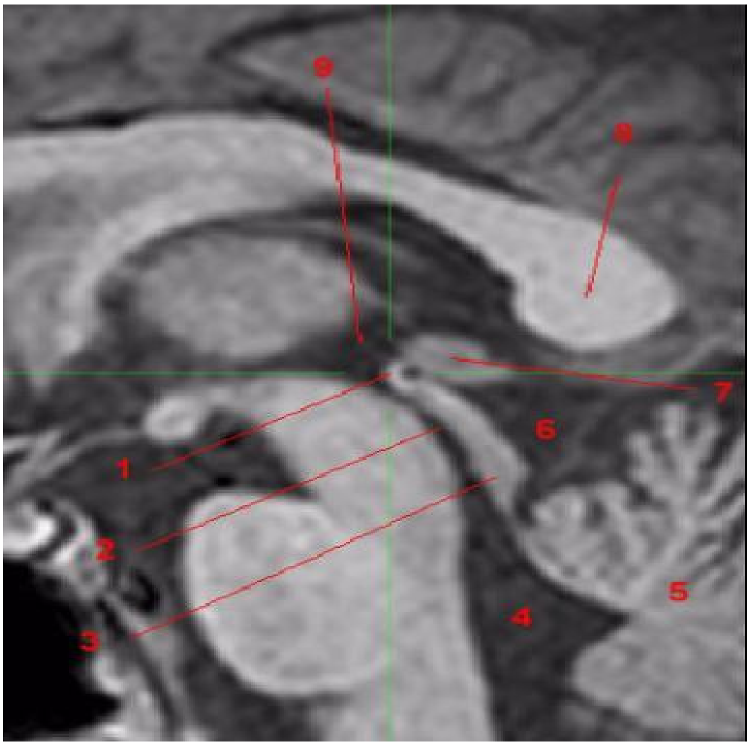

Fig (2-13): T1-weighted sagittal view.
Demonstrate (1, Posterior commissure. 2, Cerebral aqueduct (of Sylvius). 3, Tectum. 4, Fourth ventricle. 5, Cerebellum. 6, Quadrigeminal cistern. 7, Pineal gland. 8, Splenium, corpus callosum. 9, Third ventricle.) (B. Sun, et al, 2009)

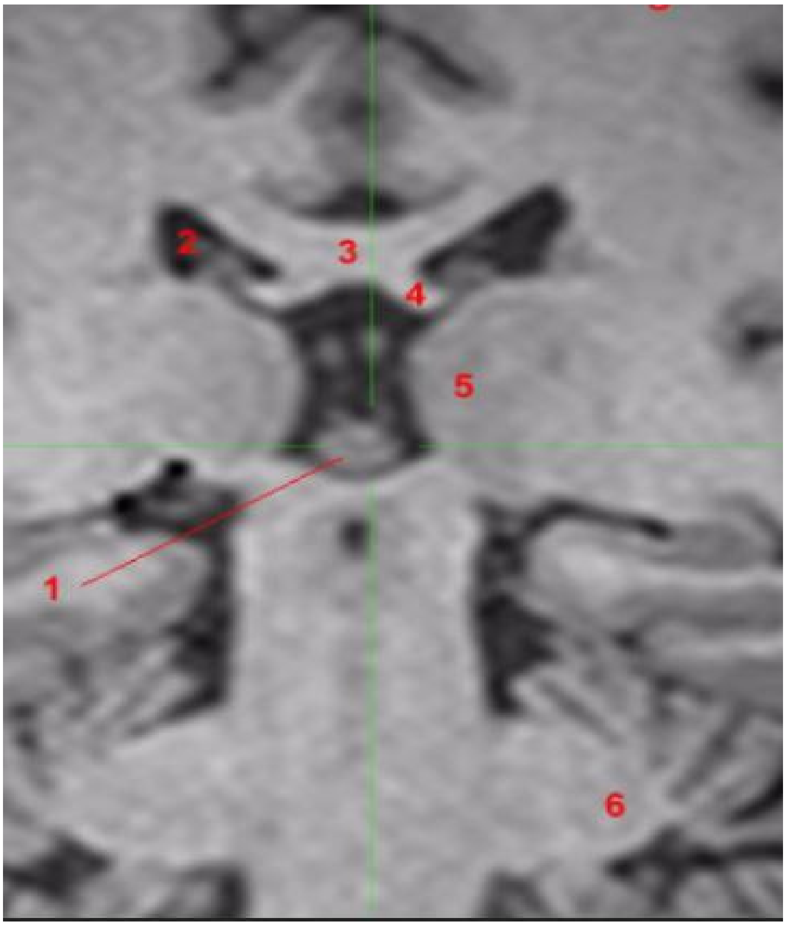

Fig (2-14):T1-weighted coronal view.

Demonstrate (1, Pineal gland. 2, Lateral ventricle. 3, Corpus callosum. 4, Fornix. 5, Thalamus. 6, Middle cerebellar peduncle)

(B. Sun, et al, 2009)

2.3 Volume Estimations:

2.3.1 Planimetry method:

This method estimate volume based on the Cavalieri principle From these, planimetry which involves manually tracing the boundaries of objects of interest on images of sections is the most commonly used technique for estimation of volume. (N. Acer et al, 2008)

2.3.2 Point-counting method:

The point-counting method uses a regular grid of test points. (B. Sahin et al, 2006). Its requires beginning from a uniform random starting within the sectioning interval, a structure of interest is exhaustively sectioned with a series of parallel plane probes a constant distant apart. An unbiased estimate of volume is obtained by multiplying the total area of all sections through the structure by sectioning interval t as follows:

$$estV = t \times (a1 + a2 + \cdots + an), \qquad \text{………}\textit{Equation (1)}$$

Wherea1, a2, . . . , an show the section areas and t is the sectioning interval (N. Roberts et al , 2000)(M. Garc´ıa-Finana et al ,2003).

2.3.3 Disk Summation Method:

The DSM, the measurement is dependent on the picture element (pixel-px), by counting the total number of px per unit area (only pineal area excluding the rest of FOV, and is represented in (px^2). Then the px are converted into units of area in (mm^2).that is done by multiplying the area in (px^2) by conversion constant(x) Then multiplying the product by slice thickness in (mm),which represents slice height an Z-axis ,and consequently the product is in unit volume (mm^3) for the single slice. (*Mazin. Abdullah et al* 2014). As shown in following equations:

- ***Px^2 (number of pixels)^2 x $(0.26)^2$=Area in $(mm)^2$………Equation (2)***
- ***Area$(mm)^2$ x slice thickness (mm) = volume $(mm)^3$………Equation (3)***
- ***Total volume of kidney = ∑slices volumes. ………Equation (4)***

2.3.4 Other Methods:

Some software about volumetric measurements has an ROI function such as DICOM viewer. Using planimetry or point-counting technique, we can also estimate the volume of any organ using these methods. .(Niyazi A, et al. 2012).

2.4 Feature Extraction:

The transformation of an image into its set of features is known as feature extraction. Useful features of the image are extracted from the image for classification purpose. It is a challenging task to extract good feature set for classification. There are many techniques for Feature extraction e.g. texture Features (Andrzej et al ,1998) (R. M. Haralick et al, 1973). Gabor features (Liu & Wechsler ,2002) feature based on wavelet transform(M. Kociołek et al ,2001) principal component analysis, minimum noise fraction transform, discriminates analysis, decision boundary feature extraction, non-parametric weighted feature extraction and spectral mixture analysis (D. LU & Q. WENG , 2007).

2.4.1 Texture Features:

The texture of an image region is determined by the waythe gray levels are distributed over the pixels in the region. Although there is no clear definition of "texture" inliterature, often it describes an image looks by fine orcoarse, smooth or irregular, homogeneous or inhomogeneous etc. The features are described to quantify properties of an image region by exploiting space relationsunderlying the gray-level distribution of a given image. (Namita Aggarwal, et al - 2012).

2.4.1.1 First Order Statistics:

First Order Statistics: FOS can be used as the most basic texture feature extraction methods, which arebased on the probability of pixel intensity values occurring in digital images. The parameters in the followingstatistical formulas are xi, the intensity value of pixel i, N, the total number of pixels, maxV , the maximum intensity value within a patch and Hi, the histogram of an image patch. (Mazin B. et al, 2018).

Mean: Calculates the mean intensity value of all pixels. The function μ= mean2(IP) can be used to compute this feature.

$$\mu = \frac{1}{N}\sum_{i=1}^{N} x_i$$

………Equation (5)

Standard Deviation:

The standard deviation of all the intensity values of a patch is used as a texture feature. The corresponding Matlab function is σ= std2 (IP).

$$\sigma = \sqrt{\frac{1}{N}\sum_{i=1}^{N}(x_i - \mu)^2}$$

………Equation (6)

Coefficient of variation:

The coefficient of variation can be seen as the relative standard deviation. It is calculated by dividing the standard deviation with the mean value.

$$c_v = \frac{\sigma}{\mu}$$

………Equation (7)

Entropy:

The entropy of a gray-scale image is a measure of intensity value randomness. It is calculated from the histogram counts of an image giving a probability p of certain pixel values occurring in the image.

$$s = -\sum(p. * log2(p))$$

………Equation (8)

Skewness:

Another statistical measure which is used for texture analysis is skewness. It measures the symmetry of a distribution curve of pixel intensity oc-currencesas seen in a histogram. The function ϒ1= skewness(IP) can beused to compute the skewness.

$$\gamma_1 = \frac{\frac{1}{N}\sum_{i=1}^{N}(x_i - \mu)^3}{(\frac{1}{N}\sum_{i=1}^{N}(x_i - \mu)^2)^{\frac{3}{2}}}$$

………Equation (9)

Kurtosis:

The kurtosis measures the atness of a histogram relative to a normal distribution.A curve has a high kurtosis

when it has a clear peak close to the mean value. The Matlab function for the kurtosis is ϒ2= kurtosis(IP).

$$\gamma_2 = \frac{\frac{1}{N}\sum_{i=1}^{N}(x_i - \mu)^4}{(\frac{1}{N}\sum_{i=1}^{N}(x_i - \mu)^2)^2} - 3$$

………Equation (10)

2.4.1.2 Second Order Statistics:

Also known as Co-occurrence matrix which is based features is local in nature. These features do not consider spatial information into consideration. So for this purpose gray-level spatial co-occurance matrix hd (i,j) based features are defined which are known as second order histogram based features. These features are based on the joint probability distribution of pairs of pixels. Distance d and angle θ within a given neighborhood are used for calculation of Joint probability distribution between pixels. Normally d=1, 2 and θ=0o, 45 o, 90 o, 135 o are used for calculation. Co-occurrence matrix calculation. Texture features can be described using this co-occurrence matrix. Following equations define these features. (Andrzej et al ,1998).

Angular second moment (Energy):

$$\sum_{i=0}^{G-1} \sum_{j=0}^{G-1} [p(i,j)]^2$$

.........Equation (11)

Correlations:

$$\sum_{i=0}^{G-1} \sum_{j=0}^{G-1} \frac{ij\, p(i,j) - \mu_x \mu_y}{\sigma_x \sigma_y}$$

.........Equation (12)

Inertia:

$$\sum_{i=0}^{G-1} \sum_{j=0}^{G-1} (i-j)^2\, p(i,j)$$

.........Equation (13)

Absolute value:

$$\sum_{i=0}^{G-1} \sum_{j=0}^{G-1} |i-j|\, p(i,j)$$ ....*Equation (14)*

Inverse Difference:

$$\sum_{i=0}^{G-1} \sum_{j=0}^{G-1} \frac{p(i,j)}{1+(i-j)^2}$$ ....*Equation (15)*

Entropy:

$$H = -\sum_{i=0}^{G-1} \sum_{j=0}^{G-1} p(i,j) \log_2[p(i)]$$ ....*Equation (16)*

Maximum:

$$\max_{i,j} p(i,j)$$ ....*Equation (17)*

2.4.1.3 Wavelet Transform:

Wavelets are mathematical functions that decompose data into different frequency components and then study each component with a resolution matched to its scale. Wavelet provides a more flexible way of analyzing both space and frequency contents by allowing the use of variable sized windows. Hence, Wavelet Transform provides better representation of an image for feature extraction (S. G. Mallat at el, 1980).

The Continuous Wavelet Transform (CWT) of a signal x(t) is calculated by continuously shifting a scalable Wavelet function ψ and is defined as :

$$W(s,\tau) = \int_{-\infty}^{\infty} x(t) \frac{1}{|s|^{1/2}} \psi^{*}\left(\frac{t-\tau}{s}\right) dt$$

.... Equation (18)

Where s and τ are scale and translation coefficients respectively. Discrete Wavelet Transform (DWT) is derived from CWT which is suitable for the analysis of images. Its advantage is that discrete set of scales and shifts are used which provides sufficient information and offers high reduction in computation time (S. G. Mallat at el, 1980). The scale parameter (s) is discredited on a logarithmic grid. The translation parameter (τ) is then discredited with respect to the scale parameter. The discredited scale and translation parameters are given by, s = 2–m and, where m and n are positive integers. Thus, the family of wavelet functions is represented by:

$$\psi_{m,n}(t) = 2^{m/2} \psi\left(2^{m} t - n\right)$$

...........Equation (19)

The DWT decomposes a signal x[n] into an approximation (low-frequency) components and detail (high frequency) components using wavelet function and scaling functions to perform multi-resolution analysis, and is given as (S. G. Mallat at el, 1980).

$$x[n]=\begin{cases}\sum_{i=1 to I}\sum_{k\in Z}c_{i,k}\ g\left[n-2^{i}k\right] \\ \quad +\sum_{k\in Z}d_{I,k}\ h_{I}\left[n-2^{I}k\right]\end{cases}$$

………..Equation (20)

where ci,k, $i = 1\ \Lambda I$ are wavelet coefficients and di,k , $i = 1\ \Lambda I$ are scaling coefficients.

The figure below shows the process of an image I being decomposed into approximate and detailed components up to level 3. As the level of decomposition is increased, compact but coarser approximation of the image is obtained. Thus, wavelets provide a simple hierarchical framework for better interpretation of the image information (J. Koenderink , 1984).

Mother wavelet is the compressed and localized basis of a wavelet transform. (S. Chaplot et al , 2006) Employedlevel 2 decomposition on MRI brain images using Daubechies-4 mother wavelet an constructed 4761 dimensional feature vector from approximation part for the classification of two types of MRI brain images i.e. image from AD patients and normal person (E.-S. A. Dahshan at el, 2010) pointed out that the number of features extracted using Daubechies-4 wavelet were too large and may not be suitable for the classification. In their proposed method, they extracted 1024 features using level 3 decomposition of image using HAAR Wavelet and further reduced features using PCA. Though PCA reduce the dimension of feature vector, but it has following disadvantages: 1)

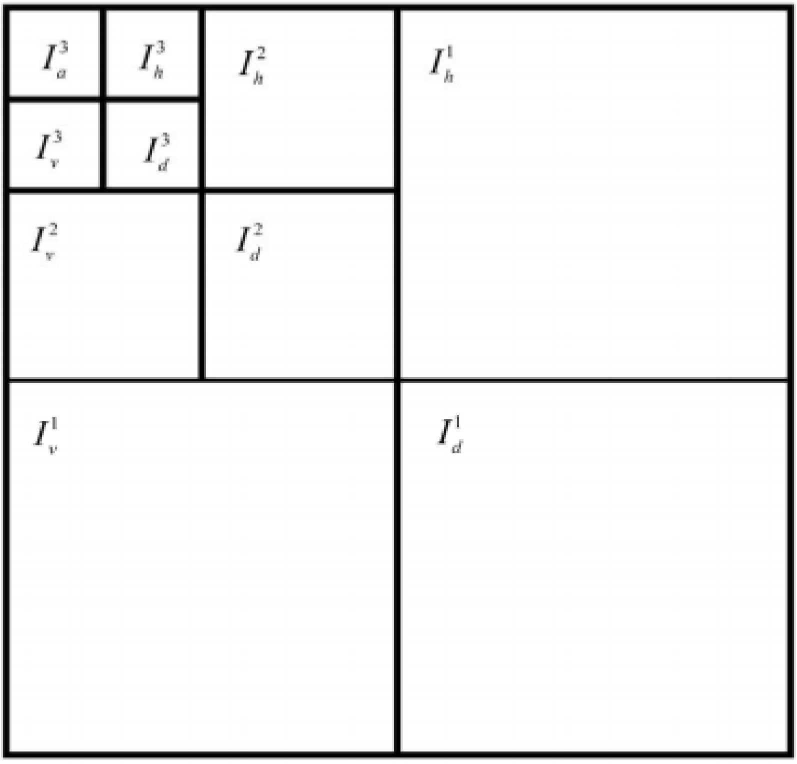

Fig (2-15):Pyramidal structure of DWT up to level 3.
(Namita Aggarwal at el , 2012)

2.5 Previous Study:

There have been a few studies about pineal volume estimation using different methods such as elliptic approaches and ROI on MRI as noted in (G. Bersani, et al, 2002)(B. Sun, et al ,2009).

Although many studies have estimated the pineal gland volume using different techniques such as study done by .(Niyazi A, et al. 2012) which was determined the pineal gland volume using stereological methods and by the region of interest (ROI) on MRI. In this study the pineal gland volumes were calculated in a total of 62 subjects (36 females, 26 males) who were free of any pineal lesions or tumors. The mean ± SD pineal gland volumes of the point-counting, planimetry, and ROI groups were 99.55 ± 51.34, 102.69 ± 40.39, and 104.33 ± 40.45 mm3, respectively. No significant difference was found among the methods of calculating pineal gland volume (P> 0.05). From these results, it can be concluded that each technique is an unbiased, efficient, and reliable method, ideally suitable for in vivo examination of MRI data for pineal gland volume estimation.

(M. Sumida et al , 1996) concern to measure the development of human pineal gland by use MRI The size of the pineal gland was significantly smaller in patients younger than 2 years old than in older patients. The size of the pineal gland increased until 2 years of age and remained stationary between the ages of 2 and 20 years. We found a large variation in size among all age groups. No difference in size was noted between males and females. This study establishes norms for pineal gland size in infants younger than 2 years old and in children and adolescents 2 to 20 years old as detected with MR imaging. Knowledge of the size of thenormal pineal gland is important in the detection of abnormalities of the pineal gland, particularly neoplasms.

Some previous studies have looked for the mystery gland and its relationship with variables in humans. One of these studies was undertaken to evaluate the variations in appearance of the normal pineal gland. The findings of 1000 consecutive MR imaging examinations obtained at 0.5 T were studied. The age of the patients ranged from 1 day to 83 years, and findings in children and adults were compared. In all age groups the pineal gland appeared mainly in three forms: (1) nodule-like, (2) crescent-like and (3) ring-like. Overall prevalences of these forms were 52%, 26% and 22%, respectively. Apparent differences in frequencies were evident in children and adults with respect to the crescent- and ring-like types. Cystic form pineal lesions 5 mm or larger in one diameter (anteroposterior, sagittal or transverse) were taken to be true pineal cysts, when compared with the gland's ring-like appearance (less than 5 mm). Pineal cysts had a prevalence of 0.6% in children and 2.6% in adults. No symptomatic pineal cyst with mass effect on the lamina tecti was detected in the series. Besides identifying the three anatomical types of the pineal gland as seen on MR imaging and addressing the potential significance of differences in their frequencies in children and adults, the author tries to explain the previous discrepancy between the MR imaging and autopsy series findings with respect to frequencies of the pineal cysts

(Pediatr Radiol , 1996)

Also (AFROZ.H, et al, 2014) created A descriptive study in the Department of Anatomy to see the morphological shape of the human pineal gland.the result pea-shaped pineal glands were found 60% in group A, 30% in group B, 5% in both group C and D, while pine cone shaped were found 25% in group A, 37.5% in group B, 25% in group C and 12.5% in group D. Besides, fusiform shaped glands were found 18.2% in group A, 63.6% in group B, 9.1% in both group C and D, where as piriform shaped found 66.7% in group B, and 16.7% in both group C and D. Moreover, cone-shaped glands were found 28.6% in group B, 57.1% in group C and 14.3% in group D.

(Qurat-Ul-Ain et al-2014) extracted texture feature from brain MR images. Second phase classify brain images on the bases of these texture feature using ensemble base classifier. After classification tumor region is extracted from those images which are classified as malignant using twostage segmentation process. Segmentation consists of skull removal and tumor extraction phases. Quantitative results show that our proposed system performed very efficiently and accurately. We achieved accuracy of classification beyond 99%. Segmentation results also show that brain tumor region is extracted quite accurately.

Chapter Three:

Material and Methods :

3.1 Materials:

3.1.1 MRI Machine and Selective protocol:

MRI machine Toshiba ™ 1.5 T as used at Al-Mouleem Hospital, the sequence was: Ultrafast Gradient Echo 3D with preparation Pulse T1W (3D-FEE) SENSE + head Coil; Specific Absorption Rate =0.3199, Flip Angle 30 degree,ETL=1 Echo No.=1 , Slice Thickness =1.6mm, Gap BetweenSlice = 50%(0.80)mm.TR=0.8ms / TE = 2.6ms.Matrix 256 px X 256px.

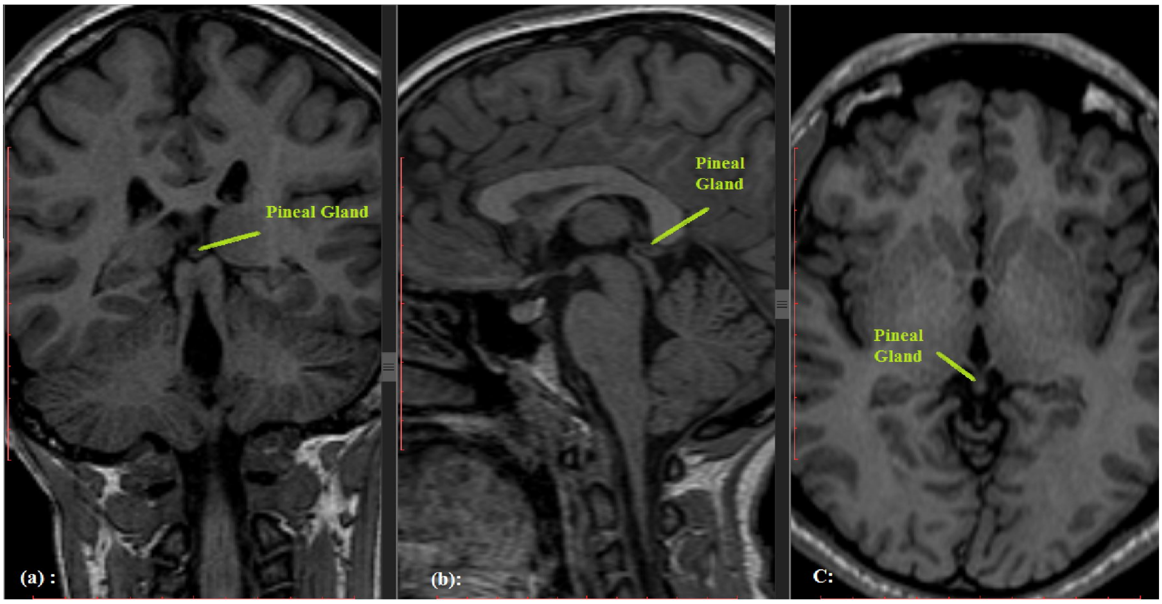

Fig (3-1):MRI brain scan 3D-T1 W with Axial, sagittal and coronal demonstrates pineal gland.

3.1.2 Software:

- Interactive Data Language (IDL 6.1) program as platform for the generated codes.
- - RadioAnt DICOM Version 5.1 64 bit use to reformatting images.
- SPSS® to Statistical analysis.

3.2 Methods:

3.2.1 Study Design:

This study adept analytic cross-sectional design focuses on measure the volume of pineal gland and describes shape using MR images.

3.2.2 Study Period and Area:

Thisstudy was conducted fromAugust 2016 to 2018 at Khartoum state Al-Moalum hospital.

3.2.3 Study Population:

Patients who had undergone 3D-T1 Brian MRI Scan were obtaining for study purpose.

3.2.4 Study Sampling and sample size:

159 consecutive Patients (male=93, Female 66) their ages were between (19-31) years. Excluded Patients were those who had mid brain & endocrine diseases. Detailed Demographic Information of

Population including; age, gender, weight, height, and BMI was recorded.

3.3 Volume estimation method:

The Disk Summation Method (DSM) used to measure the normal pineal gland in normal individuals. In DSM the measurement is dependent on the picture element (pixel-px), by counting the total number of pxs per Area (ROIs which the pineal gland appear excluding the rest of FOV) and is representing in (px)2. Than the (px)2 were converted into units of Area in (mm)2.that was done by multiplying the (px)2 by conversion factor. Than multiplying the product by slice thickness in (mm), which represents slice height an Z-axis, and consequently the product is unit of volume (mm)3 for single slice. Than dividing the value in $(mm)^3$ over 1000 to convert to $(cm)^3$.This step above was applied to each separate slice to final the total volume of pineal gland. As shown in following equations:

A $(mm)^2$=px^2(Number of pixel with ROIs) X convert factor…..Equation (21)

Volume in $(cm)^3$= A$(mm)^2$X Slice Thickness (mm)/1000. .   …..Equation (22)

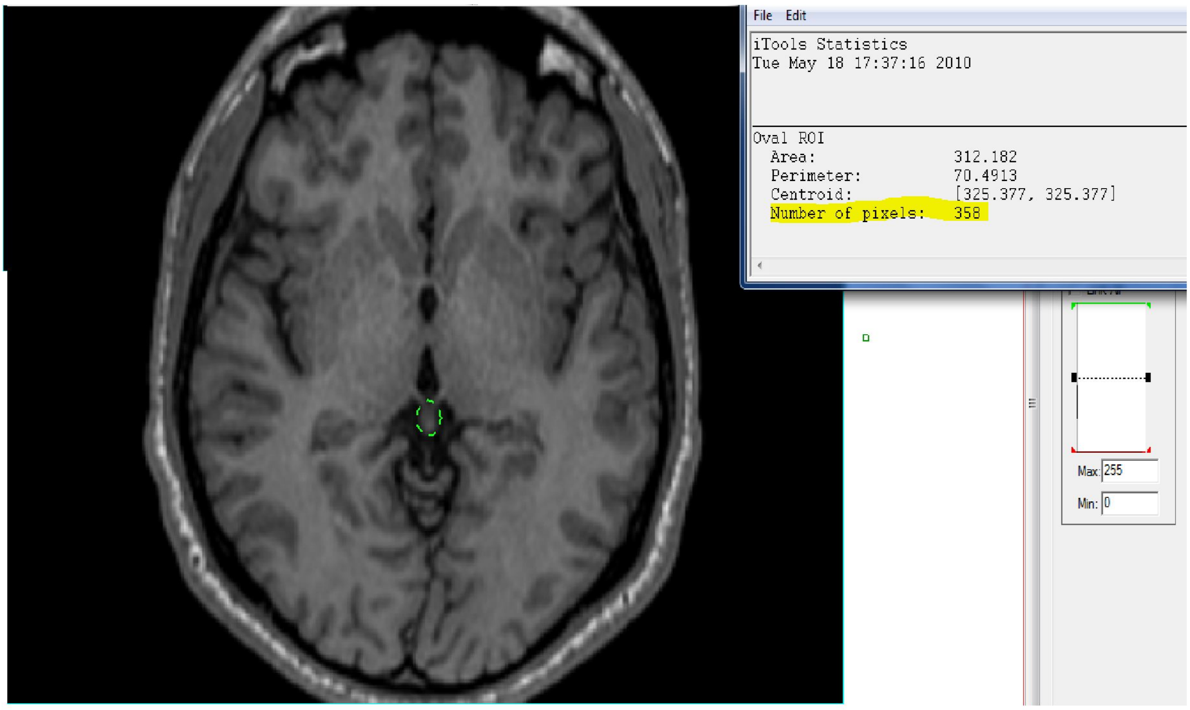

Fig (3-2):MRI 3D-T1 W with Axial demonstrates pineal gland method of contouring and pixel accounting polygon**.**

3.4 Shape evaluation method:

The pineal gland shape was evaluated in Axial & Sagittal image plane for ALL including patients. The shape describe as pear shape: tapered at the top and wider at bottom, fusiform shape: like spindle wider in the middle and tapering lowered the ends. And cone shape: smoothly from a flat base to appoint called apex or vertex.

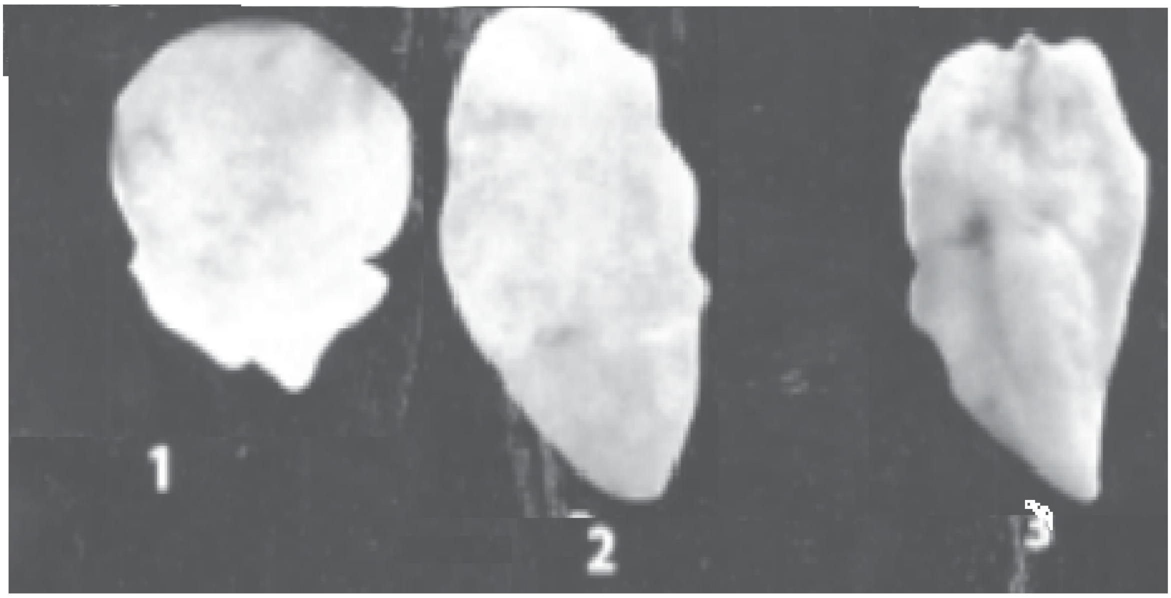

Fig (3-3): Different shapes of the pineal gland seen through magnifying glass (1. pea shaped, 2.fusiform shaped, and 3. cone shaped**.**

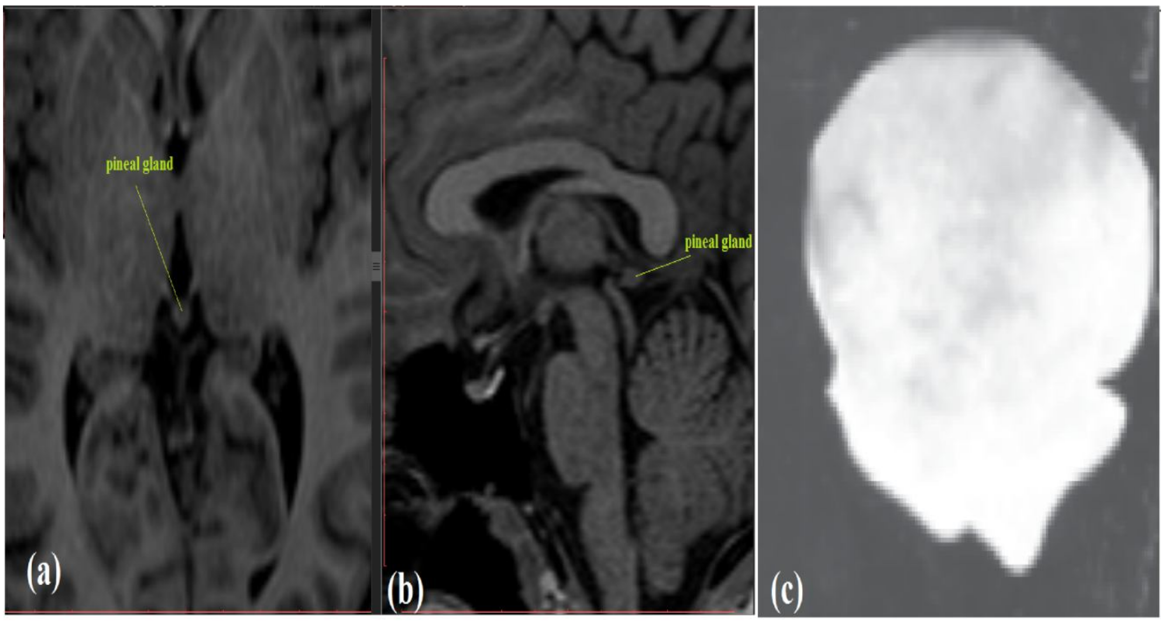

Fig (3-4): The Axial (a) and Sagittal (b) MRI showed the Pear shape(c) of pineal gland

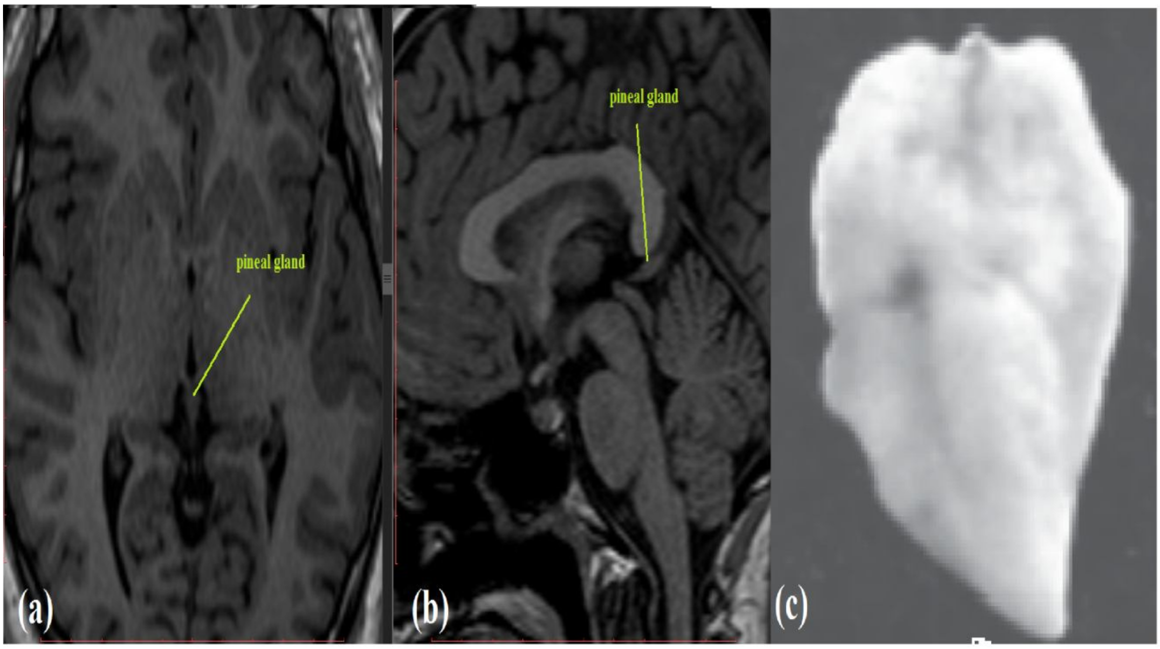

Fig (3-5): The Axial (a) and Sagittal (b) MRI showed the cone-shape(c) of pineal gland**.**

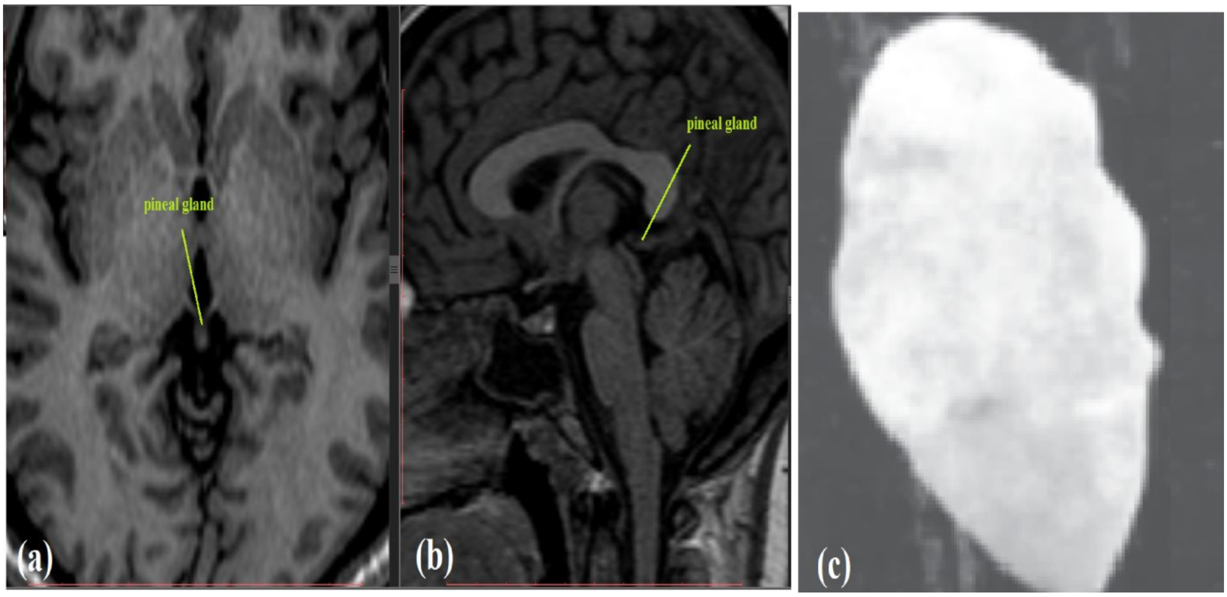

Fig (3-6): The Axial (a) and Sagittal (b) MRI showed the fusiform shape(c) of pineal gland.

3.5 Statistical Methods:

First Order Statistics: FOS can be used as the most basic texture feature extraction methods, which are based on the probability of pixel intensity values occurring in digital images (ROIs). The parameters in the following statistical formulas are xi, the intensity value of pixel I, N, the total number of pixels, maxV , the maximum intensity value within a patch and Hi, the histogram of an image patch.

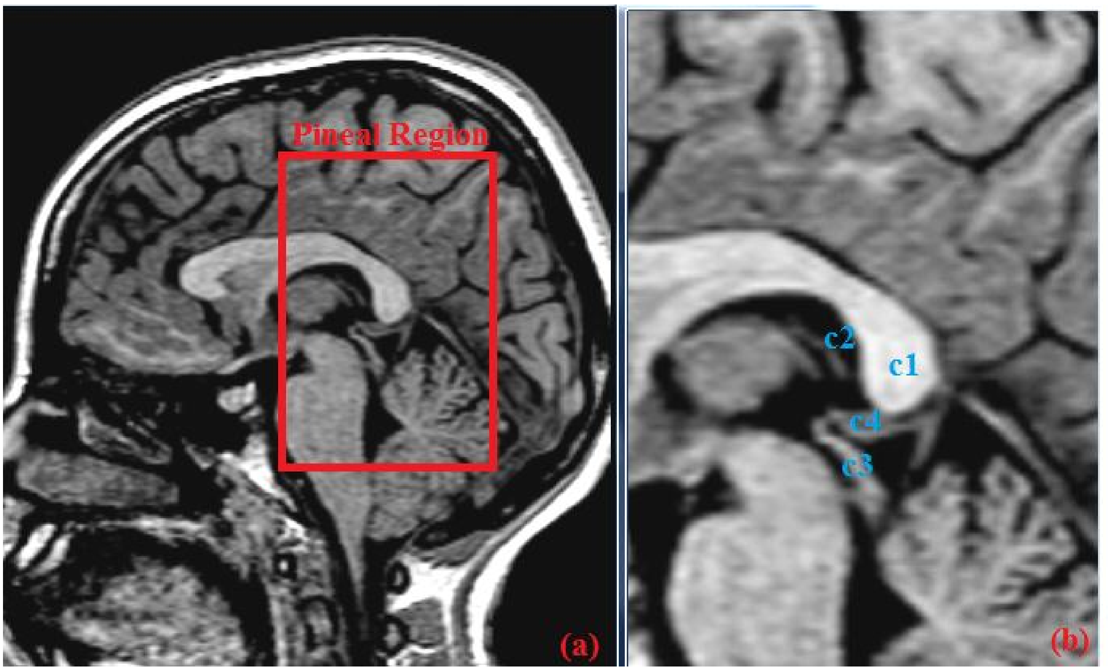

Fig (3-7):(a) T_1-Weighted Image sagittal for pineal Region, (b) class of pineal region (class 1) Splenium of corpus callosum ,(class 2) Third ventricle, (class 3) Tectum and Pineal Gland .

3.6 Data Analysis:

Variables including height; which was measured in (cm) weight in (Kg), Age (yrs), and gender (Male and Female) were evaluated, for measuring dependent variable Body Mass Index (BMI) Calculate by use:

$$BMI= weight / (height)^2 X\ 100 \ldots\ldots\ldots\ldots Equation\ (23)$$

Statistical package for the social sciences, SPSS version 20 from IBM was used to analyze the data. Data were expressed as means± standard deviation. Statistical differences between the groups were evaluated by independent sample t test and linear discriminate .Differences yielding P-values <0.05 were considered statistically significant. Along with used of Microsoft Excel 2007 to draw plot of linear regression and formula.

3.7 Ethical Consideration:

The ethical approval obtained from of Sudan university research committee council all the analytic procedures were conducted with follow the guidance of institutional patient care.

Summary:

In order to characterize the pineal gland use Magnetic Resonance Imaging by Disk summation method and texture analysis as described for result.

Chapter Four

Results:

This study adept analytic cross-sectional design focuses on measure the volume of pineal gland describes it shape and features extraction for pineal region using MR images. Statistical analyses of data were performed using Excel Microsoft 2007 Data were expressed as means± standard deviation. Statistical differences between the groups were evaluated by independent sample ***t*** test and linear discriminate. Differences yielding P-values <0.05 were considered statistically significant. The data present as tables and figures.

4.1 For the Volume Estimation and shape Description:

	Mean	Median	STD	Min	Max
Age	24.98	25	2.92	19	31
High	177.98	177	8.63	159	195
Weight	69.71	70	9.41	51	93
BMI	21.89	22	1.42	19	25
Volume	0.136	0.136	0.007	0.123	0.159

Table (4-1): Statistical descriptive for all patients.

	Gender	Mean	Std. Deviation	Std. Error Mean
Age	Female	23.48	2.731	.341
	Male	25.96	2.589	.267
BMI	Female	21.36	1.384	.173
	Male	22.27	1.321	.136
Volume cm^3	Female	.134672	.0063130	.0007891
	Male	.137690	.0064676	.0006671

Table (4-2): Show correlates the gender with pineal gland volume and patients information

		Sum of Squares	Mean Square	F	Sig.
BMI	Between Groups	82.635	6.357	3.917	.000
	Within Groups	235.327	1.623		
	Total	317.962			
Age	Between Groups	.001	.000	1.876	.037
	Within Groups	.006	.000		
	Total	.007			

Table (4-3): Shown the ANOVA test of Age and BMI with volume of pineal gland.

Shapes	*Cases*	*Percentage %*
Pear Shape	22	13.8
Fusiform Shape	61	38.4
Cone Shape	76	47.8
Total	***159***	***100***

Table (4-4): Show frequency and percentage distribution of shape of pineal gland.

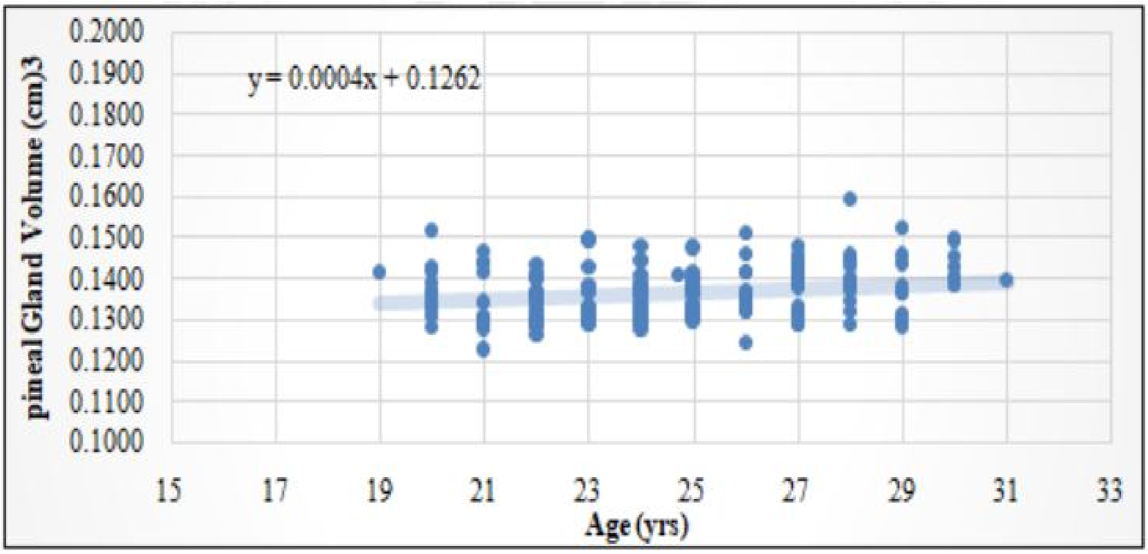

Fig (4-1): Scatter plot Show correlate between the pineal gland volumes with patient's Ages.

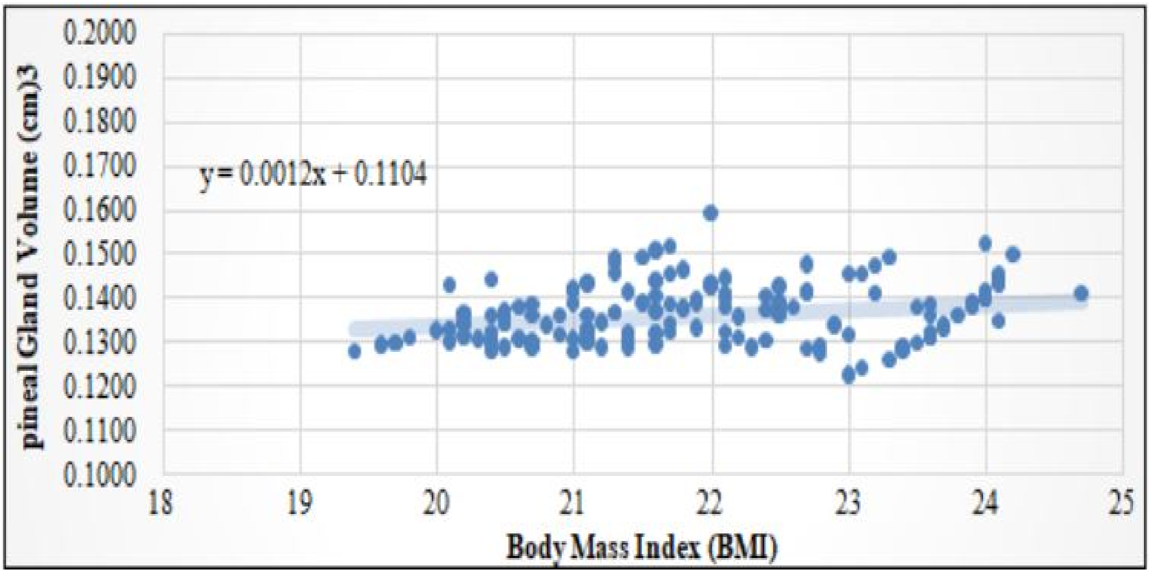

Fig (4-2): Scatter plot Show correlate between pineal gland volumes with body mass index.

4.2 pineal gland Region classification:

features extracted from MRI using First order statistic and All these features were calculated for all images and then the data were ready for discrimination which was performed using step-wise technique in order to select the most significant feature that can be used to classify the MR brain imaging for Pineal Gland and the results show that:

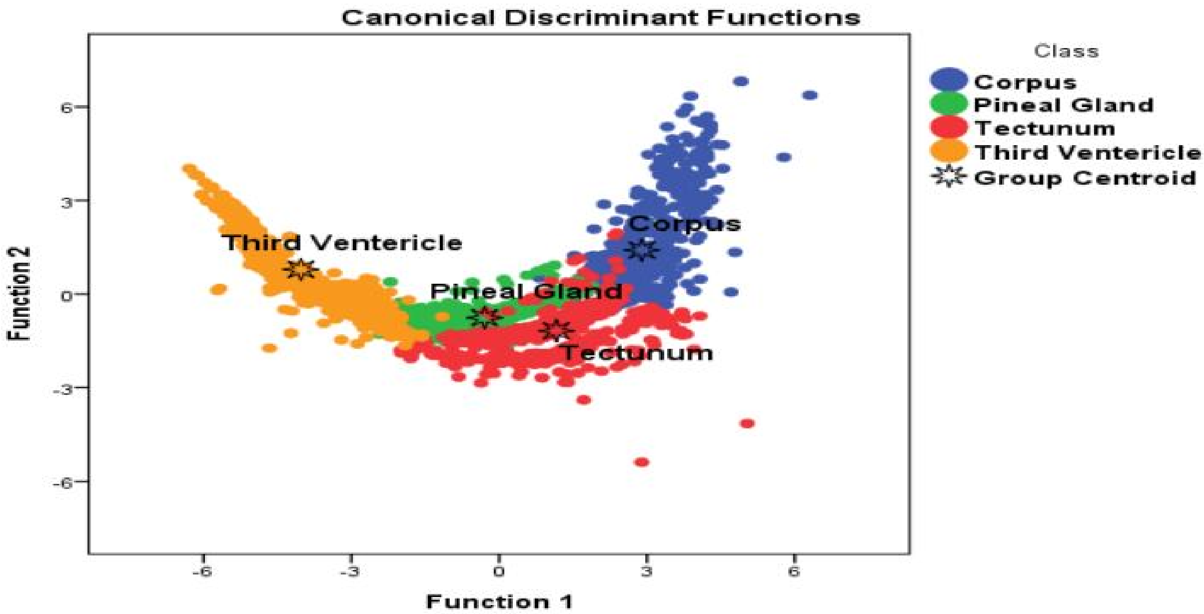

Fig (4-3): Scatter plot Show classification Map that created using linear discriminate analysis function.

Classes		*Predicted Group Membership*				*Total*
		Corpus	*Pineal Gland*	*Tectunum*	*Third Ventericle*	
Original	Corpus	93.3	2.8	4.0	.0	100.0
	Pineal Gland	.8	97.9	1.3	.0	100.0
	Tectunum	1.9	8.3	89.9	.0	100.0
	Third Ventricle	.0	10.7	.8	88.5	100.0

92.7% of original grouped cases correctly classified.

Table (4-5):show classification score matrix generated by linear discriminate analysis**.**

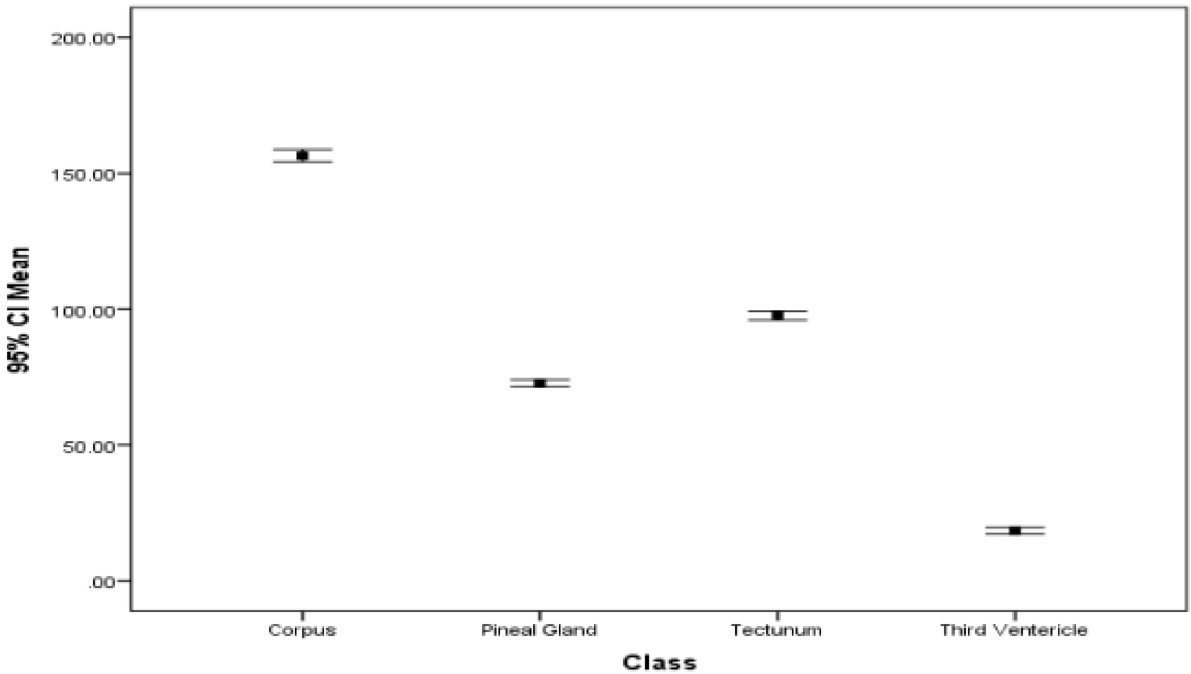

Fig (4-4):show error bar plot for the *CI mean* textural features that selected by the linear stepwise discriminate function as a discriminate feature where it discriminates between all features.

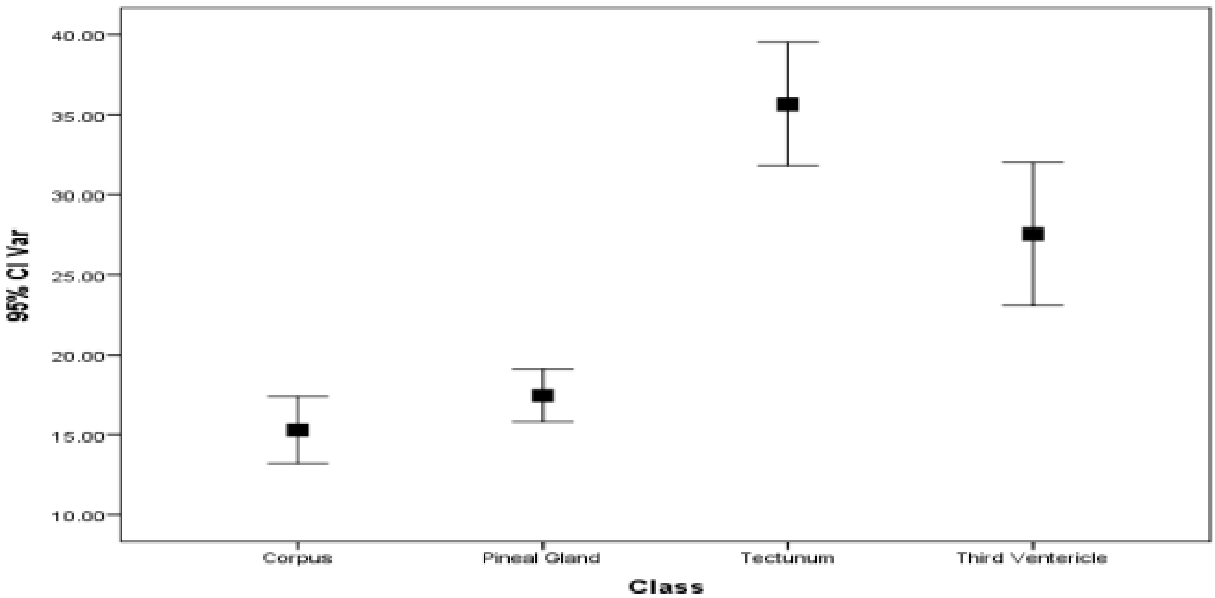

Fig (4-5):show error bar plot for the *variance* textural features that selected by the linear stepwise discriminate function as a discriminate feature where it discriminates between all features.

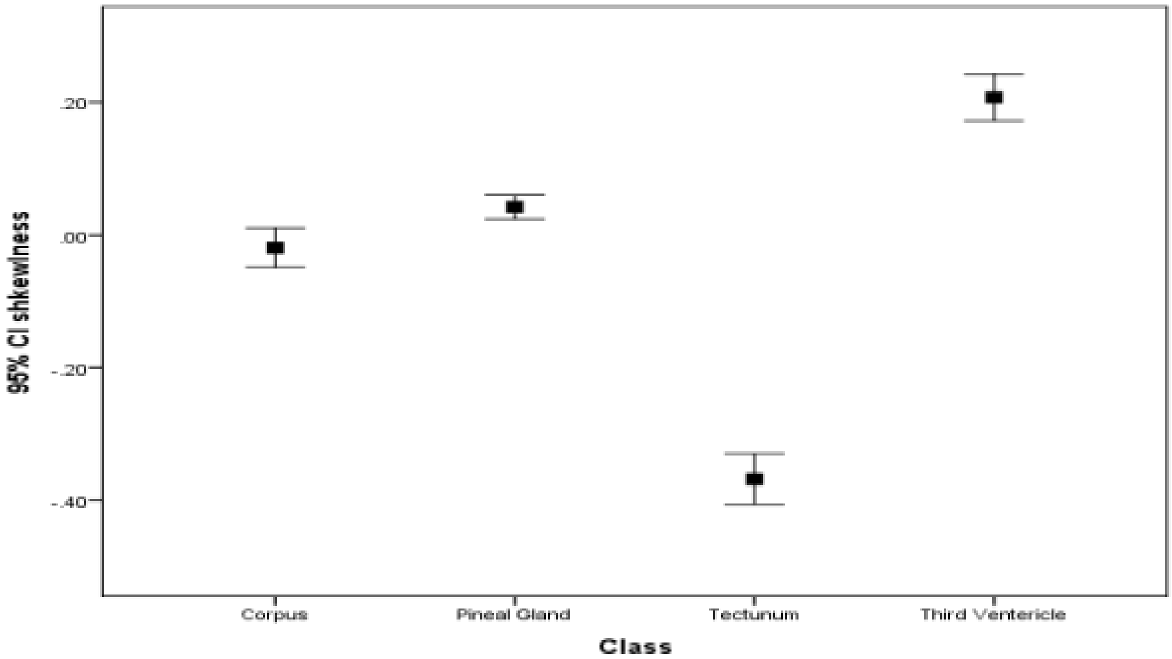

Fig (4-6):show error bar plot for the *shkewness* textural features that selected by the linear stepwise discriminate function as a discriminate feature where it discriminates between all features.

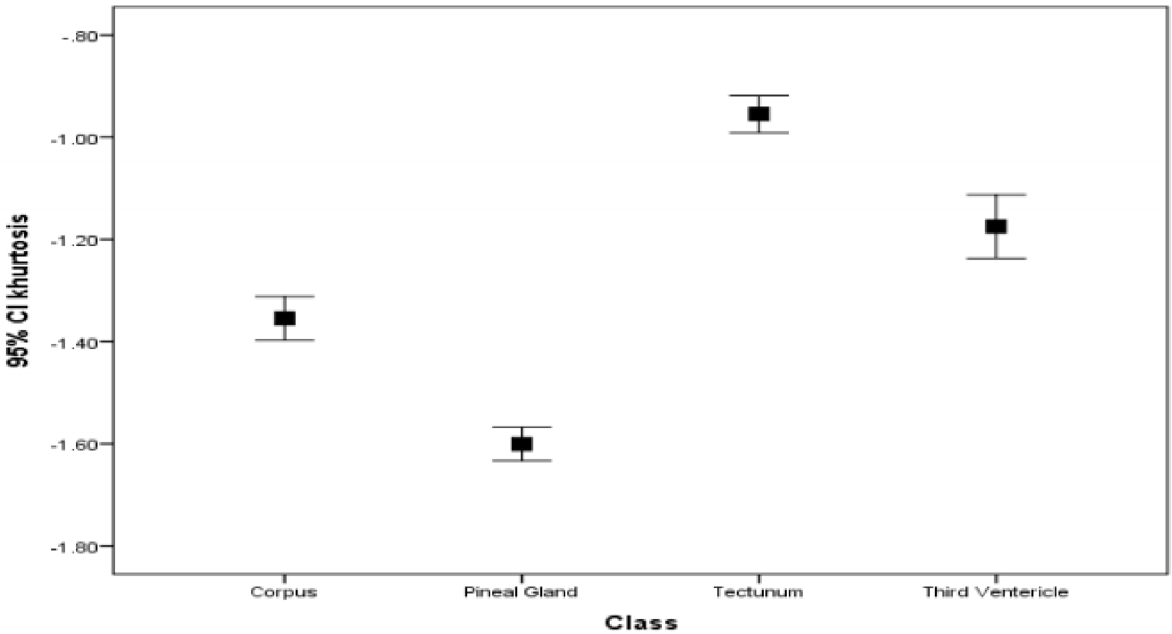

Fig (4-7):show error bar plot for the *Khurtosis* textural features that selected by the linear stepwise discriminate function as a discriminate feature where it discriminates between all features.

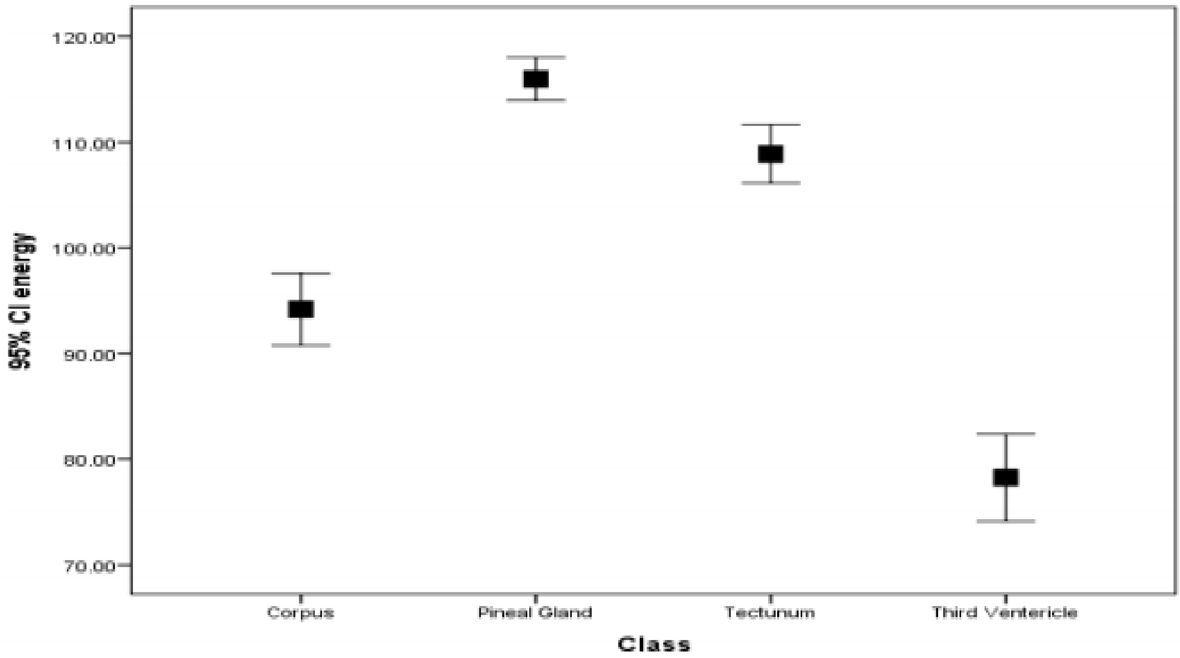

Fig (4-8):show error bar plot for the *Energy* textural features that selected by the linear stepwise discriminate function as a discriminate feature where it discriminates between all features.

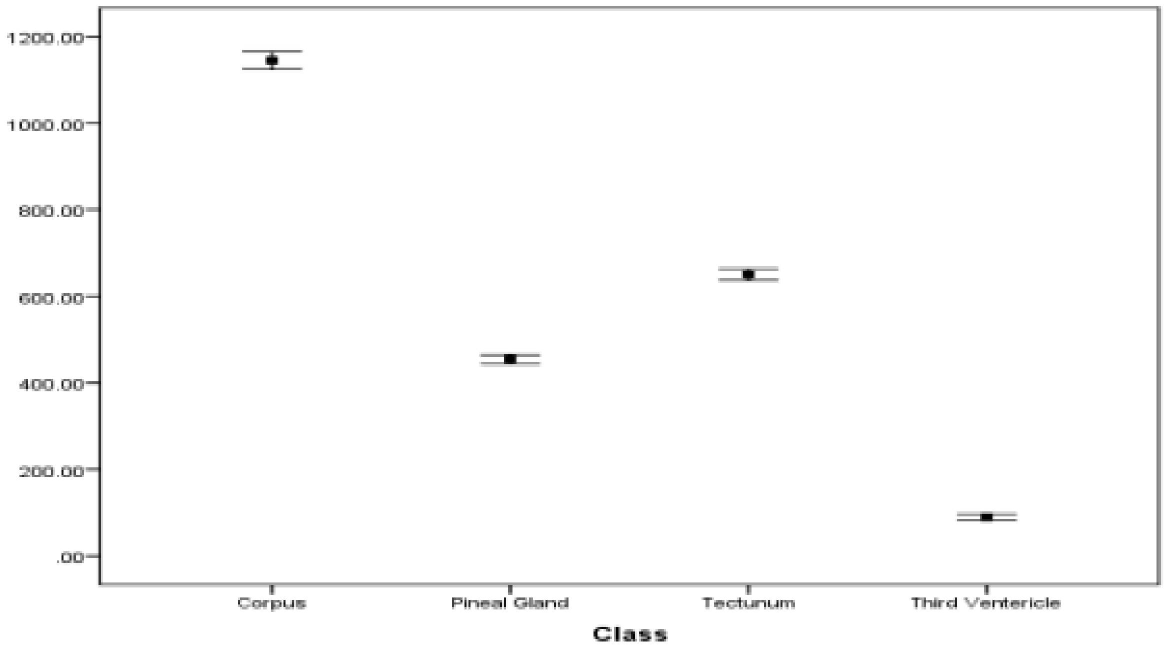

Fig (4-9):show error bar plot for the *Entropy* textural features that selected by the linear stepwise discriminate function as a discriminate feature where it discriminates between all features.

Chapter Five:
Discussion, Conclusions and Recommendation:

5.1 Discussion:

In present study, established the volume of the pineal gland and it shapes in normal Sudanese adult using Magnetic Resonance Imaging.159 consecutive patients scanned for Brian with MRI to pineal region by use MRI machine 1.5 T the sequence was 3D-T1.The classification processes of MRI brain were defining the corpus; pineal gland, Tectum, and third ventricle were carried out using Interactive Data Language (IDL) program as platform for the generated codes.

Table (4-1) shows statistical description for demographic information and volume for all patients as mean, median, standard deviation, minimum and maximum. For the age the mean ± standard deviation was 24.98±2.92, for patients high, weight, body mass index and the Pineal Gland volume was 177.98±8.63 cm, 69.71±9.1 kg, 21.89±1.42 kg/cm2 and 0.136±0.007 cm3 respectively. Also in Table (4-2) the correlates the gender with pineal gland volume and patients information Presented compare the gender with pineal gland volume and patient's information for the age the mean of female was 23.48 years and for male 25.96 years, the body mass index and the pineal gland volume shows slightly difference between the gender were the female 21.36 $kg/cm^2$and the male 22.27 kg/cm^2, the pineal gland volume for female 0.1 35 cm^3 and for male 0.137 cm^3.Table (4-3) Shown the ANOVA test of Age and BMI with volume of pineal gland. Volumes with age were the *p*.value show there is significant difference between the body mass index and the pineal gland volume with age.Table (4-4) The distribution of shape of pineal gland showed three different shape pear, fusiform and cone shape were the pear shape found in 22 case with percentage 13.8%, the fusiform shape found in 61 case with percentage 38.4% and the cone shape in 76 case with percentage 47.8%. **Fig (4-1)** show correlate between the pineal gland volume with patients age, and found that the volume increase with rate 0.0004 for each year.Fig (4-2) show correlate between pineal gland volumes with body mass index were the volume was increase with rate 0.0012 for each (kg/cm2) unit from body mass index.

Some studies have found correlation between pineal volume and age (B. Sun et al 2009).in this study showed a significant difference between the Age and Pineal gland volume ($P>0.037$).Also the results of (Niyazi Acer et al 2011) determined significant correlations between pineal volume and age. (B. Sun et al -2009) was reported that pineal volume was 94.2 ± 40.65 mm3 in healthy young adults, (Nolte et al 2009) found that the pineal gland volume was 125 ± 54 mm3. (G.Bersani et al 2002) reported the pineal volume was 64.05 ± 20.69 mm3 for schizophrenics and 74.62 ± 33.53 mm3 for controls. In the present study, the mean ± S.D pineal gland volumes for Disk Summation Method were found to be 0.1364 ± 0.00655 cm3. From the present study notice the volume was higher than (Nolte et al-2009, B. Sun et al -2009 and G. Bersani et al-2002) and this difference comes from the measurement methods for each studies.

For the pineal gland shape (Kelly.W et al 1984) the pineal gland is cone-shape while (Berkovitz1988) and (Rogers et al 1992) found it as fusiform and pea shapes respectively.

For classify the MR brain imaging for Pineal Gland and the results show that: Fig (4-3) Scatter plot generated using discriminate analysis function for Four classes represents: Corpus, pineal gland, Tectum, third ventricle the classification showed that the pineal gland were classified well from the rest of the tissues although it has characteristics mostly similar to surrounding tissue. Table (4-5) show classification score matrix generated by linear discriminate analysis and the overall classification accuracy of corpus 93.3%, were the classification accuracy of pineal gland 97.9%, Tectum 89.9%, While the third ventricle showed a classification accuracy 88.5%.

Figures (4, 5,6,7,8 and 9-4) show error bar plot for the ALL texture features that selected by the linear stepwise discriminate function as a discriminate feature where it discriminates between all features. From the discriminate power point of view in respect to the applied features the ALL texture features can differentiate between all the classes successfully.

5.2 Conclusions:

Estimation of volume and shape of the pineal gland in normal adults, were the pineal gland volume shows slightly difference between the gender were the female 0.135±0.0063 cm3 and for the male 0.137±0.0063 cm3, using ANOVA test for the age with body mass index BMI and the pineal gland volume were the p. value show there is Significant difference between the body mass index 0.000 and pineal gland volume 0.037 with age.

The distribution of shape of pineal gland showed three different shape pears, fusiform and cone shape were the pear shape found in 22 cases with percentage 13.8%, the fusiform shape found in 61 cases with percentage 38.4% and the cone shape in 76 cases With percentage 47.8%.

The pineal gland volume can be estimated using the following linear equations: Equation for the regression values between pineal gland volume and patients age and body mass index:

Pineal Gland Volume cm^3= 0.0004 (Age/ys) + 0.1262 …Equation (24)

Pineal Gland Volume cm^3= 0.0012 (BMI) + 0.1104 ……Equation (25)

The classification processes of MRI brain were defining the corpus; pineal gland, Tectum, and third ventricle were carried out using Interactive Data Language (IDL) program as platform for the generated codes.

The result of the classification showed that the pineal gland areas were classified well from the rest of the tissues although it has characteristics mostly similar to surrounding tissue.

Several texture features are introduced from FOS and the classification score matrix generated by linear discriminate analysis and the overall classification accuracy was 92.7%, were the classification accuracy of Corpus 93.3%, pineal gland 97.9%, Tectum 89.9%, while the third ventricle showed classification accuracy 88.5%.

Using linear discrimination analysis generated a classification function which can be used to classify other image into the mention classes as using the following multi-regression equation:

- ***Corpus = (Mean + 2.233) * variance + (-0.046) *(Skewness + 1.398) * (kurtosis + 0.203) * (energy + (-0.013)) * entropy + (-0.239)) -38.185 ………Equation (26)***

- ***Pineal Gland = (Mean + 2.123) * variance + (-0.033) *(Skewness + 1.584) * (kurtosis + (-0.977)) * (energy +0.011) * entropy + (-0.247)) -23.713 ……… Equation (27)***

- ***Tectum = (Mean + 2.453) * variance + (-0.023) *(Skewness + (-1.520) * (kurtosis + 2.021) * (energy +0.001) * entropy + (-0.281)) - 28.785 ……….Equation (28)***

- ***Third Ventricle = (Mean + 0.687) * variance + (-0.003) *(Skewness + 2.124) * (kurtosis + (-2.148)) * (energy +0.023) * entropy + (-0.083)) -6.36 ………Equation (29)***

5.3 Recommendations:

In this study was investigated features based on First Order Statistics the classification accuracy may difference when use Second Order or wavelet-based feature extraction technique.

The performance of our proposed approach can be evaluated on other disease MRI images to evaluate its efficacy. The researcher also explore some feature extraction/construction techniques which provide invariant and minimal number of relevant features to distinguish two or more different kinds of MRI.

Reference:

A. E. Burgess, “Comparison of receiver operating characteristic and forced choice observer performance measurement methods,” *Medical Physics*, vol. 22, pp. 643-655, 1995

A. Materka and M. Strzeleck, (1998). “Texture Analysis Methods —A Review,” Institute of Electronics, Technical University of Lodz, Brussels. , COST B11 report.

AFROZ.H, NURUNN.ABI ASM et al (2014)"Different Shapes of the Human Pineal Gland "– A Study On 60 Autopsy Cases: J Dhaka Med Coll. 23(2): 211-214.

B. Sahin and H. Ergur, (2006) “Assessment of the optimum section thickness for the estimation of liver volume using magnetic resonance images:" a stereological gold standard study,” European Journal of Radiology, vol. 57, no. 1, pp. 96–101.

B. Sun, D. Wang, Y. Tang et al.,(2009) “The pineal volume: a three-dimensional volumetric study in healthy young adults using 3.0 T MR data,” International Journal of Developmental Neuroscience, vol. 27, no. 7, pp. 655–660.

Bryden, M.M.; Griffiths, D.J.; Kennaway, D.J.; Ledingham, J. (1986) "The pineal gland is very large and active in newborn antarctic seals Experiential, [Cross Ref] [Pub Med] 42, 564–566.

Buch S, Cheng YN, Hu J, Liu S, Beaver J, Rajagovindan R, et al. (2016) .Determination of detection sensitivity for cerebral microbleeds using susceptibility-weighted imaging. NMR in biomedicine. [Pub Med]. 90, 584–8779

Bumb, J.M.; Schilling, C.; Enning, F.; Haddad, L.; Paul, F.; Lederbogen, F.; Deuschle, M.; Schredl, M. ; Nolte, I (2014) . "Pineal gland volume in primary insomnia and healthy controls: A magnetic resonance imaging study". J. Sleep Res., [Cross Ref] [Pub Med] 23, 276–282.

C. H. Mortiz, V. M. Haughton, D. Cordes, M. Quigley and M. E. Meyerand (2000) “Whole-Brain Functional MR Imaging Activation from Finger Tapping Task Examined with Independent Component Analysis,” American Journal of Neuroradiology, Vol. 21, No. 9, , pp. 1629- 1635.

C. K. Abbey, F. O. Bochud, “Modeling Visual Detection Tasks in Correlated Image Noise with Linear Model Observers,” Handbook of Medical Imaging, vol. 1. *Physics and Psychophysics*, eds. J.Beutel, H.L.Kundel, and R.L.Van Metter. Bellingham, WA: SPIE Press, 2000.

Cuello, A.C.; Tramezzani, J.H. (1969) "The epiphysis cerebri of the Weddell Sea" [Cross Ref] 12, 154–164.

D. LU & Q. WENG, (2007) A survey of image classification methods and techniques for improving classification performance, International Journal of Remote Sensing, Vol. 28, No. 5, ,pp 823–870.

Drake RL, Vogl AW, Adam WM. ;(2009) .Gray’s Anatomy for Students. 2nd ed. ASIN: B004LGYXQQ. London: Churchill Livingstone

E. M. Purcell, H. C. Torrey, R. V. Pound, “Resonance Absorption by Nuclear Magnetic Moment in a Solid,” *Physical Review*, vol. 69, no. 37, 1946.

E.-S. A. Dahshan, T. Hosny and A.-B. M. Salem, “A Hybrid Technique for Automatic MRI Brain Images Classification,” *Digital Signal Processing*, Vol. 20, No. 2, 2010, pp. 433-441.

Edmund Tapp ; (2008) " The Histology and Pathology of the Human Pineal Gland " Elsevier Volume 52, 1979, Pages 481-500 .

F. Bloch, W. W. Hansen, “Nuclear Induction,” *Physics Review*, pp. 69, 1946.

G. Bersani, A. Garavini, A. Iannitelli et al (2002)., “Reduced pineal volume in male patients with schizophrenia: no relationship to clinical features of the illness, ” Neuroscience Letters, vol. 329, no. 2, pp. 246–248,.

Grosshans, M.; Vollmert, C.; Vollstaedt-Klein, S.; Nolte, I.; Schwarz, E.; Wagner, X.; Leweke, M.; Mutschler, J.; Kiefer, F.; Bumb, J.M.(2016)" The association of pineal gland volume and body mass in obese and normal weight individuals: A pilot study. Psychiatr.Danub., 28, 220–224. [Pub Med].

H.M.Duvernoy, B.Parratte, L.Tatu, andF.Vuillier (2000) “The human pineal gland: relationships with surrounding structures and blood supply, ” Neurological Research, vol. 22, no. 8, pp. 747–790,

Haacke EM, Mittal S, Wu Z, Neelavalli J, Cheng YC.(2009) Susceptibility-weighted imaging: technical aspects and clinical applications, part 1. AJNR Am J Neuroradiol.; 30(1):19–30. Pub Med Central PMCID: PMC3805391. doi: 10.3174/ajnr.A1400 PMID: 19039041

I. Nolte, A. T. Lutkhoff, B. A. Stuck et al. (2009) "Pineal volume and circadian melatonin profile in healthy volunteers: an interdisciplinary approach," Journal of Magnetic Resonance Imaging, vol. 30, no. 3, pp. 499–505,

J. Golan, K. Torres, G. J. Staskiewicz, G. Opielak, and R.´Maciejewski, (2002) "Morph metric parameters of the human pineal gland in relation to age, body weight and height," Folia Morphologica, vol. 61, no. 2, pp. 111–113,

J. Koenderink, "The Structure of Images," *Biological Cybernetics*, Vol. 50, No. 5, 1984, pp. 363-370.

Kathiravan S and Kanakaraj J "A Review of Magnetic Resonance Imaging Techniques" *Smart Computing Review*, vol.3, no.5, October 2013.

Klein P, Rubinstein LJ (1989) Benign symptomatic glial cysts of the pineal gland: a report of seven cases and review of the literature. J Neurol Neurosurg Psychiatry 52:991 –995.

Liu & Wechsler (2000) "Gabor Feature Based Classification Using the Enhanced Fisher Linear Discriminate Model for Face Recognition , IEEE Trans. Image Processing, Vol. 11.,pp.467-476.

Louis DN, Ohgaki H, Wiestler OD, Cavenee WK (2007) WHO classification of tumors of the central nervous system. IARC Press, Lyon.55-98

M. Garc´ıa-Finana, L. M. Cruz-Orive, C. E. Mackay, B.˜ Pakkenberg, and N. Roberts, (2003)"Comparison of MR imaging against physical sectioning to estimate the volume of human cerebral compartments," Neuro Image, vol. 18, no. 2, pp. 505– 516,

M. Kociołek, A. Materka, M. Strzelecki P. Szczypiński,(2001) "Discrete wavelet transform–derived features for digital image texture analysis" Proc. of International Conference on Signals and Electronic Systems, Lodz, Poland , , pp. 163-168.

M. P. Eckstein, C. K. Abbey, F. O. Bochud. "A practical guide to model observers for visual detection in synthetic and natural noisy images," *Handbook of Medical Imaging,* vol,1: Physics and Psychophysics, SPIE, 2000.

M. Sumida, A. James Barkovich, and T. Hans Newton, (1996). "Development of the pineal gland: measurement with MR, " American Journal of Neuro radiology, vol. 17, no. 2, pp. 233– 236,

Macchi MM ,Bruce JN ;(2004)" Human pineal physiology and functional significance of melatonin." , Front Neuroendocrinol .; 25(3-4):177-95.

Mazin B. A. Hassib, Ahmed B. A. Hassib,Abbas K. A. Ibrahim, M. E. M. Garelnabi(2018) "Characterization of Pineal Region in MR Brain Images using Texture Analysis"-IOSR Journal of Applied Physics (IOSR-JAP) e-ISSN: 2278-4861.Volume 10, Issue 5 Ver. II 32-37

Mazin. Abdullah et al (2014)" Establishment of Reference Values for Normal Adult Sudanese Using MRI Disc Summation Method" Global Journal of Medical Research Vol 14,No 2-D

N. Acer, B. Sahin, M. Usanmaz, H. Tatoglu, and Z. Irmak,(2008)"Comparison of point counting and planimetry methods for the assessment of cerebellar volume in human using Magnetic resonance imaging: a stereological study," Surgical and Radiologic Anatomy, vol. 30, no. 4, pp. 335–339,

N. Acer, N. Ugurlu, D. D. Uysal, E. Unur, M. Turgut,ˇ and M. C¸ amurdanoglu(2010) "Comparison of two volumetricˇ techniques for estimating volume of intracerebral ventricles using magnetic resonance imaging: a stereological study," Anatomical Science International, vol. 85, no. 3, pp. 131–139,

N. Roberts, M. J. Puddephat, and V. McNulty,(2000)"The benefit of stereology for quantitative radiology," British Journal of Radiology, vol. 73, no. 871, pp. 679–697,

Namita Aggarwal, R. K. Agrawal (2012)"First and Second Order Statistics Features for Classification of Magnetic Resonance Brain Images" Copyright © SciRes. JSIP, 146-153 , March 11 th, 2012.

Nandigam RN, Viswanathan A, Delgado P, Skehan ME, Smith EE, Rosand J, et al. (2009) "MR imaging detection of cerebral microbleeds: effect of susceptibility-weighted imaging, section thickness, and field strength" AJNR American journal of neuroradiology.; 30(2):338– 43. Pub Med Central PMCID: PMC2760298. doi: 10.3174/ajnr.A1355 PMID: 19001544

Niy a zi Acer , Ahmet Turan Ilıca, Ahmet Tuncay Turgut, Ozlem¨ Ozc¨ ¸elik, Birdal Yıldırım, and Mehmet Turgut (2012) "Comparison of Three Methods for the Estimation of Pine al Gland Volume Using Magnetic Resonance Imaging" -The Scientific World Journal Volume, Article I D 123412, 9 pages doi:10.1100/2012/123412.

P. Lauterbur, "Image Formation by Induced Local Interactions: Examples Employing Nuclear Magnetic Resonance," Nature, pp. 242, 1973.

P. Mansfield, "Multi-planar image formation using NMR spin echoes, "*Journal of Physics* C: Solid State Physics, vol. 10, no. 15, 1977.

P. Xue, C. W. Thomas, G. C. Gilmore, D. L. Wilson, “An adaptive reference/test paradigm with applications to pulsed fluoroscopy perception,” *Behavior Research Methods, Instruments, and Computers*, vol. 30, pp. 332-348, 1998.

Pediatr Radiol (1995)"The pineal gland: a comparative MR imaging study in children and adults with respect to normal anatomical variations and pineal cysts." Sener RN1; 25(4):245-8.

Qurat-Ul-Ain, Ghazanfar Latif, Sidra Batool Kazmi, M. Arfan Jaffar, Anwar M. Mirza(2014)"Classification and Segmentation of Brain Tumor using Texture Analysis" ISSN: ISBN: 1790-5109 978-960-474-154-0,

R. M. Haralick, K. Shanmugan and I. Dinstein (1973) “Textural Features for Image Classification,” IEEE Transactions on Systems: Man, and Cybernetics SMC, Vol. 3, , pp. 610- 621. doi:10.1109/TSMC.1973.4309314.

R. N. Bracewell (1999), “The Fourier Transform and Its Applications,” 3rd Edition, McGraw-Hill, New York,

R.R. Ernst, A. Kumar, et al., “NMR Fourier zeugmatography, ”*Journal of Magnetic Resonance*, vol. 18, no. 1, 1975.

S. Chaplot, L. M. Patnaik and N. R. Jagannathan, (2006) “Classification of Magnetic Resonance Brain Images Using Wavelets as Input to Support Vector Machine and Neural Network,” Biomedical Signal Processing and Control, Vol. 1, No. 1, pp. 86-92. doi:10.1016/j.bspc..05.002.

S. G. Mallat, “A Theory of Multiresolution Signal Decomposition: The Wavelet Representation,” *IEEE Transactions on Pattern Analysis and Machine Intelligence*, Vol. 11, No. 7, 1980, pp. 674-693.

S. Keller, C. E. Mackay, T. R. Barrick, U. C. Wieshmann, M. A. Howard, and N. Roberts,(2002)“Voxel-based morphometric comparison of hippocampal and extrahippocampal abnormalities in patients with left and right hippocampal atrophy,” Neuro Image, vol. 16, no. 1, pp. 23–31.

S. S. Keller and N. Roberts, (2009) “Measurement of brain volume using MRI: software, techniques, choices and prerequisites,” Journal of Anthropological Sciences, vol. 87, pp. 127–151

S. Sahiner, H.-P. Chan, and N. Petrick et al.(1998) "Computerized characterization of masses on mammograms: the rubber band straightening transform and texture analysis", Medical Physics . Vol.25(4), , pp.516-526.

Surawicz TS, McCarthy BJ, Kupelian V et al (1999) Descriptive epidemiology of primary brain and CNS tumors: Central Brain Tumor Registry of the United States, 1990-1994. NeuroOncol 1(1):14–25

Tan, D.X.; Manchester, L.C.; Sainz, R.M.; Mayo, J.C.; León, J.; Reiter, R.J. (2005) Physiological ischemia/reperfusion phenomena and their relation to endogenous melatonin production: A hypothesis. Endocrine, [Cross Ref] 27, 149–158.

W. Gerlach, O. Stern, "Das magnetische Moment des Selberatoms," *Zeitschrift fur Physik*, vol. 9, no. 1, pp. 2, 1922.

International Journal of Science and Research (IJSR)
ISSN: 2319-7064
Index Copernicus Value (2016): 79.57 | Impact Factor (2017): 7.296

Estimation of Pineal Gland Volume for Normal Adult Sudanese Using MRI

Mazin B. A. Hassib[1, 2], M. E. M. Garelnabi[1, 2], Ahmed B. A. Hassib[1], Suhaib Alameen[2]

[1]Faculty of Radiology and Medical Imaging Sciences - National University, Sudan-Khartoum

[2]College of Medical Radiologic Sciences- Sudan University of Science and Technology, Sudan-Khartoum

Abstract: ***In present study, we established the volume of the pineal gland and it shapes in normal Sudanese adult using Magnetic Resonance Imaging.159 consecutive patients scanned for Brian with MRI to pineal region by use MRI machine 1.5 T the sequence was 3D-T1. Detailed Demographic Information of Population including; age, gender, weight, height, and BMI was recorded. The Disk Summation Method (DSM) used to measure the normal pineal gland in normal individuals, and the shape of pineal gland were evaluated in Axial & Sagittal images. The results shows that the pineal gland volume shows slightly difference between the gender were the female 0.135±0.0063 cm3and for the male 0.137±0.0063 cm3, using analysis of variance test for the age with body mass index BMI and the pineal gland volume were the p.value show there is significant difference between the body mass index 0.000 and pineal gland volume 0.037 with age. The distribution of shape of pineal gland showed three different shape pear, fusiform and cone shape were the pear shape found in 22 case with percentage 13.8%, the fusiform shape found in 61 case with percentage 38.4% and the cone shape in 76 case with percentage 47.8%. The pineal gland volume can be estimated using the following linear equations: pineal gland V = 0.0004 (Age/ys) + 0.1262, pineal gland V= 0.0012 (BMI) + 0.1104 in our study, the mean ± S.D pineal gland volumes using Disk Summation Method were found to be 0.136 ± 0.007 cm3.also the different morphologic Characteristics of the pineal gland were found three shapes in normal Sudanese adult pear shape 14%, fusiform shape 38% and cone shape 48% from total sample.***

Keywords: Pineal gland volume, Disk Summation Method, morphologic Characteristics of pineal gland

1. Introduction

The pineal gland also called the pineal body, epiphysis cerebri, epiphysis or the “third eye: is a small reddish-grey pine cone-like endocrine gland of a major regulatory importance located in between the superior colliculi. It is inferior to the splenium of the corpus callosum from which it is separated by the telachoroidea of the third ventricle and the contained cerebral veins. The pineal is about 8 mm long. Septa extend into the pineal gland from the surrounding pia mater [1].

To the present day, the functions of the pineal gland are not fully understood. Unlike most parts of the brain, it lies outside the blood-brain barrier and is not separated from the bloodstream. Current knowledge indicates that by secretion of melatonin, the pineal gland plays an important role in the regulation of the sleep-wake cycle and of reproductive function (e.g. onset of puberty) [2], with melatonin also acting as a neuroprotector or antioxidant [3, 4]. Anatomically, the pineal gland is a rounded or crescent-shaped structure like a pine cone and it is attached by the stalk to the diencephalon and the stalk lines the pineal recess whose inferior lip links the pineal gland to the posterior commissure, and superior lip to the habenular commissure [5]. It has been stated that the pineal gland grows in size from birth until two years of age and then remains constant between 2 to 20 years of age [6]. Formerly, it was believed that the pineal gland played an important functional role in the onset of puberty [7, 8].

The size is individually variable and the average weight of pineal gland in human is around 150 mg [9], the size of a soybean. Pineal glands are present in all vertebrates [10]. Pineal-like organs are also found in non-vertebrate organisms such as insects [11-13]. It appears that the sizes of pineal glands in vertebrates are somehow associated with survival in their particular environments and their geographical locations. The more harsh (colder) their habitant, the larger their pineal glands are. A general rule is that the pineal gland increases in size in vertebrates from south to north or from the equator to the poles [14].

Recent advances in MRI imaging have led to the development of novel gradient echo (GRE) imaging techniques such as SWMR, which is based on magnetic susceptibility and sensitive to materials distorting the local magnetic field. SWMR allows for a reliable differentiation of calcifications from tissue artifacts, hemorrhage and other causes of susceptibility differences by using T2. Diagnostic accuracy of SWMR for the evaluation of pineal gland calcification weighted magnitude and GRE filtered-phase information to generate a unique contrast [15-19].

Some of radiological studies of the pineal gland have been mainly conducted by computed tomography (CT) on pineal calcification over different populations of healthy subjects [20, 21]. There have been a few studies about pineal volume estimation using different methods such as elliptic approaches and ROI on MRI [22–23].

2. Material and Methods

159 consecutive patients (male=93, Female 66) their ages were between (19-31) years who had undergone 3D-T1 Brian MRI Scan were obtain at period (11) Months between July/2017 to June/2018 for study purpose. Excluded Patients were those who had mid brain & endocrine diseases. Detailed Demographic Information of Population including; age, gender, weight, height, and BMI was recorded.

MRI machine Toshiba ™ 1.5 T as used at Al-Mouleem Hospital, the sequence Were: Ultrafast Gradient Echo 3D with preparation Pulse T_1W (3D-FEE) SENSE + head Coil ;Specific Absorption Rate =0.3199, Flip Angle 30 degree, ETL=1 Echo No.=1, Slice Thickness =1.6mm, Gap Between Slice = 50%.TR=0.8ms / TE = 2.6ms.Matrix 256 px X 256 px.

The Disk Summation Method (DSM) used to measure the normal pineal gland in normal individuals. In DSM the measurement is dependent on the picture element (pixel-px), by counting the total number of pxs per Area (ROIs which the pineal gland appear excluding the rest of FOV) and is representing in $(px)^2$.than the $(px)^2$ were converted into units of Area in $(mm)^2$.that was done by multiplying the $(px)^2$ by conversion factor. Than multiplying the product by slice thickness in (mm), which represents slice height an Z-axis, and consequently the product is unit of volume $(mm)^3$ for single slice. Than dividing the value in $(mm)^3$ over 1000 to convert to $(cm)^3$.

This step above was applied to each separate slice to final the total volume of pineal gland. As shown in following equations:

$$A\ (mm)^2 = px^2 (\text{Number of pixel with ROIs}) \times \text{convert factor}.$$

$$\text{Volume in } (cm)^3 = A(mm)^2 \times \text{Slice Thickness } (mm)/1000.$$

The pineal gland shape was evaluated in Axial & Sagittal image plane for ALL including patients. The shape describe as *pear shape*: tapered at the top and wider at bottom, *fusiform shape*: like spindle wider in the middle and tapering lowered the ends. And *cone shape*: smoothly from a flat base to appoint called apex or vertex.

Variables including height ; which was measured in (cm) ; weight in (Kg), Age (yrs), and gender (Male and Female) were evaluated, For measuring dependent variable Body Mass Index (BMI) Calculate by use :

$$BMI = weight / (height)^2 X\ 100$$

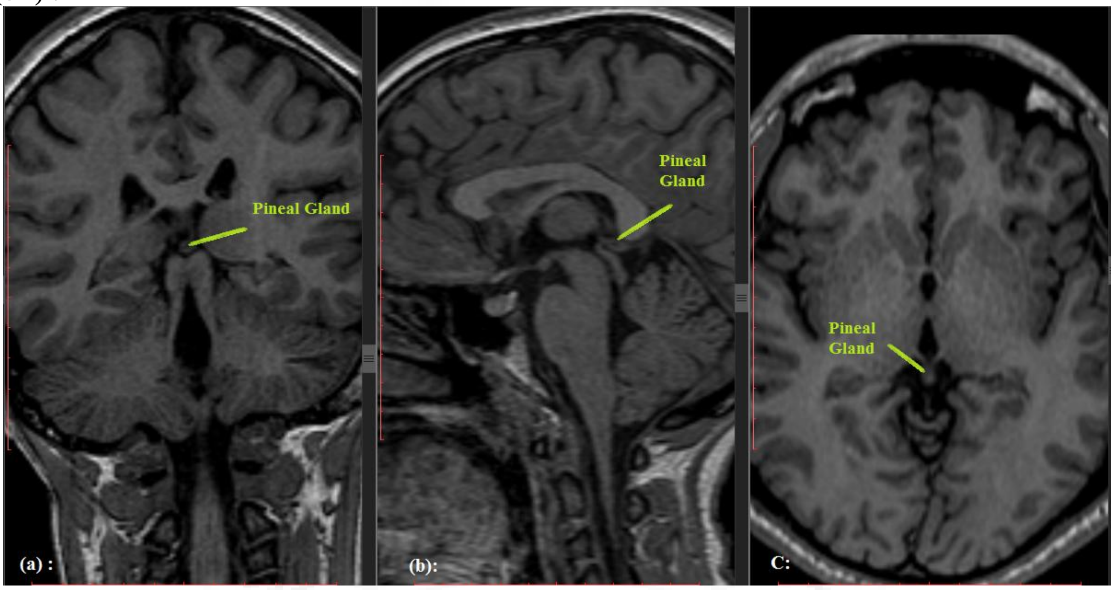

Figure 1: MRI brain scan 3D-T_1 W with Axial, sagittal and coronal demonstrates pineal gland.

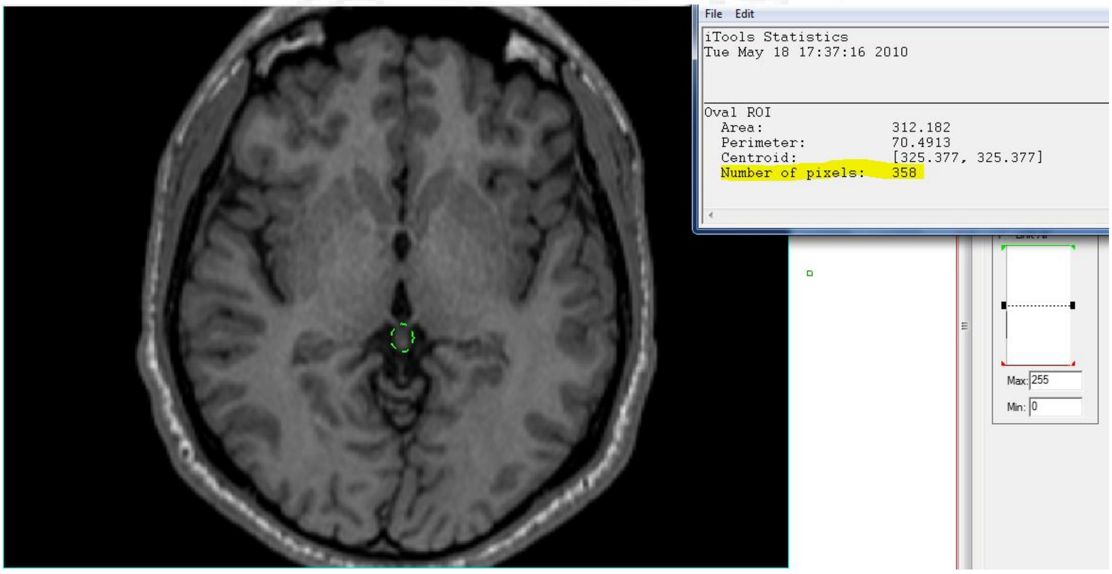

Figure 2: MRI 3D-T_1 W with Axial demonstrates pineal gland method of contouring and pixel accounting polygon

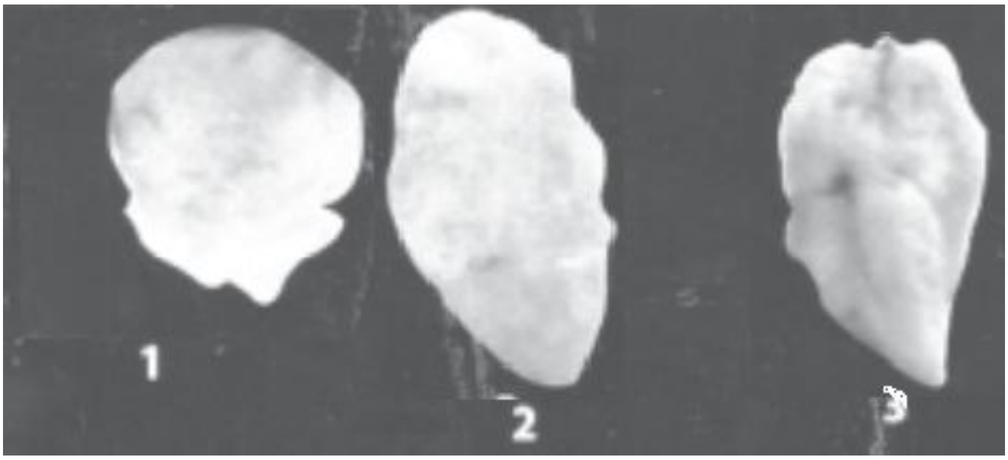

Figure 3: Different shapes of the pineal gland seen through magnifying glass (1. pea shaped, 2.fusiform shaped, and 3. cone shaped

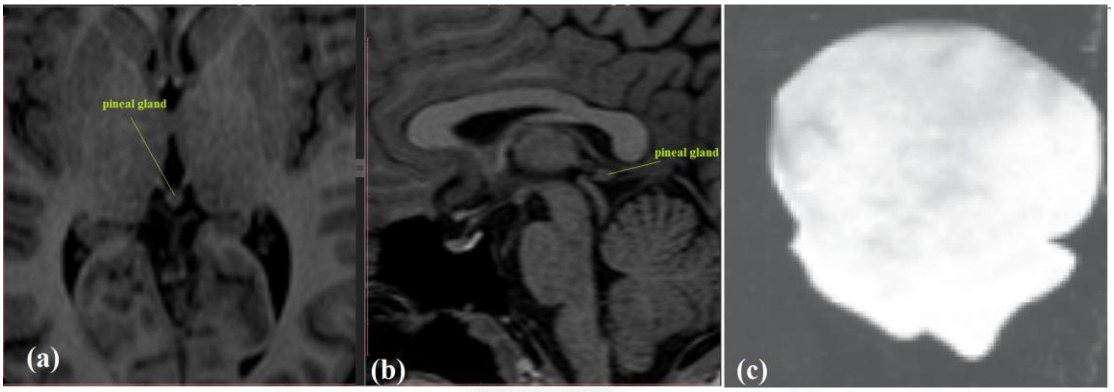

Figure 4: The Axial (a) and Sagittal (b)MRI showed the Pear shape(c) of pineal gland

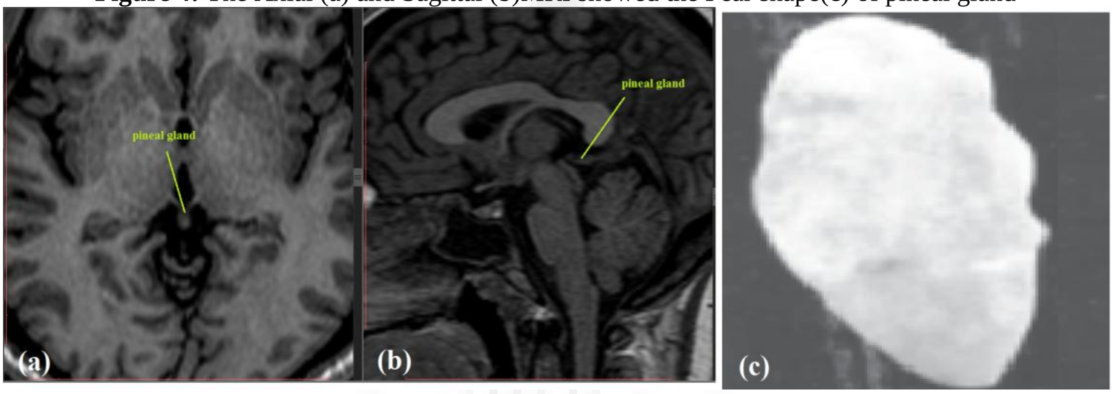

Figure 5: The Axial (a) and Sagittal (b) MRI showed the fusiform shape(c) of pineal gland

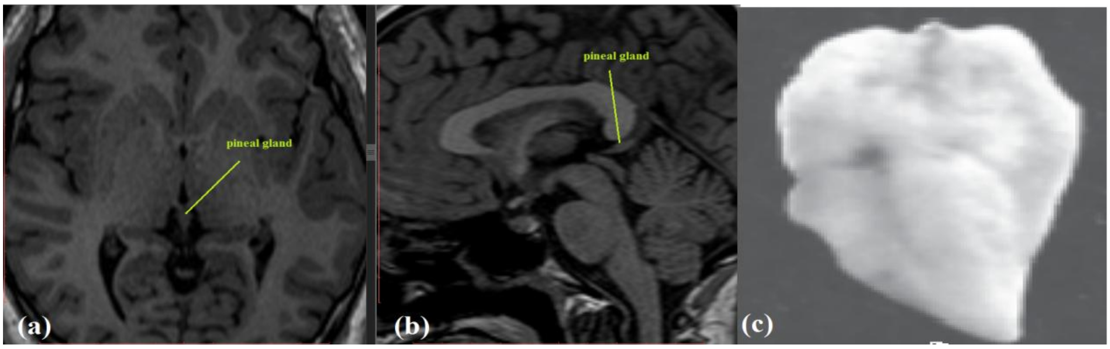

Figure 6: The Axial (a) and Sagittal (b) MRI showed the cone-shape(c) of pineal gland

3. Result and Discussion

This study adept analytic cross-sectional design focuses on measure the volume of pineal gland and describes shape using MR images.

Table 1: Statistical descriptive for all patients:

	Mean	Median	STD	Min	Max
Age	24.98	25	2.92	19	31
High	177.98	177	8.63	159	195
Weight	69.71	70	9.41	51	93
BMI	21.89	22	1.42	19	25
Volume	0.136	0.136	0.007	0.123	0.159

Table 1 shows statistical description for demographic information and volume for all patients as mean, median, standard deviation, minimum and maximum. For the age the mean ± standard deviation was 24.98±2.92, for patients high, weight, body mass index and the PINEAL GLAND volume was 177.98±8.63 cm, 69.71±9.1 kg, 21.89±1.42 kg/cm^2 and 0.136±0.007 cm^3 respectively.

Table 2: Show correlate the gender with pineal gland volume and patients information:

	Gender	Mean	Std. Deviation	Std. Error Mean
Age	Female	23.48	2.731	.341
	Male	25.96	2.589	.267
BMI	Female	21.36	1.384	.173
	Male	22.27	1.321	.136
Volume cm^3	Female	.134672	.0063130	.0007891
	Male	.137690	.0064676	.0006671

In table 2. Presented compare the gender with pineal gland volume and patients information for the age the mean of female was 23.48 years and for male 25.96 years, the body mass index and the pineal gland volume shows slightly difference between the gender were the female 21.36 kg/cm^2 and the male 22.27 kg/cm^2, the pineal gland volume for female 0.135 cm^3 and for male 0.137 cm^3

Table 3: Shown the ANOVA test of BMI with volume of pineal gland

		Sum of Squares	Mean Square	F	Sig.
BMI	Between Groups	82.635	6.357	3.917	.000
	Within Groups	235.327	1.623		
	Total	317.962			
Volume cm3	Between Groups	.001	.000	1.876	.037
	Within Groups	.006	.000		
	Total	.007			

Table 4 show ANOVA test for the body mass index and the pineal gland volume with age were the p.value show there is significant difference between the body mass index and the pineal gland volume with age.

Table 5: Show frequency and percentage distribution of shape of pineal gland:

Shapes	*Cases*	*Percentage %*
Pear Shape	22	13.8
Fusiform Shape	61	38.4
Cone Shape	76	47.8
Total	***159***	***100***

The distribution of shape of pineal gland showed three different shape pear, fusiform and cone shape were the pear shape found in 22 case with percentage 13.8%, the fusiform shape found in 61 case with percentage 38.4% and the cone shape in 76 case with percentage 47.8%.

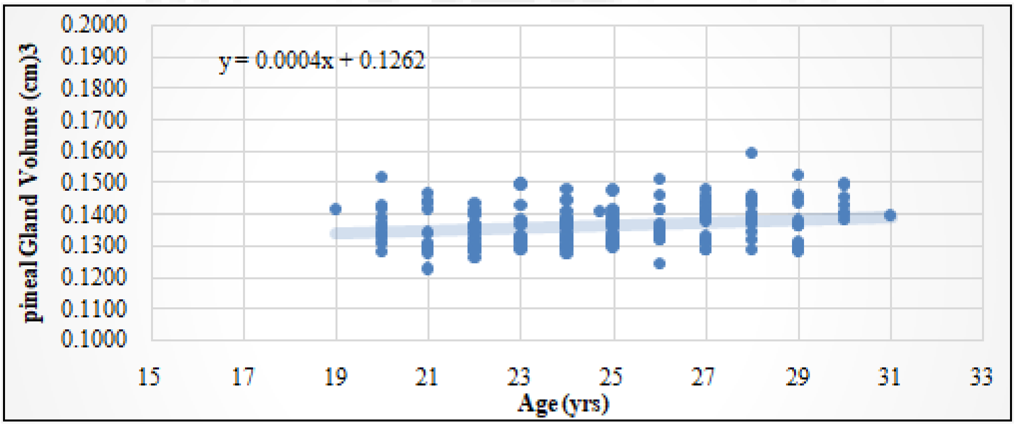

Figure 7: Show correlate between the pineal gland volume with patients age

Figure 7. show correlate between the pineal gland volume with patients age, and found that the volume increase with rate 0.0004 for each year.

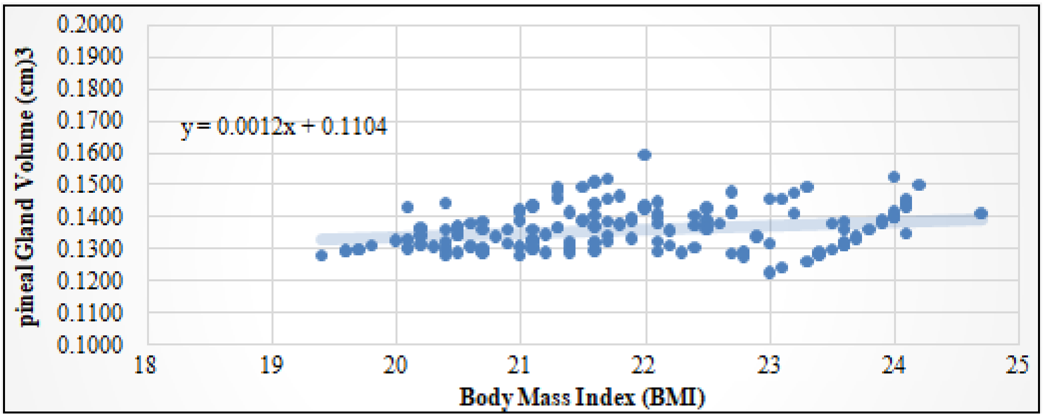

Figure 8: Show correlate between pineal gland volumes with body mass index

Figure 8. show correlate between pineal gland volume with body mass index were the volume was increase with rate 0.0012 for each (kg/cm^2) unit from body mass index

Some studies have found correlation between pineal volume and age *(B. Sun et al 2009)*.in this study showed a significant difference between the Age and Pineal gland volume*(P<0.037)*.Also the results of *(Niyazi Acer et al 2011)* determined significant correlations between pineal volume and age.

(B. Sun et al -2009) was reported that pineal volume was 94.2 ± 40.65 mm3 in healthy young adults, *(Nolte et al 2009)* found that the pineal gland volume was 125 ± 54 mm^3. *(G.Bersani et al 2002*) reported the pineal volume was 64.05 ± 20.69 mm^3 for schizophrenics and 74.62 ± 33.53 mm^3 for controls. In the present study, the mean ± S.D pineal gland volumes for Disk Summation Method were found to be 0.1364 ± 0.00655 cm^3. From the present study notice the volume was higher than *Nolte et al-2009, B. Sun et al -2009* and *G. Bersani et al-2002 and this difference comes from the measurement methods for each studies.*

For the pineal gland shape *Kelly.W et al 1984* the pineal glandis cone-shape while *Berkovitz 1988 and Rogers et al 1992*found it as fusiform and pea shapes respectively.

4. Conclusion

Estimation of volume and shape of the pineal gland in normal adults, were the pineal gland volume shows slightly difference between the gender were the female 0.135±0.0063 cm^3 and for the male 0.137±0.0063 cm^3, using ANOVA test for the age with body mass index BMI and the pineal gland volume were the p. value show there is significant difference between the body mass index 0.000 and pineal gland volume 0.037 with age. The distribution of shape of pineal gland showed three different shape pear, fusiform and cone shape were the pear shape found in 22 case with percentage 13.8%, the fusiform shape found in 61 case with percentage 38.4% and the cone shape in 76 case with percentage 47.8%.

The pineal gland volume can be estimated using the following linear equations:
Equation for the regression values between pineal gland volume and patients age and body mass index*:*

Pineal Gland Volume cm^3= 0.0004 (Age/ys)+ 0.1262
Pineal Gland Volume cm^3= 0.0012 (BMI) + 0.1104

References

[1] Drake RL, Vogl AW, Adam WM. Gray's Anatomy for Students. 2nd ed. ASIN: B004LGYXQQ. London: Churchill Livingstone; 2009.
[2] Rocha CS, Rato L, Martins AD, Alves MG, Oliveira PF. Melatonin and male reproductive health: relevance of darkness and antioxidant properties. Current molecular medicine. 2015; 15(4):299–311. PMID: 25941822
[3] Mahlberg R, Walther S, Kalus P, Bohner G, Haedel S, Reischies FM, et al. Pineal calcification in Alzheimer's disease: an in vivo study using computed tomography. Neurobiology of aging. 2008; 29(2):203–9. doi: 10.1016/j.neurobiolaging.2006.10.003 PMID: 17097768
[4] Srinivasan V, Pandi-Perumal SR, Brzezinski A, Bhatnagar KP, Cardinali DP. Melatonin, immune function and cancer. Recent Pat Endocr Metab Immune Drug Discov. 2011; 5(2):109–23. PMID: 22074586
[5] H.M.Duvernoy, B.Parratte, L.Tatu, andF.Vuillier, "The human pineal gland: relationships with surrounding structures and blood supply, " *Neurological Research*, vol. 22, no. 8, pp. 747–790, 2000.
[6] M. Sumida, A. James Barkovich, and T. Hans Newton, "Development of the pineal gland: measurement with MR, " *American Journal of Neuroradiology*, vol. 17, no. 2, pp. 233– 236, 1996.
[7] J. I. Kitay, "Pineal lesions and precocious puberty: a review, " *Journal of Clinical Endocrinology and Metabolism*, vol. 14, pp. 622–625, 1954.
[8] R. J. Wurtman and M. A. Moskowitz, "The pineal organ. I, " *The New England Journal of Medicine*, vol. 296, no. 23, pp. 1329–1333, 1977.
[9] Golan, J.; Torres, K.; Sta´skiewicz, G.J.; Opielak, G.; Maciejewski, R. Morphometric parameters of the human pineal gland in relation to age, body weight and height. Folia Morphol. **2002**, 61, 111–113.
[10] Tan, D.X.; Manchester, L.C.; Fuentes-Broto, L.; Paredes, S.D.; Reiter, R.J. Significance and application of melatonin in the regulation of brown adipose tissue metabolism: Relation to human obesity. Obes. Rev. **2011**, 12, 167–188. [CrossRef] [PubMed]

[11] Hintermann, E.; Jenö, P.; Meyer, U.A. Isolation and characterization of an arylalkylamine N-acetyltransferase from Drosophila melanogaster. FEBS Lett. **1995**, 375, 148–150. [CrossRef]
[12] Itoh, M.T.; Hattori, A.; Sumi, Y.; Suzuki, T. Day-night changes in melatonin levels in different organs of the cricket (Gryllus bimaculatus). J. Pineal Res. **1995**, 18, 165–169. [CrossRef] [PubMed]
[13] Vivien-Roels, B.; Pevet, P.; Beck, O.; Fevre-Montange, M. Identification of melatonin in the compound eyes of an insect, the locust (Locusta migratoria), by radioimmunoassay and gas chromatography-mass spectrometry. Neurosci. Lett. **1984**, 49, 153–157. [CrossRef]
[14] Ralph, C.L. The pineal gland and geographical distribution of animals. Int. J. Biometeorol. **1975**, 19, 289–303. [CrossRef] [PubMed]
[15] Haacke EM, Mittal S, Wu Z, Neelavalli J, Cheng YC. Susceptibility-weighted imaging: technical aspects and clinical applications, part 1. AJNR Am J Neuroradiol. 2009; 30(1):19–30. PubMed Central PMCID: PMC3805391. doi: 10.3174/ajnr.A1400 PMID: 19039041
[16] Mittal S, Wu Z, Neelavalli J, Haacke EM. Susceptibility-weighted imaging: technical aspects and clinical applications, part 2. AJNR Am J Neuroradiol. 2009; 30(2):232–52. PubMed Central PMCID: PMC3805373. doi: 10.3174/ajnr.A1461 PMID: 19131406
[17] Chen W, Zhu W, Kovanlikaya I, Kovanlikaya A, Liu T, Wang S, et al. Intracranial calcifications and hemorrhages: characterization with quantitative susceptibility mapping. Radiology. 2014; 270(2):496–505. PubMed Central PMCID: PMCPMC4228745. doi: 10.1148/radiol.13122640 PMID: 24126366
[18] Buch S, Cheng YN, Hu J, Liu S, Beaver J, Rajagovindan R, et al. Determination of detection sensitivity for cerebral microbleeds using susceptibility-weighted imaging. NMR in biomedicine. 2016.
[19] Nandigam RN, Viswanathan A, Delgado P, Skehan ME, Smith EE, Rosand J, et al. MR imaging detection of cerebral microbleeds: effect of susceptibility-weighted imaging, section thickness, and field strength. AJNR American journal of neuroradiology. 2009; 30(2):338–43. PubMed Central PMCID: PMC2760298. doi: 10.3174/ajnr.A1355 PMID: 19001544
[20] S. A. Schmitz, I. Platzek, D. Kunz, R. Mahlberg, K. J. Wolf, and J. O. Heidenreich, "Computed tomography of the human pineal gland for study of the sleep-wake rhythm: reproducibil- ity of a semi-quantitative approach, " *Acta Radiologica*, vol. 47, no. 8, pp. 865–871, 2006.
[21] A. T. Turgut, H. M. Karakas¸, Y.Ozsunar et al., "Age-related changes in the incidence of pineal gland calcification in Turkey: a prospective multicenter CT study, " *Pathophysiology*, vol. 15, no. 1, pp. 41–48, 2008.
[22] G. Bersani, A. Garavini, A. Iannitelli et al., "Reduced pineal volume in male patients with schizophrenia: no relationship to clinical features of the illness, " *Neuroscience Letters*, vol. 329, no. 2, pp. 246–248, 2002.
[23] B. Sun, D. Wang, Y. Tang et al., "The pineal volume: a three-dimensional volumetric study in healthy young adults using 3.0 T MR data, " *International Journal of Developmental Neuroscience*, vol. 27, no. 7, pp. 655–660, 2009.

IOSR Journal of Applied Physics (IOSR-JAP)
e-ISSN: 2278-4861.Volume 10, Issue 5 Ver. II (Sep. – Oct. 2018), 32-37
www.iosrjournals.org

Characterization of Pineal Region in MR Brain Images using Texture Analysis

Mazin B. A. Hassib[1,2], Ahmed B. A. Hassib[1],Abbas K. A. Ibrahim[3], M. E. M. Garelnabi[1,2]

1 Faculty of Radiology and Medical Imaging Sciences - National University, Sudan-Khartoum
2College of Medical Radiologic Sciences- Sudan University of Science and Technology, Sudan-Khartoum
3 College of Medical Radiological Science and Nuclear Medicine, AlRibat National University,Khartoum,Sudan
Corresponding Author: MazinHassib

Abstract: *The classification processes of MRI brain were defining the corpus,pineal gland, techunum, and third ventricle were carried out using Interactive Data Language (IDL) program as platform for the generated codes. The result of the classification showed that the pineal gland areas were classified well from the rest of the tissues although it has characteristics mostly similar to surrounding tissue.*
The results show that the Gray Level variation and features give classification accuracy
Several texture features are introduced using Gray Level variation and features and the FOS gives a classification score matrix generated by linear discriminate analysis and the overall classification accuracy was 92.7%, were the classification accuracy of corpus 93.3%, pineal gland 97.9%, techunum 89.9%, while the third ventricle showed classification accuracy 88.5%. These relationshipsare stored in a Texture Dictionary that can be later used to automatically annotate new MRI with the appropriate pineal gland

Key words: *corpus, pineal gland, third ventricle, texture analysis, FOS, MRI*

Date of Submission: 23-09-2018 Date of acceptance: 08-10-2018

I. Introduction

Signs and symptoms related to pineal lesions are generally secondary to mass effect on adjacent structures. Compression of the tectal plate can result in obstruction of the sylvian aqueduct and obstructive hydrocephalus. Cerebellar, corticospinal or sensory disturbance can result from direct

compression of the midbrain [1]. Infiltrative lesions of the pineal gland may interfere with normal pineal gland function and lead to precocious puberty, less commonly hypogonadism and diabetes insipidus. Pineal parenchymal lesions account for less than 15 % of all pineal masses and less than 0.2 % of intracranial neoplasms [1,2]. These lesions commonly arise from pineocytes or their precursors and are classified by the World Health Organization (WHO) into the following entities: low-grade pineocytoma, pineal parenchymal tumour of intermediate differentiation (PPTID), papillary tumour of pineal region (PTPR) and highly malignant pineoblastoma [3].

It was reported that several physiological or pathological conditions indeed alter the morphology

of the pineal glands. For example, the pineal gland of obese individuals is usually significantly smaller than that in a lean subject [4]. The pineal volume is also significantly reduced in patients with primary insomnia compared to healthy controls and further studies are needed to clarify whether low pineal volume is the basis or a consequence of a functional sleep disorder [5]. These observations indicate that the phenotype of the pineal gland may be changeable by health status or by environmental factors, even in humans. The largest pineal gland was recorded in new born South Pole seals; it occupies one third of their entire brain [6,7]. The pineal size decreases as they grow. Even in the adult seal, however, the pineal gland is considerably large and its weight can reach up to approximately 4000 mg, 27 times larger than that of a human. This huge pineal gland is attributed to the harsh survival environments these animals experience [8].

Recent advances in MRI imaging have led to the development of novel gradient echo (GRE) imaging techniques such as SWMR, which is based on magnetic susceptibility and sensitive to materials distorting the local magnetic field. SWMR allows for a reliable differentiation of calcifications from tissue artifacts, hemorrhage and other causes of susceptibility differences by using T2 _ Diagnostic accuracy of SWMR for the evaluation of pineal gland calcification weighted magnitude and GRE filtered-phase information to generate a unique contrast [9-13].

II. Material and methods

159 consecutive patients (male=93, Female 66) their ages were between (19-31) years who had undergone 3D-T1 Brian MRI Scan. Excluded Patients were those who had mid brain & endocrine diseases. Detailed Demographic Information of Population including; age,gender, weight,height, and BMI was recorded.

MRI machine Toshiba ™ 1.5 T as used at Al-Mouleem Hospital, the sequence Were: Ultrafast Gradient Echo 3D with preparation Pulse T_1W(3D-FEE) SENSE + head Coil; Specific Absorption Rate =0.3199, Flip Angle 30 degree, ETL=1 Echo No.=1, Slice Thickness =1.6mm, Gap Between Slice = 50% .TR=0.8ms / TE = 2.6ms. Matrix 256 px X 256 px.

Statistical Methods

First Order Statistics: FOS can be used as the most basic texture feature extraction methods, which are based on the probability of pixel intensity values occurring in digital images. The parameters in the following statistical formulas are xi, the intensity value of pixel i, N, the total number of pixels, maxV , the maximum intensity value within a patch and Hi, the histogram of an image patch.

Mean: Calculates the mean intensity value of all pixels. the function µ= mean2(IP) can be used to compute this feature.

$$\mu = \frac{1}{N}\sum_{i=1}^{N} x_i$$

Standard Deviation :

The standard deviation of all the intensity values of a patch is used as a texture feature. The corresponding Matlab function is σ= std2(IP).

$$\sigma = \sqrt{\frac{1}{N}\sum_{i=1}^{N}(x_i - \mu)^2}$$

Coefficient of variation

The coefficient of variation can be seen as the relative standard deviation. It is calculated by dividing the standard deviation with the mean value.

$$c_v = \frac{\sigma}{\mu}$$

Entropy

The entropy of a gray-scale image is a measure of intensity value randomness. It is calculated from the histogram counts of an image giving a probability p of certain pixel values occurring in the image.

$$s = -\sum(p. * log2(p))$$

Skewness

Another statistical measure which is used for texture analysis is skewness. Itmeasures the symmetry of a distribution curve of pixel intensity occurrencesas seen in a histogram. The function ϒ1= skewness(IP) can be used tocompute the skewness.

$$\gamma_1 = \frac{\frac{1}{N}\sum_{i=1}^{N}(x_i - \mu)^3}{(\frac{1}{N}\sum_{i=1}^{N}(x_i - \mu)^2)^{\frac{3}{2}}}$$

Kurtosis

The kurtosis measures the atness of a histogram relative to a normal distribution.A curve has a high kurtosis when it has a clear peak close to themean value. The Matlab function for the kurtosis is ϒ2= kurtosis(IP).

$$\gamma_2 = \frac{\frac{1}{N}\sum_{i=1}^{N}(x_i-\mu)^4}{\left(\frac{1}{N}\sum_{i=1}^{N}(x_i-\mu)^2\right)^2} - 3$$

III. Results and discussion

In this paper were features extracted from ***MRI*** using First order statistic and All these features were calculated for all imagesand then the data were ready for discrimination which wasperformed using step-wise technique in order to select the most significant feature that can be used to classify the MR brain imaging for Pineal Gland and the results show that:

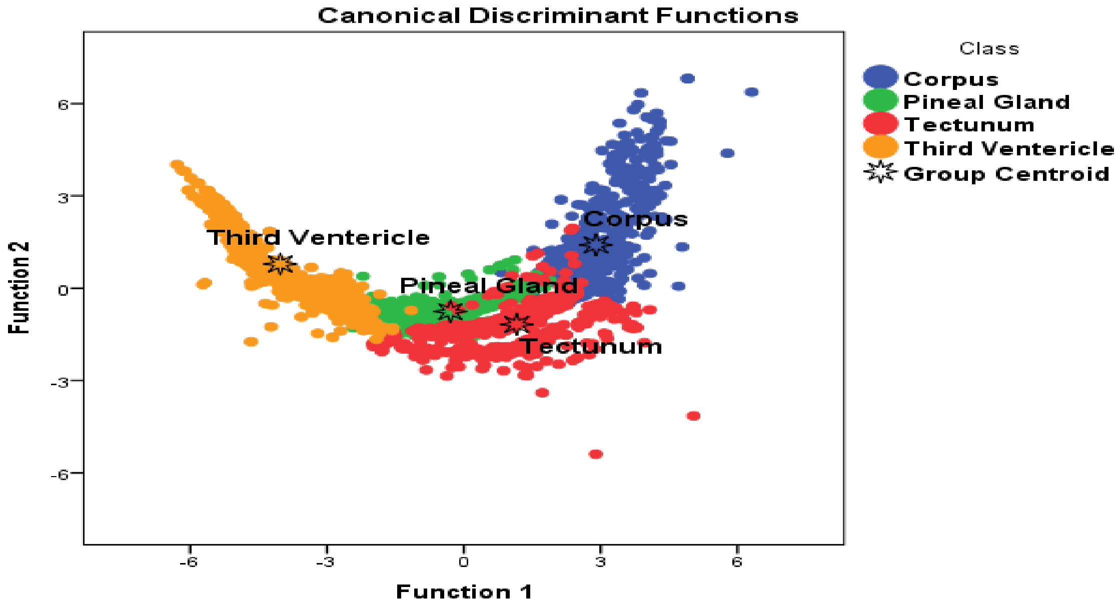

Fig 1. classification Map that created using linear discriminant analysis function.

Fig. 1. Scatter plot generated using discriminate analysis function for Four **classes** represents: Corpus, pineal gland, techunum, third ventricle the classification showed that the pineal gland wereclassifiedwell from the rest of the tissues although ithas characteristics mostly similar to surrounding tissue.

Table 1: Showed the classification accuracy of the Pineal Gland using linear discriminant analysis:

Classes		***Predicted Group Membership***				**Total**
		Corpus	***Pineal Gland***	***Tectunum***	***Third Ventericle***	
Original	**Corpus**	**93.3**	**2.8**	**4.0**	**.0**	**100.0**
	Pineal Gland	**.8**	**97.9**	**1.3**	**.0**	**100.0**
	Tectunum	**1.9**	**8.3**	**89.9**	**.0**	**100.0**
	Third Ventricle	**.0**	**10.7**	**.8**	**88.5**	**100.0**

92.7% of original grouped cases correctly classified.

Table (1) show classification score matrixgenerated by linear discriminate analysis andthe overall classification accuracyof corpus 93.3%, were the classificationaccuracy of pineal gland 97.9%, techunum 89.9%, While the third ventricle showed aclassification accuracy 88.5%.

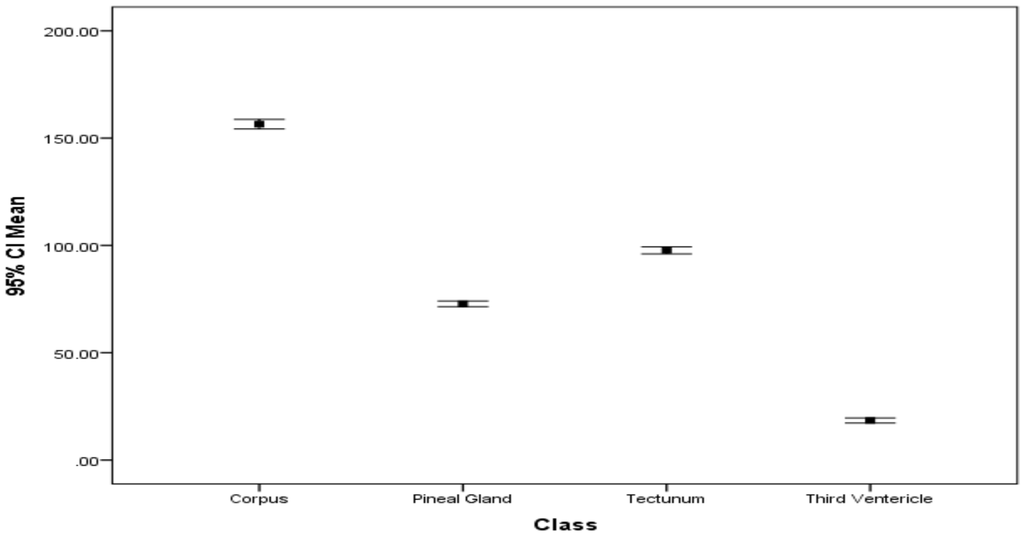

Fig .1 show error bar plot for the CI mean texturalfeatures that selected by the linear stepwise discriminatefunction as a discriminate feature where it discriminates between all features. From the discriminate power point of view in respect tothe applied features the mean candifferentiate between all the classes successfully.

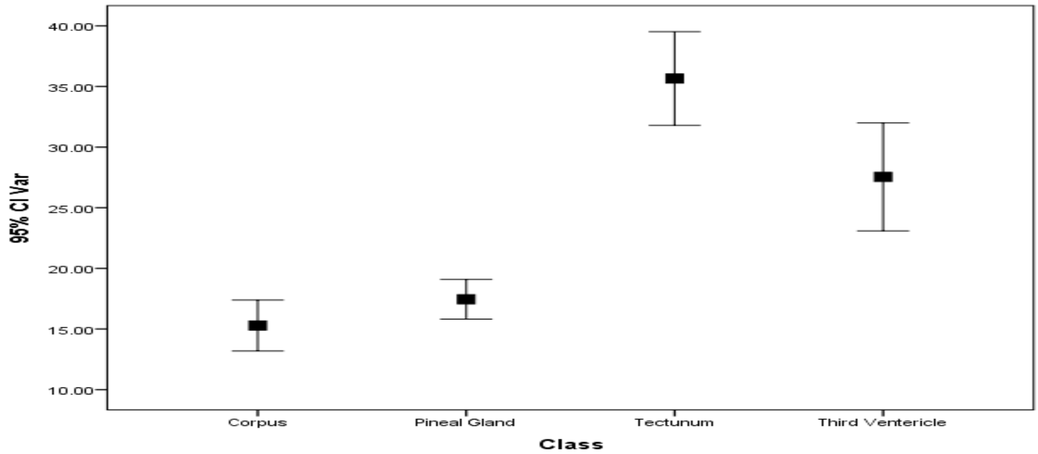

Fig .2 show error bar plot for the variance textural featuresthat selected by the linear stepwise discriminate function as adiscriminate feature where it discriminates between allfeatures.

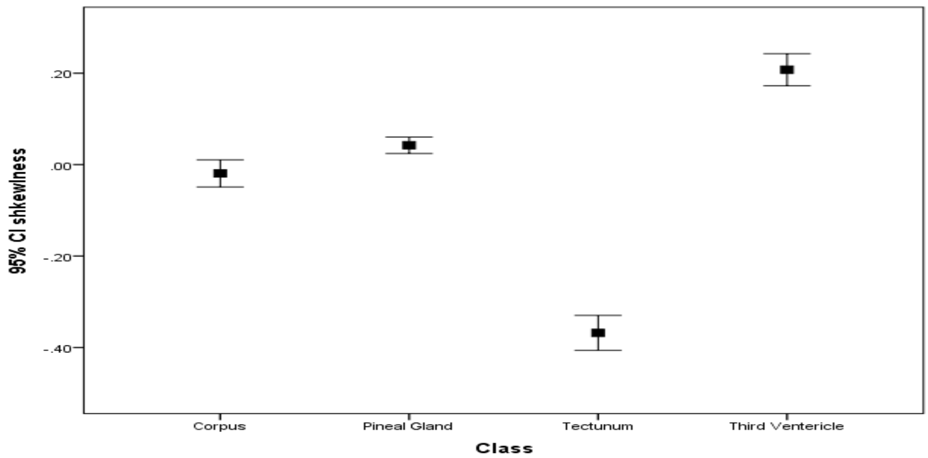

Fig .3 show error bar plot for the shkewness textural featuresthat selected by the linear stepwise discriminate function as adiscriminate feature where it discriminates between allfeatures.

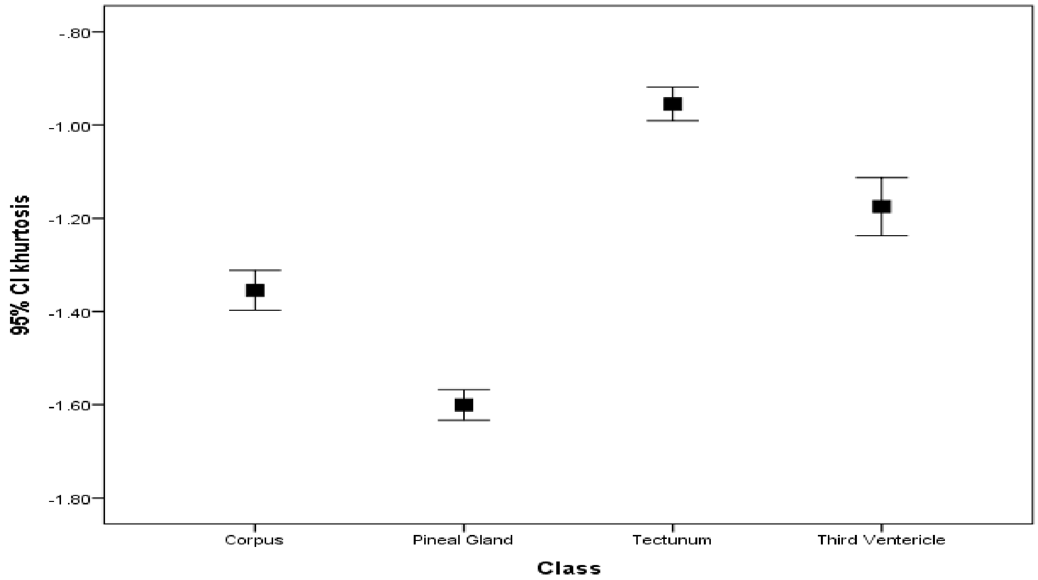

Fig .4 show error bar plot for the kurtosis textural featuresthat selected by the linear stepwise discriminate function as adiscriminate feature where it discriminates between allfeatures.

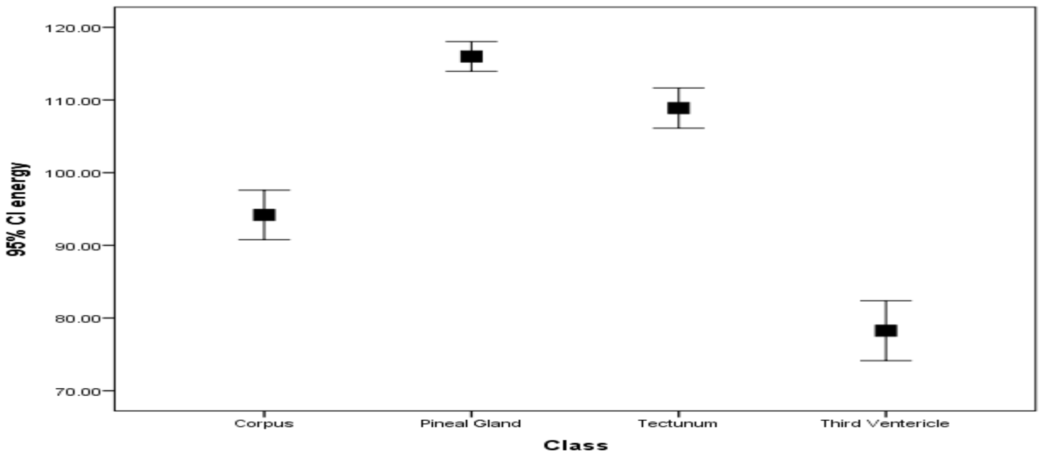

Fig .5 show error bar plot for the energy textural featuresthat selected by the linear stepwise discriminate function as adiscriminate feature where it discriminates between allfeatures.

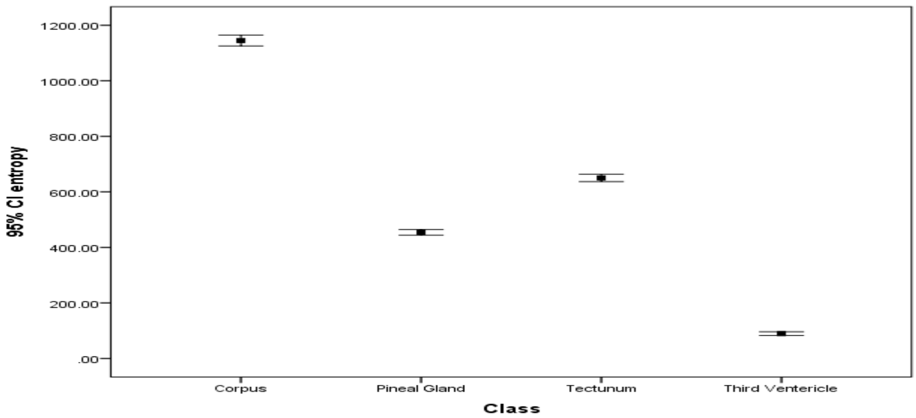

Fig .6 show error bar plot for the CI entropy texturalfeatures that selected by the linear stepwise discriminatefunction as a discriminate feature where it discriminates between all features. From the discriminate power point of view in respect tothe applied features the entropy candifferentiate between all the classes successfully.

IV. Conclusion

Theclassification processes of ***MRI*** brain were defining the corpus,pineal gland, techunum, and third ventricle were carried out using Interactive Data Language (IDL) program as platform for the generated codes. The result of the classification showedthat the pineal gland areas were classified well from the rest of the tissues although it has **characteristics mostly similar tosurrounding tissue.**

Several texture features are introduced from FOS and the classification score matrix generated by lineardiscriminate analysis and the overall classification accuracy was 92.7%, were the classificationaccuracy of corpus 93.3%,pineal gland 97.9%, techunum 89.9%, While the third ventricle showed aclassification accuracy 88.5%.

Using Linear discrimination analysis generated aclassification function which can be used to classify otherimage intothe mention classes as using the following multi-regressionequation;

Corpus = (Mean + 2.233) * variance + (-0.046) *(Skewness + 1.398) * (kurtosis + 0.203) * (energy + (-0.013)) * entropy + (-0.239)) -38.185
Pineal Gland = (Mean + 2.123) * variance + (-0.033) *(Skewness + 1.584) * (kurtosis + (-0.977)) * (energy + 0.011) * entropy + (-0.247)) -23.713
Tectunum = (Mean + 2.453) * variance + (-0.023) *(Skewness + (-1.520) * (kurtosis + 2.021) * (energy + 0.001) * entropy + (-0.281)) - 28.785
Third Ventricle = (Mean + 0.687) * variance + (-0.003) *(Skewness + 2.124) * (kurtosis + (-2.148)) * (energy + 0.023) * entropy + (-0.083)) -6.36

References

[1]. Klein P, Rubinstein LJ (1989) Benign symptomatic glial cysts of the pineal gland: a report of seven cases and review of the literature. J NeurolNeurosurg Psychiatry 52:991–995

[2]. Surawicz TS, McCarthy BJ, Kupelian V et al (1999) Descriptive epidemiology of primary brain and CNS tumors: results from the Central Brain Tumor Registry of the United States, 1990-1994. NeuroOncol 1(1):14–25

[3]. Louis DN, Ohgaki H, Wiestler OD, Cavenee WK (2007) WHO classification of tumors of the central nervous system. IARC Press, Lyon.

[4]. Grosshans, M.; Vollmert, C.; Vollstaedt-Klein, S.; Nolte, I.; Schwarz, E.; Wagner, X.; Leweke, M.; Mutschler, J.; Kiefer, F.; Bumb, J.M. The association of pineal gland volume and body mass in obese and normal weight individuals: A pilot study. Psychiatr.Danub. 2016, 28, 220–224. [PubMed]

[5]. Bumb, J.M.; Schilling, C.; Enning, F.; Haddad, L.; Paul, F.; Lederbogen, F.; Deuschle, M.; Schredl, M.; Nolte, I. Pineal gland volume in primary insomnia and healthy controls: A magnetic resonance imaging study. J. Sleep Res. 2014, 23, 276–282. [CrossRef] [PubMed]

[6]. Bryden, M.M.; Griffiths, D.J.; Kennaway, D.J.; Ledingham, J. The pineal gland is very large and active in newborn antarctic seals. Experientia 1986, 42, 564–566. [CrossRef] [PubMed]

[7]. Cuello, A.C.; Tramezzani, J.H. The epiphysis cerebri of the Weddell seal: Its remarkable size and glandular pattern. Gen. Comp. Endocrinol. 1969, 12, 154–164. [CrossRef]

[8]. Tan, D.X.; Manchester, L.C.; Sainz, R.M.; Mayo, J.C.; León, J.; Reiter, R.J. Physiological ischemia/reperfusion phenomena and their relation to endogenous melatonin production: A hypothesis. Endocrine 2005, 27, 149–158. [CrossRef]

[9]. Haacke EM, Mittal S, Wu Z, Neelavalli J, Cheng YC. Susceptibility-weighted imaging: technical aspects and clinical applications, part 1. AJNR Am J Neuroradiol. 2009; 30(1):19–30. PubMed Central PMCID: PMC3805391. doi: 10.3174/ajnr.A1400 PMID: 19039041

[10]. Mittal S, Wu Z, Neelavalli J, Haacke EM. Susceptibility-weighted imaging: technical aspects and clinical applications, part 2. AJNR Am J Neuroradiol. 2009; 30(2):232–52. PubMed Central PMCID: PMC3805373. doi: 10.3174/ajnr.A1461 PMID: 19131406

[11]. Chen W, Zhu W, Kovanlikaya I, Kovanlikaya A, Liu T, Wang S, et al. Intracranial calcifications and hemorrhages: characterization with quantitative susceptibility mapping. Radiology. 2014; 270(2):496–505. PubMed Central PMCID: PMCPMC4228745. doi: 10.1148/radiol.13122640 PMID: 24126366

[12]. Buch S, Cheng YN, Hu J, Liu S, Beaver J, Rajagovindan R, et al. Determination of detection sensitivity for cerebral microbleeds using susceptibility-weighted imaging. NMR in biomedicine. 2016.

[13]. Nandigam RN, Viswanathan A, Delgado P, Skehan ME, Smith EE, Rosand J, et al. MR imaging detection of cerebral microbleeds: effect of susceptibility-weighted imaging, section thickness, and field strength. AJNR American journal of neuroradiology. 2009; 30(2):338–43. PubMed Central PMCID: PMC2760298. doi: 10.3174/ajnr.A1355 PMID: 19001544

MazinHassib. "Characterization of Pineal Region in MR Brain Images using Texture Analysis." IOSR Journal of Applied Physics (IOSR-JAP) , vol. 10, no. 5, 2018, pp. 32-37.

Image sample:

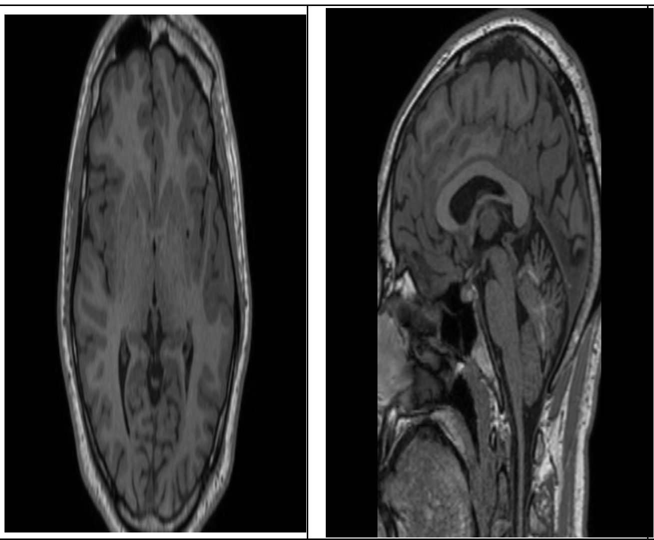	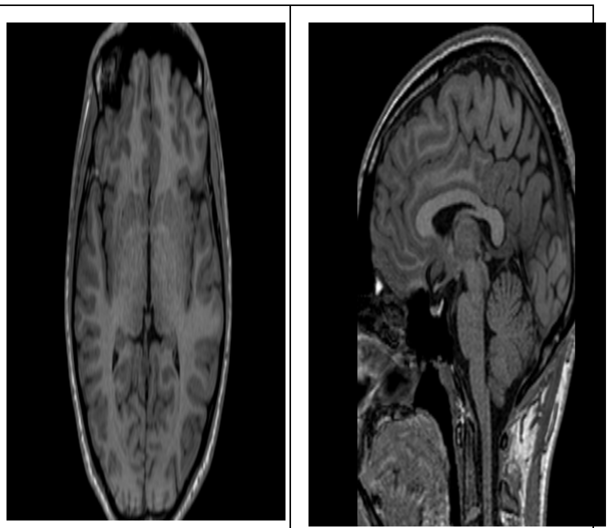
Case 1 MRI 3D T_1 –FEE (axial , sagittal)	**Case 2 MRI 3D T_1 –FEE (axial , sagittal)**
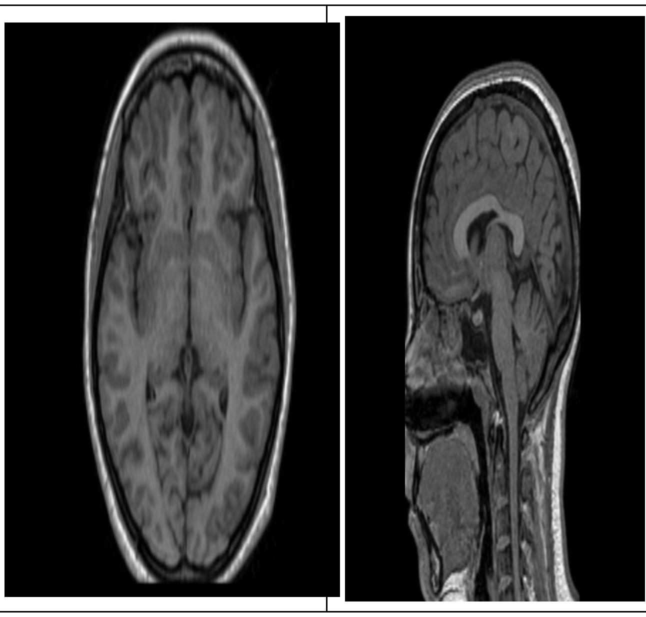	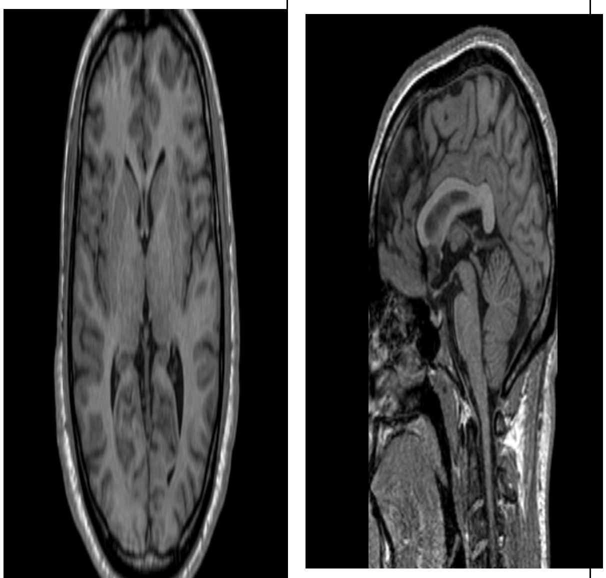
Case 3 MRI 3D T_1 –FEE (axial , sagittal)	**Case 4 MRI 3D T_1 –FEE (axial , sagittal)**

samples Pineal region feature values:

1- Corpus c.:

Mean	*Var*	*shkewlness*	*khurtosis*	*energy*	*entropy*
116	2.75	-0.292375	-1.2663	146.444	795.541
116.111	1.11111	0.381807	-1.33038	142.333	796.454
106.556	1.77778	0.457172	-1.16725	148.556	717.712
110.556	2.77778	0.778071	-0.653574	79.2222	750.537
103.222	3.94444	-0.186308	-1.46956	105.444	690.541
110.222	0.694444	-0.346071	-1.63277	60.6667	747.781
104.333	0.25	0.592579	-1.81483	48.3333	699.562
104.667	1	-0.0740673	-1.37037	90.2222	702.284
103.111	0.611111	-0.149324	-1.53566	108	689.617
96.1111	0.611111	-0.149324	-1.53566	78.7778	633.052
121.667	0.75	0.57023	-1.55143	40.7778	842.763
130.333	1	0.0740876	-1.37037	6.33333	915.735
122.111	1.61111	-0.179778	-1.39415	36.1111	846.489
121.444	0.527778	-0.70121	-1.02689	43.4444	840.903
119.111	1.11111	-0.756613	-0.85036	80	821.416
125.778	0.444444	0.175922	-1.12037	5.33333	877.269
134.778	6.44444	-0.0239735	-1.62602	51.6667	953.508
127.222	3.94444	-0.186308	-1.46956	4.11111	889.457
128.333	2.5	0.187403	-1.31703	2.33333	898.827
133.111	12.1111	-0.636145	-1.4781	36.8889	939.356
93.5556	5.52778	-0.651861	-0.986641	110.444	612.617
96.4444	0.527778	-0.70121	-1.02689	114.444	635.729
98.6667	0.5	0.419036	-1.22222	92.8889	653.62
104	2	0.235702	-1.55556	122.667	696.858
101.111	0.111111	2.07405	2.62954	211.111	673.38
103	1.5	0	-1.22222	114.333	688.719
90.3333	12.25	0.00172573	-1.76743	149.667	587
122.556	8.27778	0.0610515	-1.34533	37	850.247
128.222	1.44444	0.396651	-1.55973	1.33333	897.884
130.222	2.44444	0.373987	-1.16377	7.11111	914.801
129.667	2	0.288071	-1.55556	4.55556	910.097
127.111	1.11111	0.381807	-1.33038	1.77778	888.505
191.444	2.02778	-0.247024	-1.43718	101.667	1451.31
183.889	3.61111	-0.24867	-1.80682	140.111	1383.35
183	3	0	-1.81481	211.667	1375.38
184	6	0	-1.22222	69.3333	1384.36
180.333	4.75	0.0715589	-1.26326	126.111	1351.53
109.556	0.527778	-1.03752	-0.495015	84.6667	742.299
99.2222	17.4444	-0.184732	-1.30789	47.2222	658.214
93.3333	16.75	-0.0280959	-1.54235	135.778	610.918
90.1111	25.6111	0.0194507	-1.80073	93	585.331
109.222	0.444444	-0.175922	-1.12037	97	739.56
139.444	0.777778	0.147991	-1.04384	131.667	993.343
145.111	0.861111	-0.181975	-1.94061	37.5556	1042.05

134.556	8.77778	0.155601	-1.66007	50.7778	951.627
142.333	4	-0.324067	-1.45371	123.667	1018.15
141.556	3.02778	0.107269	-1.47306	129.556	1011.46
113.889	1.11111	-0.381807	-1.33038	171.667	778.036
107.778	0.194444	-1.1199	-0.798934	153.111	727.708
111.778	3.69444	-0.00309196	-1.75411	95.7778	760.612
114.333	3.25	-0.4425	-1.81481	104.333	781.727
95.7778	38.4444	-0.182194	-1.76938	162.222	630.632
130.222	6.19444	-0.0946769	-1.78679	10.4444	914.82
125.778	11.1944	0.0112796	-1.52566	14.8889	877.323
144	1.25	-0.477028	-1.43556	86.4444	1032.47
146.556	1.02778	-0.452883	-1.27979	89.2222	1054.52
139.556	2.77778	0.202071	-1.26797	136	994.304
130.222	6.19444	-0.0946769	-1.78679	10.4444	914.82
125.778	11.1944	0.0112796	-1.52566	14.8889	877.323
144	1.25	-0.477028	-1.43556	86.4444	1032.47
146.556	1.02778	-0.452883	-1.27979	89.2222	1054.52
139.556	2.77778	0.202071	-1.26797	136	994.304
98.8889	6.86111	0.14411	-1.46747	114	655.454
97.1111	5.11111	0.224602	-1.35147	133.778	641.119
97	5	-0.178885	-1.70222	112.111	640.225
101.444	1.77778	0.105327	-1.91724	109.444	676.092
93.5556	7.52778	-0.166307	-1.47979	112.222	612.63
110.222	2.44444	-0.323748	-1.65963	62.2222	747.792
113	0.75	0	-1.81481	140.333	770.684
111	0.75	0	-1.81481	33.6667	754.185
107	0	NaN	NaN	185	721.337
105.444	13.7778	0.0917888	-1.54493	122.778	708.706
158.333	11.5	0.0531876	-1.24015	105.444	1156.96
163.111	2.11111	0.483869	-0.661234	125.333	1198.83
164.556	1.77778	0.457172	-1.16725	114.778	1211.54
161.111	1.36111	-0.184869	-0.878906	102	1181.26
99.6667	-92.5	0.000831921	-1.77082	117	662.287
86.1111	0.111111	2.07405	2.62954	218.778	553.534
82.4444	0.277778	0.187403	-2.17037	141.333	524.79
85	0.5	0	-1.22222	114.333	544.802
66.1111	43.1111	0.0565328	-1.7587	113.889	400.18
75.6667	0.5	0.419036	-1.22222	179.222	472.284
199.667	3.25	-0.0126503	-1.6465	104.333	1525.75
203.333	0.5	-0.419007	-1.22223	185.778	1559.1
200.444	2.02778	0.445603	-1.32908	158.444	1532.82
176.333	54.5	-0.0600172	-1.80399	109	1316.03
193.778	21.1944	-0.372209	-1.75702	107.333	1472.44
130.556	1.52778	0.0639205	-1.80541	7.88889	917.62
126.556	4.52778	0.796749	-0.541888	6.11111	883.84
123	0	NaN	NaN	25	853.929
115.333	7.75	-0.274668	-1.60762	110.444	790.038
102.889	18.6111	-0.0323227	-1.4809	106.667	687.923

145.333	0.25	0.59262	-1.81479	44.6667	1043.96
144.556	4.27778	0.0806188	-1.79473	107.222	1037.27
142.444	6.02778	-0.413585	-1.73266	100.222	1019.11
142.778	0.444444	0.175953	-1.12036	190.333	1021.95
138.667	1	-0.0740876	-1.37037	114.667	986.684
214.111	6.11111	0.019791	-1.76178	224.111	1657.71
213	6	0	-1.22222	147.667	1647.51
224.444	1.77778	-0.457172	-1.16725	115.556	1752.96
223.222	0.694444	-0.346096	-1.63276	51	1741.66
199.889	81.3611	-0.356101	-1.28608	91.8889	1528.02
151.778	0.694444	0.346096	-1.63276	54	1099.76
158.556	4.02778	-0.690669	-1.42383	55.4444	1158.87
154.222	9.94444	0.350283	-1.16127	99.1111	1121.06
143.111	2.11111	-0.385496	-1.59197	88	1024.83
148.111	19.6111	-0.249879	-1.80273	165.889	1068.05
170.778	2.94444	-0.092299	-1.44584	154.333	1266.49
169.222	3.19444	-0.644865	-1.30291	166.111	1252.73
176	30	0	-1.60148	112	1312.97
177.556	2.77778	-0.0859286	-1.57517	97.3333	1326.73
171.222	0.194444	1.11985	-0.799011	76.3333	1270.42
164.556	37.7778	0.0735737	-1.37324	118.333	1211.68
139.444	9.52778	-0.235825	-1.2053	111	993.383
144.889	28.8611	0.127542	-1.65954	111.778	1040.26
136.111	101.611	-0.456261	-1.02824	99.2222	965.329
158	4.25	-0.532627	-1.68358	135.778	1154.01
96.8889	4.11111	-0.426873	-1.70931	118.222	639.325
99.5556	4.27778	-0.371479	-1.30898	101.778	660.821
98.3333	1	0.0740673	-1.37037	113	650.935
93.1111	2.36111	-0.162586	-1.64552	110	609.045
97.8889	4.61111	-0.681041	-1.20605	85.8889	647.377
195.889	4.11111	0.0529939	-1.60412	89.8889	1491.49
195.333	3.25	0.0126503	-1.6465	99.3333	1486.46
202.222	2.19444	0.0750992	-1.64276	134.889	1548.99
190.111	7.11111	-0.0701712	-1.47486	81	1439.3
176.444	125.028	-0.371832	-1.15081	97.1111	1317.28
90.6667	5.5	-0.160795	-1.53566	118.667	589.599
96.7778	1.19444	-0.130302	-1.61483	94.1111	638.413
84.5556	7.02778	-0.216175	-1.70739	101.667	541.364
84	3.5	0	-1.22222	147.111	536.981
79.4444	9.52778	0.12687	-1.70795	119	501.52
175.889	110.111	-0.132836	-1.29768	144.111	1312.27
180.222	20.4444	-0.0566599	-1.74596	128.444	1350.59
182.111	18.6111	-0.0174971	-1.66054	100.111	1367.48
175.111	82.8611	-0.646687	-0.829146	131.333	1305.26
148.222	188.944	-0.45399	-1.72389	64.8889	1069.75
173.556	10.2778	0.723057	-0.846427	121.778	1291.16
161.556	2.52778	-0.00682929	-1.37858	104.222	1185.16
166.444	2.02778	-0.247024	-1.43718	114.444	1228.18

180.667	7.75	-0.528735	-1.81481	135.333	1354.52
174.556	32.5278	-0.433774	-1.71361	119.889	1300.13
168.333	4.75	0.0715589	-1.26326	151.889	1244.87
169	0.75	0	-1.81481	145.667	1250.75
162	5	0.178885	-1.70222	79.5556	1189.08
164.556	1.02778	0.18694	-1.42004	85.6667	1211.53
155.333	5.5	-0.459417	-1.18305	97.7778	1130.73
170.222	4.94444	-0.550476	-1.0699	137.333	1261.58
164.556	2.27778	0.293683	-1.66781	143.667	1211.54
162.111	1.86111	0.0885983	-1.42829	84.3333	1190.04
178.222	2.44444	0.373987	-1.16377	135.111	1332.67
160.778	44.1944	-0.322287	-1.25742	146.556	1178.51
97.2222	1.69444	-0.359466	-1.44024	95.4444	641.99
103.778	1.19444	-0.130302	-1.61483	75.7778	695.044
96.6667	1.75	0.255981	-1.23431	101.556	637.523
98.1111	0.861111	0.65232	-0.542076	126.111	649.143
102.222	1.19444	0.130302	-1.61483	153.556	682.399
204.111	3.61111	0.151519	-1.68185	135.667	1566.2
212.111	6.86111	-0.14411	-1.46747	168.778	1639.36
210.556	1.77778	0.457172	-1.16725	132.556	1625.09
211.444	1.27778	0.121566	-1.58965	137.444	1633.23
209.111	6.11111	0.019791	-1.76178	156	1611.87
171.333	0.25	0.59262	-1.81479	86	1271.41
172.667	0.25	-0.59262	-1.81479	203.333	1283.23
171.222	0.944444	0.346715	-1.1074	133.889	1270.43
159.111	3.61111	-0.139934	-1.30694	89.3333	1163.74
158.333	6.25	-0.165921	-1.22317	100.778	1156.94
151.778	12.1944	-0.0857455	-1.7508	92.6667	1099.81
145.111	33.1111	-0.229368	-1.60869	94.6667	1042.19
146.444	5.27778	-0.266543	-1.76616	117.333	1053.58
154.889	5.61111	-0.284428	-1.46644	102.222	1126.85
139.444	22.7778	-0.913498	-0.114739	94.3333	993.445
201.444	5.02778	-0.0829817	-1.64204	136.333	1541.92
205.778	6.69444	-0.475958	-1.16494	110.444	1581.41
192.667	7	-0.363971	-1.37037	63.5556	1462.36
210.222	4.44444	-0.827764	-0.887859	165.333	1622.04
197	11	-0.0913671	-1.4977	105.889	1501.58
92.5556	0.527778	0.70121	-1.02689	90.5556	604.599
90.1111	3.61111	-0.139934	-1.30694	130.333	585.174
71.2222	42.6944	-0.388653	-1.07671	104.333	438.711
85.7778	1.94444	-0.882321	-0.759756	191.556	550.925
83.2222	1.44444	-0.371379	-0.991673	157.444	530.877
79	189.5	-0.239205	-1.25698	66.3333	499.578
173	9.75	0	-1.30988	127.889	1286.23
168.111	11.1111	0.184071	-1.12517	139.667	1242.93
176.778	5.69444	0.183732	-1.05218	137.222	1319.81
176.778	5.69444	0.183732	-1.05218	137.222	1319.81
143.444	2.02778	-0.247024	-1.43718	126.556	1027.7

2- Pineal Gland:

Mean	*Var*	*shkewlness*	*khurtosis*	*energy*	*entropy*
62.8889	31.6111	0.0220737	-1.72595	86.2222	376.067
72.5556	1.02778	-0.452883	-1.27979	173.667	448.476
70.4444	0.527778	-0.70121	-1.02689	127.333	432.422
65	4	-0.416667	-1.52778	75.6667	391.494
66.6667	1.75	0.255981	-1.23431	94	403.943
64.5556	8.77778	0.155601	-1.66007	79.2222	388.225
66.2222	5.19444	0.264644	-1.35035	94.8889	400.644
61	24.25	-0.0390786	-1.4329	73.2222	362.031
77.4444	2.27778	0.0941741	-1.09672	111.667	485.99
84	7.25	0	-1.5076	122	537.01
65.1111	5.11111	-0.41004	-1.27774	62.6667	392.334
59.2222	8.69444	-0.192731	-1.74049	73.2222	348.799
70	3	-0.3849	-1.37037	95.5556	429.077
62.4444	4.77778	0.321812	-1.59536	63.5556	372.499
58.3333	10.5	-0.148043	-1.5071	112.556	342.314
49.3333	0.75	0.456182	-0.761314	102	277.485
56.3333	7	0.0040009	-1.73318	136.111	327.71
52.1111	11.6111	0.0843193	-1.73346	109	297.359
52.3333	1.5	0.161286	-1.74897	123.222	298.824
57.8889	2.61111	-0.474666	-1.24905	110.778	338.981
83.7778	7.69444	0.641026	-1.13604	142	535.272
56.8889	46.1111	-0.0738185	-1.43243	120	332.19
72.4444	91.5278	0.0501111	-1.25174	124.222	448.433
98.8889	19.3611	-0.372177	-1.33751	125.111	655.536
104.111	6.61111	-0.344098	-1.59549	121.444	697.791
39.7778	24.6944	-0.0726143	-1.59481	96.6667	211.776
36.7778	27.9444	0.241547	-1.22437	97.4444	191.757
44.6667	22.25	0.00776291	-1.30369	137.556	245.144
50.3333	6.5	-0.491686	-1.81131	149.889	284.64
44	3.5	0	-1.22222	147.111	240.266
64.1111	9.61111	-0.0918938	-1.25556	79.6667	384.923
68.8889	3.86111	-0.6545	-0.877026	112.667	420.686
68	7.5	0	-1.60148	79.5556	414.018
74.4444	1.52778	-0.416956	-0.726406	138.889	462.916
71.7778	2.44444	-0.374	-1.16376	119.556	442.565
89.2222	8.69444	-0.582796	-1.74637	89.2222	578.163
88.7778	3.94444	-0.494492	-1.08868	119.667	574.61
94.2222	0.944444	0.346736	-1.10739	117.778	617.915
58.1111	20.6111	0.00715412	-1.76807	124.111	340.802
43.5556	13.0278	0.178998	-1.65087	116.667	237.342
135.222	1.44444	-0.371396	-0.991663	53.4444	957.271
111.222	47.9444	0.0817322	-1.47829	125	756.287
134.444	12.2778	-0.267964	-1.56734	52.4444	950.697
133.778	1.44444	0.371396	-0.991663	34.6667	944.972
134.556	0.277778	-0.187403	-2.17037	43.2222	951.586
123	101	0.0426914	-1.77446	57.8889	854.456

131.556	40.0278	-0.0378414	-1.63406	48.2222	926.284
126.333	19.75	-0.189046	-1.72822	20.3333	882.045
132.778	0.694444	0.346096	-1.63276	23.4444	936.468
134.667	0.5	0.419007	-1.22223	44.8889	952.533
74.8889	27.3611	0.0838282	-1.77661	142.889	466.543
90	1.25	0	-0.582222	136.667	584.276
91.5556	8.77778	-0.562176	-1.74467	141.333	596.691
73.2222	3.19444	-0.528088	-1.23033	187.444	453.582
68.6667	13.5	-0.355419	-1.80425	90.6667	419.099
75	25	-0.314667	-1.18738	129	467.377
55.3333	144.25	0.0300575	-1.45419	89.5556	322.075
86.7778	13.6944	-0.0939806	-1.6187	147	558.885
65.6667	54.5	-0.271374	-1.62144	122.333	396.976
87.3333	5.75	-0.204152	-0.936567	122.889	563.208
65.2222	12.1944	0.0857513	-1.7508	111.889	393.233
71.7778	4.94444	0.0653763	-1.70013	121.778	442.588
77.1111	0.611111	-0.149324	-1.53566	115.556	483.404
72.8889	1.86111	0.436548	-1.2572	166	451.026
75.5556	2.52778	0.988465	-0.265677	164.222	471.448
85.7778	5.19444	-0.095708	-1.43271	137.556	550.949
88.7778	5.69444	-0.1597	-1.55017	92.7778	574.622
84.3333	11.25	-0.22183	-1.38873	153.222	539.653
90.6667	1.25	-0.371016	-1.43556	114.889	589.569
93.1111	0.361111	0.0126277	-0.636643	165.111	609.031
31	44	0.0616728	-1.72429	118.333	154.496
41.3333	27.5	-0.0842379	-1.47611	140	222.359
40.5556	14.2778	0.0599029	-1.80526	121.444	216.867
51.6667	11	-0.452776	-1.55647	119.222	294.182
46.2222	2.44444	0.374	-1.16376	119.111	255.666
59.1111	1.86111	0.613752	-0.0596094	110.889	347.91
68.5556	5.77778	0.0353583	-1.59966	97	418.188
74.4444	-26.7778	0.00514686	-1.68765	161.333	463.133
59.1111	-36.1111	0.00271799	-1.73059	84.4444	348.283
69.3333	4.25	-0.0930017	-1.38831	117.556	424.046
79.3333	121.5	-0.504038	-1.7477	115.556	501.595
66.4444	17.0278	0.163795	-1.56676	106.444	402.424
71.8889	15.8611	0.3154	-1.13738	90.5556	443.53
97.2222	8.69444	-0.400766	-1.32501	73.2222	642.037
94.6667	17.5	-0.137608	-1.55504	102.667	621.585
20	42.75	0.200347	-1.81481	96.6667	87.8074
25.2222	6.94444	0.478831	-1.27335	101.889	117.624
36	51.5	-0.15513	-1.39918	90.2222	187.057
45.5556	28.2778	-0.0277691	-1.3208	137.778	251.391
39.1111	19.8611	0.349008	-1.23905	125.111	207.201
143	2	-0.942809	-0.555555	84.5556	1023.87
97.1111	-7.86111	0.00996109	-1.62054	136.222	641.137
138	9	0	-1.05761	108	981.018
126	20.75	-0.592462	-1.73086	22.4444	879.244

127	4.25	0.228269	-1.38831	4.77778	887.584
62.4444	11.0278	-0.146908	-1.47679	97.5556	372.564
76.7778	12.9444	-0.111809	-1.47507	132.111	480.938
70.6667	23	0.0920029	-1.78933	93.3333	434.311
83.5556	9.27778	-0.425607	-1.74629	106.222	533.546
78.5556	16.5278	0.0877837	-1.79955	155.444	494.692
78.5556	30.2778	-0.186902	-1.57632	139.222	494.806
80.1111	13.6111	-0.0781289	-1.24596	115.222	506.726
82.7778	24.6944	-0.0726143	-1.59481	189.667	527.583
92.8889	0.361111	-0.0126277	-0.636643	152.222	607.257
92.2222	0.694444	-0.346071	-1.63277	114.444	601.943
83.4444	212.028	-0.0430575	-1.36253	154.111	534.254
144.889	7.11111 -0	0.000141294	-1.69752	120.889	1040.16
145	4.75	-0.321987	-1.80825	122.556	1041.11
140	17	-0.466049	-1.78047	102.222	998.178
141	2.75	-0.292375	-1.2663	171.444	1006.69
52.4444	24.5278	0.169748	-1.40961	126.889	299.899
64.5556	40.0278	-0.264235	-1.52792	78.5556	388.541
104.444	7.52778	-0.188752	-1.32032	106.444	700.513
102.889	4.61111	-0.277069	-1.12244	122.667	687.835
67.6667	31	-0.232177	-1.24088	112.111	411.735
111	43	-0.555615	-1.79887	156.556	754.432
116.111	0.611111	-0.149324	-1.53566	141.889	796.452
118.556	1.77778	0.457172	-1.16725	90.7778	816.789
117.667	3.5	-0.384626	-1.6576	109.889	809.397
112.444	0.277778	0.187403	-2.17037	100	766.093
44.4444	93.2778	0.138167	-1.65197	124	244.632
34.4444	167.278	0.00282054	-1.77781	83.5556	179.103
38.4444	9.02778	-0.651656	-1.37102	120.667	202.552
35.7778	64.9444	-0.455491	-1.80488	143.111	185.873
48.6667	84.75	-0.125133	-1.5494	139.778	273.908
31.6667	4.5	-0.240551	-1.43439	96.5556	157.947
31	19.5	0	-1.72715	125	153.985
46.8889	8.86111	0.171198	-1.64179	101.556	260.409
48.4444	1.52778	-0.0639205	-1.80541	129.556	271.225
42.1111	23.6111	-0.0367774	-1.70372	116.111	227.598
134.444	28.7778	-0.464769	-0.847064	67.1111	950.777
140	1.25	-0.477028	-1.43556	145.111	998.105
122.444	16.5278	-0.693009	-0.417139	45.5556	849.36
117.222	66.1944	-0.193755	-1.23367	61.2222	806.045
119.444	39.0278	0.126195	-1.27441	79.4444	824.399
42.2222	3.19444	0.172507	-1.57876	164.222	228.045
26.4444	23.0278	0.16649	-1.57497	122.444	125.504
40.3333	4.75	0.0715542	-1.26326	151.889	215.209
38.2222	2.19444	-0.129966	-1.79658	126	200.946
43.6667	0.25	-0.592599	-1.81481	115	237.92
103.556	10.5278	0.198698	-1.3655	94.8889	693.293
78.5556	96.2778	-0.111059	-1.53909	141	495.351

98.8889	49.1111	-0.343509	-1.18903	151.556	655.731
97.3333	3	-0.584482	-1.10699	89.7778	642.893
103.111	4.86111	0.062454	-1.65785	140.222	689.643
91.7778	24.1944	-0.32385	-1.71377	82	598.568
100.333	0.5	-0.419036	-1.22222	111.667	667.085
93	70	-0.235631	-1.78376	121	608.629
108	22.25	-0.438291	-1.03437	106.889	729.661
95.3333	2.5	0.18739	-1.31704	102.222	626.825
89	15	-0.0344265	-1.56	140.556	576.448
109.667	10	-0.381814	-1.75704	117.444	743.268
115.556	1.02778	0.18694	-1.42004	155.778	791.844
91.8889	30.3611	0.053119	-1.79408	107.889	599.494
110.222	13.1944	-0.35347	-1.80892	128.667	747.855
112.111	7.11111	-0.0701712	-1.47486	116.556	763.381
105.111	-36.1111	0.00271968	-1.73059	100.889	706.123
109.556	16.2778	0.0446975	-1.23865	127.111	742.391
118.222	2.94444	0.0923108	-1.44584	98.2222	814.018
110.889	8.61111	-0.167196	-1.41915	129.778	753.315
51.6667	27.5	0.0842379	-1.47611	105.444	294.385
63.4444	6.27778	-0.958953	-0.311872	77	379.933
48.4444	18.2778 0	0.000352148	-1.4761	144.444	271.447
66.3333	1	0.0740673	-1.37037	77.4444	401.437
68.5556	2.77778	0.778071	-0.653574	94.3333	418.16
94.8889	168.361	-0.165201	-1.77927	108.222	624.398
134	48	-0.186436	-1.29225	50.2222	947.087
116.222	77.6944	-0.0289555	-1.34058	94	797.8
114.333	133.5	-0.194299	-1.54718	77.8889	782.465
110	139.25	-0.0507138	-1.54817	78	746.766
126.556	0.777778	-0.147991	-1.04384	2.77778	883.821
93.3333	117.75	0.0910168	-1.6186	140.222	611.612
102.667	45.75	-0.190542	-1.60729	85.1111	686.288
114.778	4.69444	0.383822	-1.49712	150.556	785.416
114.333	3.25	0.012639	-1.6465	132.778	781.727
27.6667	58.75	-0.0579022	-1.80091	49.6667	133.92
36.5556	60.7778	0.149864	-1.54165	110.333	190.863
74.3333	45.75	0.190542	-1.60729	76.3333	462.444
73.3333	29.5	0.0628729	-1.39654	113.333	454.66
66.7778	29.9444	-0.116765	-1.56011	105.444	405.049
125	14.25	-0.780777	-1.18447	21.6667	870.797
114.111	28.1111	-0.184864	-1.26288	104.111	780.028
120.667	11.5	-0.224129	-1.46867	64	834.457
127.556	0.527778	0.70121	-1.02689	0.666667	892.251
95.8889	114.611	-0.145193	-1.52825	137.444	632.038
32.2222	26.4444	-0.0401466	-1.73574	151.556	161.964
25.4444	21.2778	0.0591463	-1.65781	125.889	119.346
46	8	-0.500867	-1.74306	103.556	254.197
11.3333	3.25	0.0126432	-1.6465	131.333	39.8799
43.3333	10	-0.187393	-1.31704	123.111	235.77

3- Tectum :

Mean	*Var*	*shkewlness*	*khurtosis*	*energy*	*entropy*
81.2222	1.19444	-0.891084	-0.78411	84.3333	515.267
43.7778	49.9444	0.17958	-1.20576	112	239.412
64.7778	7.44444	-0.187071	-1.09949	78.3333	389.87
55.7778	16.1944	-0.132186	-1.26691	138.889	323.789
67.7778	1.44444	-0.396668	-1.55972	72.4444	412.288
88.4444	14.5278	0.201156	-1.31025	98.4444	572.049
80.1111	23.6111	-0.0367795	-1.70372	152.556	506.806
87	4.75	-0.386384	-1.1582	149.222	560.571
87.7778	2.19444	0.335046	-1.39665	140.667	566.69
80.2222	9.69444	0.14797	-1.74294	101.111	507.557
79.6667	4.75	-0.0715495	-1.26326	121.667	503.205
73.5556	20.5278	0.143063	-1.44538	166.444	456.279
78	5.5	-0.20674	-1.33976	144	490.307
75.2222	3.69444	-0.0907906	-1.41763	115	468.898
76.5556	1.77778	-0.386577	-1.02662	145	479.133
92.5556	6.52778	-0.277012	-1.21167	67.4444	604.641
95.7778	3.69444	0.278556	-1.3308	102.889	630.398
91.6667	0.5	0.419036	-1.22222	69	597.517
91.7778	2.69444	0.614711	-0.959276	119.778	598.417
95.2222	4.94444	-0.429194	-0.900228	83.2222	625.951
91.6667	1	-0.0740673	-1.37037	97.8889	597.52
75.7778	58.9444	-0.145726	-1.34651	105.778	473.637
93.4444	1.52778	-0.769992	-0.789879	114.556	611.701
89.2222	3.19444	-0.528088	-1.23033	169.667	578.123
96.2222	4.44444	-0.685452	-0.677871	103.556	633.97
56.8889	13.8611	-0.0904829	-1.54259	119.778	331.823
42.5556	30.0278	-0.203196	-1.5703	102.556	230.739
57.6667	7.25	-0.29977	-1.7359	89.2222	337.412
53	15.25	-0.716447	-0.705754	177.222	303.768
40.3333	34.5	-0.261728	-1.21127	149.889	215.695
86.6667	6	-0.246962	-1.63786	149.333	557.953
84.1111	8.86111	0.334281	-1.37764	85.2222	537.893
73.8889	2.36111	0.162586	-1.64552	142.556	458.67
83.3333	6	0.60985	-1.09465	151.556	531.781
71.5556	0.777778	-0.147991	-1.04384	114.667	440.86
57	68.5	-0.0799616	-1.48895	124.111	333.253
79.5556	44.5278	-0.0748825	-1.55488	110.889	502.666
85.5556	2.02778	0.0161486	-0.752618	125.111	549.178
85.5556	2.02778	0.0161486	-0.752618	125.111	549.178
79.3333	2.5	-0.824539	-0.463699	95.1111	500.602
98.8889	11.3611	-0.646142	-0.678101	146.444	655.484
98.4444	11.2778	-0.589935	-1.04471	115.556	651.898
81.8889	38.6111	-0.119494	-1.46323	112.556	520.757
93.8889	15.6111	-0.186185	-1.66606	125	615.35
87	10.25	-0.101576	-1.30154	154.111	560.612
152.556	34.5278	-0.490102	-1.32767	150.111	1106.66

149.222	22.6944	-0.677416	-1.03378	129.222	1077.68
142	13	-0.355577	-1.53517	122.222	1015.32
125	52	-0.147564	-1.42719	55.2222	870.991
136.556	77.0278	-0.0597572	-1.28633	84.7778	968.998
86.5556	7.77778	-0.359835	-1.5067	160.111	557.091
83.7778	0.944444	-0.346736	-1.10739	136	535.221
74.3333	17	-0.296963	-1.25759	164.556	462.199
82.4444	12.5278	-0.386944	-1.22062	152.222	524.886
84	3	0	-1.81481	146.667	536.978
98.1111	9.86111	-0.542919	-0.988507	77.2222	649.202
70.2222	64.1944	0.0405123	-1.42098	95.7778	431.32
96.1111	28.3611	-0.107879	-1.63584	131.889	633.238
95.2222	1.19444	0.130302	-1.61483	79.8889	625.925
95.2222	1.19444	0.130302	-1.61483	79.8889	625.925
78.1111	16.1111	-0.0618144	-1.6527	142.333	491.253
77.5556	29.7778	-0.0188598	-1.4191	124.889	487.075
78.4444	7.52778	-0.608368	-0.789606	101.556	493.76
82.5556	10.2778	0.116068	-1.7889	140.111	525.735
82.5556	10.2778	0.116068	-1.7889	140.111	525.735
99.7778	56.1944	-0.0353969	-1.44599	50	662.951
105.222	38.9444	-0.233986	-1.44465	126.778	707.048
118.889	6.36111	0.692394	-0.771217	88.6667	819.591
104.222	9.69444	-0.647139	-0.834973	147.333	698.716
106.556	22.7778	-0.276218	-1.2158	110.333	717.839
50.2222	25.1944	-0.137476	-1.45938	126.889	284.093
65	4	0.0833333	-1.52778	75.6667	391.493
57.3333	9.25	0.144817	-1.81481	138	335.005
57.8889	3.61111	-0.151524	-1.68185	54.7778	338.992
46.4444	20.5278	-0.143063	-1.44538	155.778	257.469
89.3333	6.25	-0.251262	-1.31419	106.889	579.026
86.1111	4.11111	-0.852773	-0.797683	108.556	553.564
86.1111	4.11111	-0.852773	-0.797683	108.556	553.564
85	5.5	-0.62022	-1.51607	175.667	544.84
66.8889	35.1111	-0.113945	-1.30544	96.4444	405.932
134.333	25	-0.234071	-1.7885	62.3333	949.813
124.333	54	-0.404142	-1.22796	33	865.401
110.111	6.61111	-0.26566	-1.60905	126.778	746.902
125.222	8.94444	-0.514228	-1.76002	15.6667	872.638
110.556	9.27778	-0.23688	-1.01654	85	750.574
40.3333	29.25	-0.558621	-1.07854	116.778	215.615
32.4444	40.7778	-0.263594	-1.49926	150.222	163.699
37.6667	10.5	-0.753284	-0.668597	148.111	197.377
44.1111	1.11111	0.381817	-1.33037	126.333	240.998
30.7778	31.1944	-0.082607	-1.56667	121.667	152.819
147.444	17.5278	-0.705216	-0.821538	80.7778	1062.27
147.333	31	-0.285392	-1.41107	116.889	1061.37
159.444	10.5278	0.250183	-1.31069	116.333	1166.68
149	15.5	-0.349592	-1.31102	113.444	1075.72

136.889	35.6111	-0.390059	-1.75056	110.667	971.649
68.5556	61.0278	-0.22799	-1.25272	89.2222	418.713
83.1111	2.61111	-0.15736	-0.292958	168.444	530.017
91.4444	12.7778	-0.221577	-1.06428	153	595.834
80.2222	18.1944	-0.196336	-1.44639	108.667	507.626
62.7778	50.9444	-0.0770646	-1.28705	89.4444	375.445
114.778	9.69444	-0.545525	-1.00522	126.556	785.444
101.889	51.1111	-0.296381	-1.51757	129.889	680.01
118	14.75	-0.305981	-0.929586	84.6667	812.232
109.778	18.4444	0.0848184	-1.63151	120.889	744.23
106.444	1.52778	-0.416956	-0.726406	181.556	716.802
159.111	14.1111	-0.0390782	-1.87232	127.111	1163.78
156.889	7.61111	-0.215318	-1.03897	73.3333	1144.32
145.333	55.5	-0.30886	-1.1672	65.3333	1044.21
144.111	79.1111	-0.11748	-1.57914	102.333	1033.78
135.778	106.194	-0.162606	-1.48873	98	962.504
106	34.75	-0.344971	-1.68477	116.667	713.371
109.889	14.8611	0.482233	-1.21666	142.111	745.122
108	3.75	-0.734432	-0.677037	118.889	729.55
107.667	32.5	-0.435779	-1.03764	129.444	726.991
91.1111	67.3611	-0.238487	-1.38163	112.222	593.572
111.333	34.5	-0.261729	-1.21127	137.778	757.127
99.1111	73.6111	-0.0343619	-1.22668	103.556	657.681
101.111	84.6111	-0.0320716	-1.2261	172.444	673.918
130.444	4.52778	0.171996	-1.0911	10	916.693
128	3.75	0	-1.43556	3.33333	896.019
79.3333	219.5	-0.440389	-1.49092	88.8889	502.431
78	119.75	-0.350013	-1.15139	103.333	491.271
79.1111	346.111	-0.149987	-1.53976	109.333	501.75
79.8889	165.361	-0.595261	-1.01864	129.222	506.282
90	101	-0.474859	-1.16693	111.556	585.004
58.3333	3	0.955125	-0.5144	105.889	342.23
56.2222	23.9444	-0.136369	-1.38857	110.222	327.099
72.3333	6	-0.297369	-1.34156	145.889	446.827
65.2222	3.94444	-0.186308	-1.46956	76.1111	393.152
40.8889	47.6111	0.0588412	-1.33315	121.333	219.655
135.444	40.0278	-0.420212	-1.57526	91	959.349
155.111	23.6111	-0.507452	-1.49564	101.778	1128.87
154.444	12.7778	-0.878385	-0.615136	113.333	1123.01
150.778	2.19444	-0.280179	-0.935188	122.556	1091.08
149	5.5	-0.62022	-1.51607	104.556	1075.68
64.3333	16	-0.207178	-1.60474	85.4444	386.643
57	15	0	-1.43556	161.889	332.644
56.5556	6.27778	-0.482096	-1.33434	132.111	329.315
60.7778	5.19444	-0.433579	-1.56448	114.556	360.192
46.5556	22.0278	-0.363527	-1.14714	139	258.267
135.889	10.1111	0.566682	-1.02645	71.2222	962.995
132.667	38	0.447451	-1.39674	55.5556	935.703

4- Third ventricle:

Mean	***Var***	***shkewlness***	***khurtosis***	***energy***	***entropy***
33.2222	82.6944	0.164727	-1.49531	96.3333	169.51
22.3333	79.25	0.373046	-1.34229	142.556	102.328
14.2222	39.4444	0.616949	-1.20837	123.556	56.1599
14.2222	39.4444	0.616949	-1.20837	123.556	56.1599
27.5556	78.5278	0.202209	-1.54138	118	133.666
48.5556	40.5278	0.0400873	-1.81083	89.6667	272.523
40.6667	32	0.0781576	-1.79644	117.778	217.9
30.3333	13.75	0.0145278	-1.55153	79	149.618
23.7778	6.44444	0.057519	-1.34064	116	108.875
20	0.75	0	-1.81481	144.667	86.4626
1.44444	0.527778	1.03751	-0.495024	2.55556	0.972765
13.8889	1.36111	0.18486	-0.878909	165.667	52.7829
14.3333	7	0.363966	-1.37037	126.333	55.3669
12.8889	16.1111	0.226757	-1.1824	95.1111	48.3411
11	1.5	0	-1.22222	122.333	38.1416
27.1111	75.1111	0.0335728	-1.75	119.111	130.885
9	9.5	0.500894	-0.926747	89.4444	29.189
12.4444	2.02778	-0.247028	-1.43717	156.667	45.3718
13.4444	0.527778	-0.701217	-1.02688	181.222	50.428
17.7778	13.9444	0.218649	-1.75773	129.333	74.3127
46	98.5	0.316426	-1.14563	127.111	255.443
45.5556	55.5278	0.325749	-1.17904	133.556	251.764
29	28.25	0.594957	-1.11739	155	141.487
24	2.25	-0.592593	-0.761317	94.4444	110.1
25.5556	0.527778	0.701217	-1.02688	141.556	119.5
31.4444	69.5278	-0.0150296	-1.75188	140.333	157.872
8.77778	6.44444	-0.0239805	-1.62602	82.7778	27.9914
27.1111	8.61111	0.193582	-1.69287	145.333	129.274
15.5556	2.27778	0.293686	-1.66781	130.222	61.6831
31	2.25	-0.592593	-1.81481	24.3333	153.627
4.55556	5.77778	0.515389	-1.24463	25.8889	10.7567
0.777778	0.444444	0.175926	-1.12037	1	0.22222
1.77778	5.19444	1.19947	0.208972	7.77778	3.24014
2.22222	8.19444	0.825126	-0.875846	12.2222	5.06774
1.55556	2.27778	0.293686	-1.66781	4.44444	2.16775
38.1111	25.6111	0.0194528	-1.80073	109.889	200.597
28.3333	10	0.381815	-1.75704	100.556	136.915
35.5556	12.2778	0.0820081	-1.76782	108.889	183.404
25.2222	0.944444	0.346736	-1.10739	125	117.474
46.3333	34.75	0.0491788	-1.27893	129.667	256.89
48.4444	40.5278	0.360421	-1.21075	107.333	271.734
51.3333	65.25	0.304126	-1.13625	104.667	292.474
92.5556	137.278	-0.0325314	-1.37926	126.778	605.553
46.5556	23.2778	0.610507	-0.955997	111.667	258.273
41.8889	2.61111	0.473364	-0.988297	135.667	225.758
60.3333	12.25	0.00172865	-1.76743	67	356.995

67.3333	19	0.000892864	-1.78404	84.8889	409.113
66.4444	24.2778	0.0968303	-1.65701	84.4444	402.494
59	21	0.561132	-0.862434	114.778	347.301
54	2	0	-1.22222	101.778	310.788
30.4444	10.7778	0.346202	-1.49111	140	150.258
32.2222	6.69444	0.475966	-1.16493	105.556	161.564
31.5556	37.5278	0.435507	-1.13777	90.4444	157.888
26.3333	1.75	0.319969	-1.81482	97.6667	124.305
25.5556	1.02778	1.46659	0.823934	113.556	119.512
5	26.5	0.537567	-1.46272	48.5556	15.3612
16.1111	45.6111	0.410972	-1.74384	129.444	66.37
6.77778	0.944444	-0.346733	-1.10739	46.7778	18.8039
2.77778	0.944444	-0.346733	-1.10739	8.55556	4.33551
3.77778	2.19444	0.540127	-1.55047	16.2222	7.6004
33.7778	18.4444	0.25314	-1.75345	104.889	171.871
40.5556	38.7778	0.213694	-1.42423	86.3333	217.25
23.4444	0.777778	0.147985	-1.04384	66.7778	106.721
30.8889	3.61111	0.917137	-0.307176	104	152.943
32	3.75	0	-1.43556	117.111	160.075
34.5556	66.5278	0.164306	-1.43505	115.444	177.844
10.2222	8.69444	0.587399	-0.91737	83.7778	34.8072
18.3333	7.5	-0.0504903	-1.65416	115.222	77.1986
21.2222	6.94444	-0.395476	-1.64199	86.7778	93.7516
30.3333	10.5	-0.55952	-0.938691	76.1111	149.554
1.77778	3.44444	1.12055	0.194666	6.22222	2.69607
11.7778	51.6944	0.393951	-1.14398	70.8889	44.834
2.77778	1.19444	0.891086	-0.784106	8.77778	4.3466
1.88889	1.11111	0.756604	-0.85037	4.55556	2.08388
9.44444	13.0278	0.41646	-1.28426	72.3333	31.4628
30.3333	6	0.609852	-1.09465	100.556	149.451
34.3333	0.75	0.456182	-0.761314	127	175.167
27.2222	0.944444	0.346736	-1.10739	144.556	129.783
33.2222	3.19444	-0.17779	-1.01256	82.5556	167.97
32.6667	0.25	-0.592599	-1.81481	43.3333	164.31
6.88889	14.3611	0.504911	-1.13142	60.2222	20.5014
29.7778	31.4444	-0.205553	-1.27308	89.7778	146.492
38.2222	7.44444	-0.600649	-0.84286	159.111	201.036
39.1111	57.3611	-0.0357998	-1.68113	101.556	207.83
4.11111	0.361111	0.0126425	-0.636642	17.2222	8.44157
11.3333	7.75	0.0961332	-1.25244	106.889	40.1384
6.55556	7.77778	0.254856	-1.55568	49.8889	18.5489
59.8889	94.1111	0.424005	-1.08178	114.778	354.587
65.6667	59.5	0.451585	-1.16113	98.3333	397.008
60.2222	7.69444	-0.0787939	-1.58646	106.444	356.129
61	4.25	0.608717	-1.01922	112.333	361.819
62.8889	5.36111	-0.203113	-1.49333	91.3333	375.799
41.4444	73.5278	0.474573	-1.24525	133.222	223.796
25.2222	2.44444	0.374	-1.16376	97.8889	117.512

23	0.75	0	-1.81481	103	104.063
27.8889	1.11111	-0.381817	-1.33037	96.1111	133.938
29.4444	13.5278	0.100299	-1.66817	111	143.981
8.33333	6	0.700575	-1.14403	74.7778	25.9281
8.33333	6	0.700575	-1.14403	74.7778	25.9281
15.6667	7.75	0.274665	-1.60762	138.556	62.5047
18.1111	2.36111	0.204927	-1.75182	74.1111	75.766
12.6667	0.5	0.419025	-1.22222	160.889	46.4227
24.3333	33	-0.0160209	-1.70285	109.444	112.935
17.5556	12.5278	-0.0340292	-1.43206	120.222	73.0366
35.8889	6.86111	0.0328204	-1.62797	156.333	185.505
46.8889	3.86111	-0.654505	-0.877021	97.1111	260.342
29	2	0.942809	-0.555555	46.3333	140.925
2.66667	1	-0.0740743	-1.37037	8	4.02941
2.11111	1.11111	0.381816	-1.33037	5.44444	2.6122
0.666667	0.5	0.419026	-1.22222	0.888889	0.22222
35.1111	18.6111	-0.0174947	-1.66054	111.556	180.597
53.4444	53.5278	-0.0112781	-1.35573	116.333	307.416
48.5556	26.2778	0.0107934	-1.59659	133.889	272.335
55.2222	19.6944	-0.00907109	-1.70815	108.778	319.81
15.4444	30.5278	0.277712	-1.37774	123.444	62.2571
28	43	-0.0260075	-1.51331	111.111	135.609
58.1111	37.6111	0.611138	-1.02984	110.778	340.981
62.3333	75.75	-0.0197741	-1.77753	84.3333	372.411
16.5556	22.0278	0.474768	-1.26927	123	67.867
13.4444	16.5278	0.160258	-1.78599	110.111	51.1926
18.3333	60	0.443879	-1.37403	105	78.9838
25.5556	76.2778	0.207219	-1.46856	123.556	121.412
2.11111	1.11111	0.381816	-1.33037	5.44444	2.6122
50.5556	11.2778	0.167476	-1.51995	91.2222	286.277
57	1.5	0	-1.22222	121.444	332.492
43.4444	0.527778	1.03752	-0.495015	95.8889	236.393
43.7778	0.194444	-1.1199	-0.798934	124.667	238.685
43.5556	0.277778	-0.187403	-2.17037	105.333	237.155
3	6.75	0.684267	-0.995427	15	6.25163
14.7778	21.4444	-0.156119	-1.46401	123.667	58.3967
10.4444	13.5278	0.314681	-1.27634	92.6667	36.1775
11.4444	9.02778	0.085667	-1.61096	110.556	40.7558
3.77778	8.94444	0.912977	-0.574876	22.2222	8.62507
4.55556	12.2778	0.918812	-0.494139	31.6667	11.5369
5.88889	26.8611	0.300608	-1.36726	58.5556	18.6852
6.11111	23.3611	0.807602	-0.700905	29.6667	18.2751
12	11.25	0.795046	-0.634897	125.556	43.587
17.2222	4.94444	0.904804	-0.342721	101.889	70.8952
11.1111	5.11111	-0.0638672	-1.54995	128	38.8991
12.4444	3.02778	0.272344	-1.42458	157.556	45.4205
18.4444	0.777778	0.147985	-1.04384	84.8889	77.588
76.7778	76.4444	0.3647	-1.11117	131.667	481.461

63.5556	0.277778	-0.187403	-2.17037	57.3333	380.697
69.7778	20.1944	0.0193474	-1.80443	136.667	427.553
68.5556	24.5278	0.0387997	-1.76027	85.2222	418.364
78.1111	44.8611	0.155812	-1.51854	167.889	491.487
74.1111	75.6111	0.312873	-1.79842	126.778	460.997
43.2222	48.1944	0.0069292	-1.69744	147.444	235.576
45.5556	2.27778	-0.0941741	-1.09672	114.667	251.023
46.2222	0.444444	-0.175922	-1.12037	117.333	255.639
46.2222	9.69444	-0.315843	-1.73822	154	255.768
2.55556	0.777778	-0.147986	-1.04384	7.22222	3.66884
22.4444	28.2778	0.0632357	-1.65947	102.222	101.552
0.444444	0.277778	0.187394	-2.17037	0.444444	0
1.66667	0.25	-0.592592	-1.81482	3	1.33333
0.777778	1.44444	0.755404	-1.3467	1.88889	0.97276
28.4444	85.2778	0.25306	-1.73532	88.4444	139.298
14.7778	37.1944	0.116808	-1.78548	137.667	59.0664
1.11111	1.11111	0.381816	-1.33037	2.22222	0.972765
3.77778	7.69444	0.453616	-1.73659	21.1111	8.53475
11.1111	33.8611	0.785345	-0.664546	68.2222	40.4246
54.2222	40.6944	-0.050991	-1.66674	131.778	312.848
67.1111	5.86111	-0.396554	-1.77728	43.3333	407.319
48.8889	56.6111	0.0391222	-1.80492	79.5556	275.082
52.4444	62.2778	0.0228149	-1.46798	103.556	300.366
12.5556	14.5278	-0.225233	-1.34675	113.667	46.6181
20.2222	10.4444	-0.611618	-1.64697	133.778	88.0671
9.77778	6.69444	-0.168053	-1.65418	101.556	32.6189
4.11111	3.11111	0.21648	-1.54894	19.6667	8.8767
11.1111	42.8611	0.218849	-1.49689	104.667	41.2025
22.5556	156.778	0.320315	-1.21377	136.111	106.032
57	195.25	0.21601	-1.73782	151.444	334.658
13.5556	12.7778	0.163196	-1.61597	138.222	51.5852
7.77778	23.1944	0.544886	-1.05571	52.6667	24.9095
1.33333	3	0.955123	-0.514404	4.44444	2.0405
46.4444	166.278	-0.060652	-1.42898	114.667	259.551
8.22222	24.6944	0.670203	-0.975801	61.1111	26.8197
1.44444	2.02778	0.4456	-1.32909	3.88889	1.86165
3.22222	3.94444	0.494491	-1.08868	13.8889	6.224
0.444444	0.527778	1.03751	-0.495024	0.666667	0.22222
23.5556	397.278	0.0129433	-1.81052	54.6667	121.815
56.4444	526.278	0.0432326	-1.75689	98.2222	334.622
41.5556	565.278	0.0891084	-1.40436	67.5556	233.143
0.666667	0.25	-0.592593	-1.81481	0.666667	0
42.5556	92.2778	0.223754	-1.35444	101	231.665
64.3333	109.5	0.073567	-1.22099	111.667	387.578
28	11	0.603023	-1.3214	111.111	134.852
30	2.5	0	-1.79111	77.3333	147.26